





Research and Development Technical Report

DELET - TR -77-0472-F

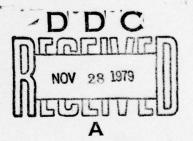


ANALYSIS OF PRESSURE PRODUCING REACTIONS IN LITHIUM-SULFUR DIOXIDE CELLS

A.N. DEY and R.W. HOLMES

P.R. MALLORY & CO., INC. LABORATORY FOR PHYSICAL SCIENCE BURLINGTON, MA 01803

NOVEMBER 1979



FINAL REPORT FOR PERIOD 15 SEPT. 1977 TO 31 JULY 1979

DISTRIBUTION STATEMENT
APPROVED FOR PUBLIC RELEASE; DISTRIBUTION UNLIMITED

PREPARED FOR:
US ARMY ELECTRONICS TECHNOLOGY AND DEVICES LABORATORY

ERADCOM

US ARMY ELECTRONICS RESEARCH AND DEVELOPMENT COMMAND FORT MONMOUTH, NEW JERSEY 07703

79 11 28 089

NOTICES

Disclaimers

The citation of trade names and names of manufacturers in this report is not to be construed as official Government indorsement or approval of commercial products or services referenced herein.

Disposition

Destroy this report when it is no longer needed. Do not return it to the originator.

SECURITY CLASSIFICATION OF THIS PAGE (When Date Entered)

	(19) REPORT DOCUMENTATION		READ INSTRUCTIONS BEFORE COMPLETING FORM
-	PORT NUMBER	2. GOVT ACCESSION NO.	3. RECIPIENT'S CATALOG NUMBER
	ELET TR-77-0472 - F		5. TYPE OF REPORT & PERIOD COVERE
. TIT	LE (end Subtitle)	and the same of th	Final Report
#	nalysis of Pressure Producing		9/15/77 to 7/31/79
in	Lithium-Sulfur Dioxide Cells	• 5	6. PERFORMING ORG. REPORT NUMBER
7. AU1	THOR(e)		8. CONTRACT OR GRANT NUMBER(s)
P	A. N./Dey R. W./Holmes] (15)	DAAB07-77-C-0472
. PEF	REPORMING ORGANIZATION NAME AND ADDRE	55	10. PROGRAM ELEMENT, PROJECT, TASK AREA & WORK UNIT NUMBERS
	P. R. Mallory & Co. Inc.	(16)	1L162705AH9411-981
	Laboratory for Physical Science	ce /	42
11. CO	Burlington Mass 01803		12. REPORT DATE
	. S. Army Elct Tech & Dvcs L	aboratory (1)	November 179
	N: DELET-PR, Fort Monmouth,		13. NUMBER OF PAGES
14. MC	NITORING AGENCY NAME & ADDRESS(II ditte	rent from Controlling Office)	15. SECURITY CLASS. (of this report)
		1287	Unclassified
		9/20	15a. DECLASSIFICATION/DOWNGRADING SCHEDULE
16. DIS	STRIBUTION STATEMENT (of this Report)		L
L	pproved for Public Release; Distribution Unlimited		
AF	inal rept. 15 S	ex 77-31	Jul 79,
17. DI:	STRIBUTION STATEMENT (of the abetract enter	réd in Block 20, il different fro	m Report)
18. SU	PPLEMENTARY NOTES		
	Y WORDS (Continue on reverse side if necessary	and identify by block number	
Su	ulfur Dioxide Battery, Lithium mermal Analysis (DTA), Energy ectrical Conductivity.	, Organic Electroly	yte, Safety, Differential
20 45	STRACT (Continue on reverse side if necessary	and identify by block number)	
b	Although the State-of-the-A y P. R. Mallory & Co. Inc. a ations, this program was initi	Art hermetically se re sufficiently abu lated to explore the	e feasibility of improving the
11	ntrinsic abuse resistance of the	he system even fur	ther by chemical and/or
i	ntrinsic abuse resistance of the	he system even fur product may be re	ther by chemical and/or ndered Safe under all user

- a. the identification of the chemical reactions responsible for the pressure buildup and/or thermal runaway,
- b. the determination of the sensitivity of these reactions to the various use and abuse variables, and
 - c. the development of methods to desensitize these reactions.

We have carried out differential thermal analysis (DTA) of the cell/constituents that may be present during the various stages of storage and discharge singly, as well as in binary and multiple combinations in order to accomplish (a) and (b) above. We carried out DTA of miniature Li/SO₂ cells in order to establish the applicability of the results to actual cells. In addition, we carried out kinetic studies of the Li + organic solvent (the most reactive couple) reactions in an effort to find organic solvent additives to guench this reaction.

We determined the exotherm initiation temperature of a variety of lithium-organic solvent combination in order to select the least reactive organic solvents. We narrowed down our selection of the prospective organic electrolytes for enhanced safety further by measuring the electrical conductivities of the actual electrolytes containing 70% SC₂. LiBr and the various promising organic solvent combinations.

The DTA results showed the Li + SO_2 couple to be the most stable showing no exothermic transition up to as high a temperature as 370° C, the upper limit of the DTA run. The Li + AN couple was found to be the least stable and as such, the most important reaction pertaining to safety. Both SC_2 & PC were found to be excellent film-forming agents to protect Li from spontaneous reactions with AN. Cn the other hand, organic solvents such as MF, DME, DG and THF although stable with Li by themselves, were found to enhance the Li + AN reactions most likely due to the enhanced solubilizing property of the mixed solvent towards the lithium film. The DTA results of the miniature Li/ SC_2 cells corroborated the DTA results on the separate reactive cell constituents.

Exotherm initiation temperature provided a measure of the lithium solvent reactivity; the higher is this temperature, the lower is the reactivity and vice a versa. We selected fifteen organic solvent combinations which showed exotherm initiation temperature in excess of 100° C and as such these combinations should be considerably safer than AN whose exotherm initiation temperature is $25^{\circ}-50$, C. We narrowed our selection of prospective organic electrolytes further to six specific ones based on their electrical conductivity (in the temperature range of -40° C to 100° C) which was found to be comparable or superior to the standard SC₂ electrolyte with AN. Two of these six electrolytes contained no AN and as such are the most promising ones from the point of view of safety.

We strongly recommend evaluation of these electrolytes in actual cells for determining their efficacy in improving the safety of the cells without sacrificing the performance.

Unclassified

CONTENTS

	Distr	ibution/
Page	Avel	abi ity Codes
111	Dist	Avail and/or special
viii	H	1

Ву___

NTIS Color DDC TAB Unamnounced Justification

		Page
	List of Figures	iii
	List of Tables	viii
1.	Introduction	1-1-1
2.	DTA of Li/SO ₂ Cell Constituents	* Buomaya
	Experimental	3
	Results and Discussion	4
	Conclusions	13
3.	DTA of Spirally-Wound Li/SO ₂ Minature Cells	15
	Experimental	15
	Results and Discussion	16
	Conclusions	21
4.	Kinetics of Lithium-Organic Solvent Exothermic Reactions	23
	Experimental	23
	Results and Discussion	24
	Conclusions	28
5.	Exotherm Initiation Temperature. Effect of Solvent Additives on the Li-Solvent Reaction	29
	Experimental	29
	Results and Discussion	30
	Conclusions	32

Contents (continued)

		Page
6.	Electrical Conductivity of the Prospective Electrolytes	34
	Experimental	34
	Results and Discussion	35
	Conclusions	36
7.	Selection of Electrolytes for Improved Safety	38
8.	Conclusions and Recommendations	41
9.	References	43
	Tables	45
	Figures	53
	Distribution List	124

List of Figures

		Page
Fig. 1.	Cross-Sectional View of the High-Pressure Hermetic Crucible.	53
Fig. 2.	Thermogram of S (0.0240 gm); 5°C/Minute.	54
Fig. 3.	Thermogram of Na ₂ S ₂ O ₄ (0.0333 gm); 5°C/Minute.	55
Fig. 4.	Thermogram of Li (0.0123 gm) + Celgard (0.0634 gm); 5°C/Minute.	56
Fig. 5.	Thermogram of Li (0.0031 gm) + LiBr (0.0799 gm); 5°C/Minute.	57
Fig. 6.	Thermogram of Li (0.008 gm) + Teflon Powder (0.0234 gm); 5°C/Minute.	58
Fig. 7.	Thermogram of Li (0.00029 gm) + SO ₂ ; 5°C/Minute.	59
Fig. 8.	Thermogram of Li (0.0010 gm) + AN (100µ1); 5°C/Minute.	60
Fig. 9.	Thermogram of Li (0.0008 gm) + PC (20µl); 5°C/Minute	61
Fig. 10.	Thermogram of Li (0.0003 gm) + AN/PC $(50:50)$ 80μ l; 5° C/Minute.	62
Fig. 11.	Thermogram of Li (0.00085 gm) + Electrolyte (40% SO ₂ , 40% AN, 20% LiBr)~25µl; 5°C/Minute	63
Fig. 12.	Thermogram of Li (000029 g) + 20µl Electrolyte (28% SO ₂ , 56% AN/AA (90/10), 16% LiBr). 5°C/Minute.	64
Fig. 13.	Thermogram of Cathode Mix (0.0661 gm) from a Discharged Li/SO, Cell; 5°C/Minute.	65
Fig. 14.	Thermogram of Cathode Mix (0.0819 gm) from a Discharged Li/SO ₂ Cell after Exposure to Air; 5°C/Minute.	66
Fig. 15.	Thermogram of Cathode Mix (0.0624 gm) from a Li/SO ₂ Cell Which was Discharged and Then Driven into Reversal for 10% of Its Discharged Capacity; 5°C/Minute.	67
Fig. 16.	Thermogram of $Na_2S_2O_4$ (0.01007 gm) + Li Powder (0.00131 gm) + Carbon (0.00284 gm); 5°C/Minute	68
Fig. 17.	Thermogram of Li (0.0015 gm) + S (0.0079 gm); 5°C/Minute.	69
Fig. 18.	Thermogram of Powdered Li $(0.00039 \text{ g}) + \text{S} (0.00147 \text{ g}) + \text{Na}_2\text{S}_2\text{O}_4 (0.00644 \text{ g})$.	70

List of Figures (continued)

		Pag
Fig. 19.	Thermogram of Li $(0.00094 \text{ gm}) + \text{Li}_2\text{SO}_3$ (0.0075 gm) As Received; 5°C/Minute.	71
Fig. 20.	Thermogram of Li (0.00572 gm) + Al (0.00720 gm); 5°C/Minute.	72
Fig. 21.	Thermogram of LiAl Alloy (0.01333 gm) + AN; 5°C/Minute.	73
Fig. 22.	(1) Thermogram of LiAl Alloy $(0.0050 \text{ g}) + S(0.0034 \text{ g})$ (2) Thermogram of Al $(0.0084 \text{ g}) + S(0.0153 \text{ g}) 5 ^{\circ}\text{C/Minute}$.	74
Fig. 23.	Thermogram of LiAl Alloy + An/SO ₂ (75:25) 20µl; 5°C/Minute.	75
Fig. 24.	Cross-Sectional View of the Miniature Li/SO2 Cell.	76
Fig. 25.	Fixtures for DTA of Minhture Cell.	77
Fig. 26.	Thermogram of a Discharged Miniature Li/SO ₂ Cell of Standard Construction; Discharged Current lmA; Discharge Capacity 193 mAHr.	78
Fig. 27.	Voltage, Differential Temperature and the Block Temperature Profiles of a Li/SO ₂ Minature Cell of Standard Construction During Discharge and Force-Discharge at 25°C at a Current of 90 mA.	79
Fig. 28.	Thermogram of the Force-Discharged Li/SO ₂ Minature Cell of Fig. 24.	80
Fig. 29.	Thermogram of the Repeat DTA Run after the One in Fig. 25.	81
Fig. 30.	Thermogram of a Miniature Li/SO ₂ Cell of Standard Construction after Being Charged at 25°C for 7 Hours at 90 mA.	82
Fig. 31.	Thermogram of a Discharged Minature Li/SO ₂ Cell with PC in the Electrolyte; Discharge Current, 10 mA; Discharge Temperature, 25°C.	83
Fig. 32.	Voltage, Differential Temperature and the Block Temperature Profiles of a Li/SO ₂ Miniature Cell with PC in the Electrolyte During Discharge and Force-Discharge at 25°C at a Current of 90 mA.	84
Fig. 33.	Thermogram of the Li/SO ₂ Miniature Cell with PC in the Electrolyte after the Force-Discharge as Shown in Fig. 29.	85
Fig. 34.	Thermogram of the Repeat DTA Run after the One	86

List of Figures (continued)

		Page
Fig. 35.	Thermogram of a Li/SO ₂ Miniature Cell with PC in the Electrolyte after Being Force-Discharged at -30°C for 3 Hours at 90 mA.	87
Fig. 36.	Thermogram of the Repeat DTA Run after the One in Fig. 32.	88
Fig. 37.	Thermogram of an Undischarged Li/SO ₂ Miniature Cell with Glass Filter Paper Separator.	89
Fig. 38.	Thermogram of a Discharged Li/SO, Miniature Cell with Glass Filter Paper Separator; Discharge Current, 10 mA; Discharge Temperature, 25°C.	90
Fig. 39.	Thermogram of a Li/SO ₂ Miniature Cell with Glass Filter Paper Separator after Being Force-Discharged at-30°C for 3 Hours at 90 mA; Upper Limit of Temperature was 170°C.	91
Fig. 40.	Thermogram of a Li/SO ₂ Miniature Cell with Glass Filter Paper Separator after being Force-Discharged at -30°C for 3 Hours at 90 mA; the Upper Limit of the Temperature was 250°C.	92
Fig. 41.	Thermogram of an Undischarged Li/SO ₂ Miniature Cell with LiAsF ₆ Electrolyte.	93
Fig. 42.	Thermogram of the Repeat DTA Run after the One in Fig. 38.	94
Fig. 43.	Thermogram of a Discharged Li/SO ₂ Miniature Cell with LiAsF ₆ Electrolyte; Discharge Current 10 mA; Capacity, 160 mAHr; Temperature, 25°C.	95
Fig. 44.	Thermogram of a Li/SO ₂ Miniature Cell with LiAs F ₆ Electrolyte after Being Force-Discharged at 25°C, for 5 Hours with 90 mA.	96
Fig. 45.	Thermogram of a Li/SO ₂ Miniature Cell with LiAsF ₆ Electrolyte after Charging at 25°C for 7 Hours with 90 mA.	97
Fig. 46.	Typical Isothermal DTA Thermograms of Li + AN System at Various Temperatures.	98
Fig. 47.	Arrhenius Plots of the Li + AN System; (1) with Li Discs Aged in Dry Box, (2) Freshly Cut Li Discs. (3) with 0.32 M LiBr in AN.	99

<u>List of Figures</u> (continued)

		Page
Flg. 48.	Arrhenius Plots of the Li + AN + PC System; (1) 0% AN, (2) 50% AN, (3) 80% & 95% AN, (4) 100% AN, and (5) 0% PC and 3% SO ₂ .	100
Fig. 49.	Arrhenius Plots of the Li + AN/BL System; (1) 0% AN, (2) 80% AN, (3) 95% AN and (4) 100% AN.	101
Fig. 50.	Arrhenius Plots of Li + AN + MF System; (1) 0% AN, (2) 80% AN, and (3) 95% AN.	102
Fig. 51.	Isothermal DTA Thermograms (a) Normal Runs, (b) for Reactions with Short Induction Periods as with Li + AN/MF (80/20).	103
Fig. 52.	Arrhenius Plots of Li + AN + DME System; (1) 0% DME, (2) 5% DME, and (3) 20% DME.	104
Fig. 53.	Arrhenius Plots of (1) Li + AN/THF (95/5), (2) Li + AN/DG (95/5), (3) Li + AN/THF (80/20), and (4) Li - AN/DG (80/20) Systems.	105
Fig. 54.	Thermograms at 5°C/Min. Showing the Determination of the Exotherm Initiation Temperature (1) Li + AN/bromobenzene (95/5), (2) Li + AN/acetic anhydride (95/5).	106
Fig. 55.	Thermograms for the Li + AN/BL Reaction.	107
Fig. 56.	Exothern Initiation from DTA @ 5°C/min. 0.00029 g Li + 20µl of Indicated AN/DME/PC.	108
Fig. 57.	Exotherm Initiation from DTA @ 5°C/Min. 0.000291 g Li + 20µl of Solvent Mixture.	109
Fig. 58.	Exotherm Initiation from DTA @ 5°C/Min. 0.000291 g Li + 20µl of AN/BL Mixture.	110
Fig. 59.	Exotherm Initiation Temperature of the Li + AN Reaction as a Function of SO ₂ Concentration.	111
Fig. 60.	Conductivity Cell for SO ₂ Electrolytes.	112
Fig. 61.	Specific Conductance vs. Temperature for SO ₂ Electrolytes, In Aluminum Cell.	113
Fig. 62.	Specific Conductance vs. Temperature Electrolyte 3A: LiBr, AN, SO ₂ .	114
Fig. 63.	Specific Conductance vs. Temperature for Electrolyte 4: LiBr, AN/BL (90/10), SO ₂ .	115
Fig. 64.	Specific Conductance vs. Temperature Electrolyte 5: LiBr, PC, SO ₂ .	116

List of Figures (continued)

		Page
Fig. 65.	Specific Conductance vs. Temperature Electrolyte 6: LiBr, THF, SO ₂	117
Fig. 66.	Specific Conductance vs. Temperature Electrolyte 7: LiBr, AN/PC/DME(85/10/5), SO2	113
Fig. 67.	Specific Conductance vs. Temperature Electrolyte 8: LiBr, DME, SO ₂	119
Fig. 68.	Specific Conductance vs. Temperature Electrolytes 9 and 10 Electrolyte 9: LiBr, BL, SO ₂ and Electrolyte 10: LiBr, PC, SO ₂	120
Fig. 69.	Specific Conductance vs. Temperature Electrolytes 11 and 12 Electrolyte 11: LiBr AN/MF(50/50) SO ₂ and Electrolyte 12: LiBr, AN/PC/BL(90/5/5), SO ₂	121
Fig. 70.	Specific Conductance vs. Temperature Electrolytes 13 and 14 Electrolyte 13: LiBr, DME/PC(50/50), SO ₂ and Electrolyte 14: LiBr, DME/BL(50/50), SO ₂	122
Fig. 71.	Specific Conductance vs. Temperature Electrolytes 15 and 15 Electrolyte 15: LiBr, AN/PC/MeOH(35/10/5), SO ₂ Electrolyte 15: LiBr, AN/BL/DME(85/10/5), SO ₂	123

List of Tables

		Page
Table 1.	List of Possible Chemicals Present in Li/SO ₂ Batteries at the Various Stages and Types of Use and Abuse.	45
Table 2.	Summary of DTA Results of the Various Chemicals and their Combinations from Table 1; Heating Rate 5°C/Minute.	46
Table 3.	The Activation Energy and the Frequency Factor of Various Li-Organic Solvent Heterogeneous Reactions Determined by Isothermal DTA Method.	48
Table 4.	Solvent and Additive Search for System to Protect Lithium in SO ₂ Cells. DTA @ 5 °C/min. 0.00029g Li + $20\mu l$ of Indicated Solution.	49
Table 5.	SO ₂ Electrolyte Compositions for Conductivity Study.	51
Table 6.	Conductivity of SO ₂ Electrolytes in Order of Higher to Lower Conductivities. (SO ₂ and LiBr were common to all).	52

1. Introduction:

The Li/SO, battery is the most highly developed high-energy density battery system obtainable today and is available in a growing volume from several manufacturers in response to the rising demand for its use in various applications. The rising demand is motivated by the need for a light-weight power source that has a high-rate capability, a good low temperature performance, and good high temperature storability. The Li/SO, system has all these characteristics to a greater extent than does any other battery system and for this reason, it has acquired a dominant position in the emerging new primary battery technology. Improvements made at a rapid pace in the Li/SO, technology in the areas of efficient manufacturing technology, product reliability (hermetic structures) and abuse tolerance (ventable structures). In this report, we address ourselves to the area of abuse tolerance. Although, the State-of-the-Art hermetically sealed high-rate D cells made by P. R. Mallory & Co. Inc. are sufficiently abuse resistant (3-5) for various applications, we have initiated a program for exploring the feasibility of improving the intrinsic abuse resistance of the system even further by chemical and/or mechanical means, if possible, so that the product may be rendered Safe under all user conditions. The approach that we have pursued involves:

- a. the identification of the chemical reactions responsible for the pressure buildup and/or thermal runaway;
- b. the determination of the sensitivity of the above reactions to the various use and abuse variables; and
 - c. the development of methods to desensitize the above reactions.

We have carried out differential thermal analysis (DTA) of all the cell constituents that may be present at the various stages of storage and discharge, singly, as well as in binary and multiple combinations in order to accomplish (a) and (b) above. We successfully used this method earlier

for the Safety studies of the Li/SOCl₂ cells (6). In addition, we carried out DTA of miniature Li/SO₂ cells in order to establish the applicability of the results from the DTA of individual cell constituents to the actual cells. We also carried out kinetic studies of the Li-organic solvent heterogenious reactions (the most significant reactions affecting the safety) at various temperatures using an isothermal DTA method. The purpose was to determine the effectiveness of the various organic solvent additives in reducing the Li-organic solvent reactions for enhanced safety.

A variety of organic solvents were studied in order to find an effective additive to AN for improving the safety of Li-SO₂ cells with acetonitrile (AN) as the major organic solvent. We also examined solvents with the intention of altogether eliminating the reactive AN from the cell. The promising organic solvents were first selected based on their exotherm initiation temperature with Li as determined from DTA thermograms run at the programmed temperature increase of 5.0°C/min. The higher the initiation temperature, the lower the lithium-solvent reactivity and hence safer.

Another area of interest was the conductivity of various SC_2 electrolytes of interest. To maintain the excellent discharge performance of the Li-SC_2 cell it is essential that the electrolyte conductivity be at least as good as that of the standard electrolyte currently in use, which employs AN as the organic solvent. We measured the conductivity of the SC_2 electrolytes with various promising solvents and solvent additives in hermetically sealed pressurized conductivity cells.

The experimental details and the results of the above studies are reported here. Several promising SO_2 electrolytes are recommended for further study in actual cell configurations. The recommended electrolytes all promise enhanced safety and equivalent or improved conductivity compared to the standard SO_2 electrolyte with AN.

2. DTA of Li/SO2 Cell Constituents:

Experimental:

The Mettler TA2000 Differential Thermal Analysis System was used for the DTA experiments. High-pressure crucibles made of a corrosion resistant alloy (Nemonic) and having a gold diaphragm capable of withstanding pressures of 1000 PSI were used for most of the experiments. A cross-sectional view of the crucible is shown in Fig. 1. The sealing of the crucible was accomplished by means of the screw cap which when tightened, cuts into the gold diaphragm providing a hermetic seal. In certain experiments with reactive liquids, the crucible was sealed by means of a septum made of viton rubber and the liquid reactants were injected into the crucible. The corrosive gaseous samples were first prepared in a Kovar tube which was hermetically sealed by means of welding and then placed inside the crucible which was sealed by means of the screw-cap and the gold diaphragm as above.

The DTA System was calibrated with indium metal samples in order to obtain quantitative data on the caloric output of the reactions. Thus, the DTA thermograms were useful in determining both the temperature at which a thermal transition (exothermic and/or endothermic) occurred as well as the total heat of such transitions.

All the chemicals were used as received. Since a majority of the above chemicals, shown in Table 2, were moisture sensitive, the transfer of the materials to the high-pressure crucible and the sealing of the crucible were carried out in an argon filled dry box.

The DTA runs were carried out at heating rates of 5°C/minute, from room temperature to approximately 450°C and back. Thermograms were recorded for both the heating and the cooling modes, the latter was occasionally useful in identifying the reaction products generated during the heating mode.

Results and Discussion:

Li/SO $_2$ organic electrolyte cells contain Li anode, Teflon (polytetrafluoroethylene) bonded carbon cathode on expanded aluminum grid, LiBr electrolyte salt, acetonitrile organic solvent and liquid SO $_2$ depolarizer. Porous polypropylene has been most commonly used for separator. Electrolyte salts such as LiAsF $_6$ (8) and organic solvents such as propylene carbonate and methyl formate have also been used. The cell container is made of nickel-plated cold-rolled steel with glass-to-metal seal electrical feedthrough comprising tantalum or molybdenum positive terminal. The cell case is the negative terminal. A list of all the possible chemicals that may be present in a Li/SO $_2$ battery at the various stages of use and abuse is provided in Table 1. The list includes (a) the possible starting materials mentioned above, (b) the possible impurities and (c) the possible chemicals generated during the various use and abuse regimes. Lithium dithionite is the main discharge product according to the cell reaction,

$$2 \text{ Li} + 2 \text{ SO}_2 \longrightarrow \text{ Li}_2 \text{S}_2 \text{O}_4$$
 [1]

The formation of Li_2SO_3 , Li_2SO_4 , Br_2 , SOBr_2 and S_2Br_2 as a result of prolonged high temperature storage has been postulated (7, 8) to be due to the reactions between LiBr and SO_2 ,

$$8 \text{ LiBr} + 8 \text{ SO}_2 \longrightarrow 4 \text{ Li}_2 \text{SO}_3 + 4 \text{ SOBr}_2$$
 [2]

$$4 SOBr_2 \longrightarrow 2 SO_2 + S_2Br_2 + 3 Br_2$$
 [3]

$$4 \operatorname{Li}_{2} \operatorname{SO}_{3} + 2 \operatorname{Br}_{2} \longrightarrow 2 \operatorname{Li}_{2} \operatorname{SO}_{4} + 4 \operatorname{LiBr} + 2 \operatorname{SO}_{2}$$
 [4]

$$4 \operatorname{LiBr} + 4 \operatorname{SO}_{2} \longrightarrow 2 \operatorname{Li}_{2} \operatorname{SO}_{4} + \operatorname{S}_{2} \operatorname{Br}_{2} + \operatorname{Br}_{2}$$
 [5]

The formation of CH_4 and LiCN during reversal of an unbalanced Li/SO₂ cell has been reported (9). The formation of CS_2 , H_2S and CO_2 from the reactions between CH_4 and SO_2 was predicted from thermodynamic considerations (10).

The list in Table 1 contains only the stable chemical species known to be present in Li/SO₂ cell. There are unstable species which may be formed during the electrochemical and chemical reactions that occur during storage, use and abuse of the cell. Both the nature of and the effect of these species in the abuse resistance of the cells are uncertain. Since all these stable and unstable chemicals may be present simultaneously in the cell, any and all of these may be important in determining the abuse resistance of the Li/SO₂ cells. In this program, we have attempted to identify the chemicals and the chemical combination which contribute to the unsafe behavior (thermal runaway, etc.) of the cell from the DTA of the chemicals and their combinations shown in Table 1. Chemical combinations which produce exothermic transitions at ambient temperatures may be responsible for the initiation of a thermal runaway, whereas the chemicals and/or combinations thereof that produce exothermic transitions at elevated temperatures, may sustain a thermal runaway once initiated by other means.

The DTA results are summarized in Table 2. All the runs were made at a heating rate of $5\,^{\circ}\text{C/minute}$. The thermograms of some important chemicals and their combinations are discussed below.

Single Components:

<u>Lithium:</u> The thermogram of Li consists of one sharp endotherm at 188°C corresponding to the melting of Li. The difference between the melting point of Li (179°C) and the above temperature indicates the thermal lag of the crucible at the heating rate of 5°C/minute.

The lag would be expected to depend upon both the temperature and the heating rate. All the temperatures reported in Table 2 are the programmed furnace temperatures, Tp, the actual sample temperatures corresponding to the furnace temperature can be approximated by subtracting about 8°C from the furnace temperature. On cooling mode, the Li thermogram showed an exotherm corresponding to the freezing of Li. The identical caloric output corresponding to melting and freezing, indicated the lack of reaction of Li and the crucible.

<u>Carbon Black:</u> The thermogram of Shawinigan black, the major constituent of the carbon cathode showed no transitions.

Separator: The thermogram of Celgard 2400, the porous polypropylene separator material, showed an endothermic transition at 156°C corresponding to the melting of polypropylene and an exotherm on cooling mode for freezing of polypropylene, with identical caloric output.

<u>Acetonitrile (AN)</u>: The thermograms of both AN and PC showed no characteristic transitions within the temperature range (25° to 350°C) examined.

Teflon: The thermogram of Teflon powder (TL-120) showed a small gradual endothermic transition at 250°C most likely indicating the sintering of Teflon powder. The Teflon is used as a binder for the carbon cathode.

Sulfur: The thermogram of elemental S is shown in Fig. 2. The two overlapping endothermic transitions at 112° and 120°C correspond to the melting of two crystalline forms (rhombic and monoclinic) of sulfur and the sharp exotherm on cooling mode represents the crystallization of one type of sulfur since one form changes to the other on melting. The absence of any other transitions indicate the inertness of the crucible to sulfur.

Sodium Dithionite: Lithium dithionite, $\operatorname{Li}_2\operatorname{S}_2\operatorname{O}_4$, the primary cell reaction product of the $\operatorname{Li/SO}_2$ battery, was not commercially available. Therefore, we used commercially available $\operatorname{Na}_2\operatorname{S}_2\operatorname{O}_4$ which is chemically similar to $\operatorname{Li}_2\operatorname{S}_2\operatorname{O}_4$; the $\operatorname{Na}_2\operatorname{S}_2\operatorname{O}_4$ was approximately 90% pure, having sulfite and thiosulfate as major impurities. The DTA thermogram of $\operatorname{Na}_2\operatorname{S}_2\operatorname{O}_4$ is shown in Fig. 3. The material showed several strong exothermic transitions above $100\,^{\circ}\mathrm{C}$ on heating. The absence of endothermic transitions on cooling indicates that the above transitions represent irreversible decomposition of $\operatorname{Na}_2\operatorname{S}_2\operatorname{O}_4$. The thermogram on cooling showed an exothermic transition corresponding to the freezing of elemental S. The repeat run (not shown)

shows another endothermic transition corresponding to the melting of elemental S, thus confirming that one of the decomposition products of Na₂S₂O₄ is S. The quantity of S formed was estimated (using the DTA thermogram of elemental S shown in Fig. 2) to be 0.0056 gm. The amount of S expected based on the decomposition reactions such as

$$2 \text{ Na}_2 \text{S}_2 \text{O}_4 \longrightarrow 2 \text{ Na}_2 \text{SO}_3 + \text{SO}_2 + \text{S}$$
 [6]

$$2 \text{ Na}_2 \text{S}_2 \text{O}_4 \longrightarrow 2 \text{ Na}_2 \text{ O} + 3 \text{ SO}_2 + \text{S}$$
 [7]

is 0.0055 gm. The agreement is reasonable.

The total caloric output of the exothermic decomposition was determined by integrating the area under the three major peaks (two major peaks in the case of pre-dried material) and it turned out to be approximately - 14.4 K. Cal/mole as the heat of decomposition of $\mathrm{Na_2S_2O_4}$. Assuming reaction [6] as the decomposition reaction, the heat of formation of $\mathrm{Na_2S_2O_4}$ was calculated using the known heats of formation of $\mathrm{Na_2SO_3}$ (-260.6 K.Cal/mole), and $\mathrm{SO_2}$ (-70.96 K.Cal/mole). This turned out to be -290 K.Cal/mole. The heat of formation of $\mathrm{Na_2S_2O_4}$ calculated (11) from the date in aqueous ammonia was 296 K.Cal/mole. The agreement is reasonable. Thus, the heat of decomposition of -14 K.Cal/mole for $\mathrm{Na_2S_2O_4}$ as determined from the DTA thermogram is probably reasonable.

In another experiment, Na₂S₂O₄ was vacuum dried for about 22 hours at 100°C. DTA was run on the sample and the thermogram was similar to Figure 3 except the ripple at about 120°C, and the small peaks at about 150°C and 220°C were absent. The run demonstrated that the minor peaks in Figure 3 were the result of small side reactions due to traces of water.

<u>Lithium Bromide</u>: The thermogram of anhydrous LiBr as used in the electrolyte for the Li/SO₂ batteries was found to be completely featureless.

Combinations:

Li + Celgard: The thermogram of Li and the porous polypropylene separator (Celgard) which remains in contact with Li in the cell, is shown in Fig. 4. The endothermic transitions corresponding to melting of polypropylene and Li during heating mode and the identical exothermic peaks during the cooling mode, indicate the absence of chemical activity between the two.

<u>Li + LiBr</u>: The thermogram of a mixture of Li and LiBr, as shown in Fig. 5, consists of one exothermic peak at 124°C prior to Li melting. The exothermic peak most likely represents the reaction between Li and some trace impurities in LiBr.

<u>Li + Teflon</u>: The thermogram of Li + Teflon powder is shown in Fig. 6. The strong exothermic peak, at 279°C, beyond the lithium melting most likely represents the following reaction:

$$4 \text{ Li} + \frac{1}{n} \left(\frac{C_2 F_4}{n} \right)_n \longrightarrow 4 \text{ LiF} + 2 C$$

$$\triangle H_0 = -96 \text{ K. Cal/g atom of Li.}$$

The caloric output determined by integrating the exothermic peak was 88 K. Cal/gm atom of Li which is in reasonable agreement with the literature value. In all these experiments, the weight of Li used was very small, viz, 0.0008 gm or less and errors in the Li weight may lead to the above deviations of the experimental values from the literature values.

taking a small piece of Li in a Kovar tube which was then cooled in liquid $\rm N_2$ and $\rm SO_2$ was condensed in the tube which was then sealed by welding. This sealed tube was placed in the crucible shown in Fig. 1 and DTA run was taken. A typical thermogram is shown in Fig. 7. The endotherm at 190°C corresponding to the melting of Li indicated that the sensitivity of the system was not altered significantly by the use of the Kovar tube. The thermogram is very striking in that there was no exothermic transition below 320°C, the highest temperature used, indicating the absence of chemical reaction between molten Li and liquid $\rm SO_2$. The runs were repeated with new samples and the above results were confirmed. Also, the Kovar tubes were opened at the end of the run and the presence of unreacted Li and liquid $\rm SO_2$ was confirmed. The results demonstrate the exceptional chemical stability of Li towards $\rm SO_2$. The film is sufficiently protective even when the Li is in a molten state, thus indicating continuous regeneration of the film.

Li + AN: Li and AN were found to react exothermically at room temperature. For this reason, the DTA crucible (Fig. 1) was modified slightly to incorporate a septum top through which AN was injected and the DTA runs were started immediately after such injection. The exothermic reaction was accelerated at higher temperatures as shown in the thermogram in Fig. 8. AN was found to be one of the most reactive agents towards Li. We examined the kinetics of this heterogeneous reaction in some detail using the DTA. The results will be reported later.

 $\underline{\text{Li} + \text{PC}}$: PC was used as a co-solvent along with AN in $\underline{\text{Li}/\text{SO}_2}$ cells. Li was found to be quite inert in PC probably due to the formation of a protective film (12) of $\underline{\text{Li}_2\text{CO}_3}$. The thermogram shown in Fig. 9 indicate strong exothermic reactions at 270°C. In this respect, Li is more stable in SO₂ than in PC.

Li + PC + AN: AN and PC were mixed in equal volumes and injected through the septum of the crucible containing Li. The thermogram is shown in Fig. 10. The exothermic peak represents Li + AN reaction. Note that the temperature at which the exothermic reactions occurred was increased to 180°C from 80°C (Fig. 8). The results indicate the protective nature of PC. In similar runs with AN:PC volume rations of 95:5, the exothermic peaks occurred at 98°C. Thus, the extent of protection is dependent upon the concentration of PC. In this analysis, the relative stabilities of the various materials are judged by the temperature at which they react, the higher the temperature, the more stable the materials at ambient temperature.

 $\underline{\text{Li} + \text{SO}_2 + \text{AN} + \text{LiBr}}$: The SO₂, AN and LiBr mixture used represents an electrolyte for the Li/SO₂ battery having a pressure of one atmosphere and consists of approximately 40% SO₂, 40% AN, and 20% LiBr by weight. The thermogram is shown in Fig. 11. The exothermic transition occurring at 180° prior to the melting of Li most likely represent the Li + AN reactions. SO₂ acts as a protective agent for Li as did the PC above.

 $\underline{\text{Li} + \text{SO}_2} + \text{AN} + \text{AA} - \underline{\text{LiBr}}$: This mixture represents an electrolyte with acetic anhyolride (AA) as an additive for supressing the Li - AN reaction in the absence of SO₂. The thermogram is shown in Figure 12. The run demonstrates the feasibility

of using AA in the completed electrolytes in the presence of lithium. The reaction of Li + AN did not start until Tp = 125 °C.

The results indicate that the spontaneous reactions between Li and AN can be mixigated by the addition of either SO_2 . PC or AA. The use of a mixture of AN and PC or AN and AA as the organic co-solvent may thus be beneficial in preventing spontaneous exothermic reaction of Li and AN in a completely discharged Li/SO_2 cell which has SO_2 as the capacity limiting component. The efficacy of this approach will be reported later.

 $\frac{\text{Na}_2\text{S}_2\text{O}_4 + \text{C}:}{\text{to Li}_2\text{S}_2\text{O}_4}$ The thermogram of a mixture of $\text{Na}_2\text{S}_2\text{O}_4$ (analogous to $\text{Li}_2\text{S}_2\text{O}_4$) and carbon black was found to be similar to the thermogram of $\text{Na}_2\text{S}_2\text{O}_4$ alone as shown in Fig. 3, thus indicating the absence of any significant effect of carbon black.

Cathode Mix: The thermogram of the cathode mix consisting of carbon and Teflon did not show any transitions in the sealed crucible. However, the dried cathode mix obtained from a discharged Li/SO, cell, containing the cell discharge product. Li2S2C4, and the electrolyte salt, LiBr in addition to carbon and Teflon did. A thermogram of such a discharged cathode mix is shown in Fig. 13. The exothermic transition at 180°C is similar to that observed with dry $\mathrm{Na_2S_2O_4}$. The caloric output was approximately 13 Cal/gm of carbon mix. The thermogram of the cathode mix (from the same discharged cell) which was exposed to air is shown in Fig. 14. Note the additional exothermic peaks similar to those on the thermogram of as received $Na_2S_2O_4$ (Fig. 3). The caloric output was found to be 38 K Cal/qm of cathode mix. Another thermogram of the cathode mix from a cell which was discharged into reversal, so that the cell voltage was negative for approximately 10% of its normal capacity is shown in Fig. 15. The cathode mix was inadvertently exposed to air prior to the DTA run. The thermogram looked very similar to the previous one, except the caloric output was increased to 112 Cal/gm of the cathode mix. Thus, the behavior of the discharged cathode was very similar to the behavior of Na, S,O,. Moisture appeared to enhance the exothermic decomposition. The presence of Li in the discharged cathode (from the cell reversal) enhanced the heat output of the decomposition reactions. Carbon and Teflon did not appear to have any significant effect.

 $\text{Li} + \text{Na}_2\text{S}_2\text{O}_4 + \text{C}$: The thermogram of a physical mixture of

powdered Li, powdered $\mathrm{Na_2S_2O_4}$ and carbon black (simulating a cathode mix of a $\mathrm{Li/SO_2}$ cell which was in reversal) is shown in Fig. 16. Note that the thermogram is very similar to that in Fig. 15, except for the endotherm corresponding to Li melting. The slight differences in the temperature at which the two major exotherms occured are most likely due to the differences in the size of the sample. We found that the exothermic transitions occur at high temperatures for the smaller samples. The first peak at 198°C most likely represents the decomposition of $\mathrm{Na_2S_2O_4}$ (Figs. 3, 13) and the second strong peak at 290°C most likely represents the reaction between Li and the decomposition products of $\mathrm{Na_2S_2O_4}$ such as S and $\mathrm{Na_2SO_3}$ according to reaction [6] or [7]. The striking similarity of the thermograms shown in Figs. 15 and 16, indirectly supports the assumed similarity of $\mathrm{Na_2S_2O_4}$ and $\mathrm{Li_2S_2O_4}$ insofar as their thermochemical characteristics are concerned.

 $\underline{\text{Li} + S:}$ The thermogram, shown in Fig. 17, indicates a very strong exotherm after the melting of two forms of sulfur, corresponding to the exothermic formation of Li_2S according to,

The similarity of the strong exotherm to that observed in the thermogram of Li-Na $_2$ S $_2$ O $_4$ (in Fig. 16) suggests that the latter was due to Li + S reactions. The higher temperature of the strong exotherm in Fig. 16, is most likely due to the poor physical distributions of the trace amounts of S (formed as a result of the decomposition of Na $_2$ S $_2$ O $_4$) which may have to be in a vapor form to react with the molten Li in view of the trace amounts of S involved. The Li + S thermogram was about the same when powdered Li was used instead of Li foil.

 $\underline{\text{Li} + \text{S} + \text{Na}_2 \text{S}_2 \text{O}_4}$: The thermogram which is shown in Fig. 18, shows the melting of sulfur followed by the very sharp strong exotherm at 164°C of the Li + S reaction. The usual $\text{Na}_2 \text{S}_2 \text{O}_4$ decomposition exotherm did not follow the usual pattern indicating that the decomposition was initiated by the great heat generated by the Li + S reaction. At Tp = 264°C, a small endotherm occurred which is probably the result of the melting of a reaction product.

 $\underline{\text{Li} + \text{Li}_2 \text{SO}_3}$: $\underline{\text{Li}_2 \text{SO}_3}$ may be a product of decomposition of $\underline{\text{Li}_2 \text{S}_2 \text{O}_4}$ according to reaction [6]. The thermogram of as-received $\underline{\text{Li}_2 \text{SO}_3}$ is shown in Fig. 19. They are strong exothermic reactions prior to the melting of Li. However, with dehydrated $\underline{\text{Li}_2 \text{SO}_3}$, the thermogram of $\underline{\text{Li}} + \underline{\text{Li}_2 \text{SO}_3}$ showed only the endothermic transition due to the melting of Li, but no exothermic transition. This demonstrates the important effect of moisture (as impurity) in the various cell components on the thermal characteristics of the cell constituents.

Li + Al: Expanded Al was used as a current collector for the carbon cathode. During cell reversal, Li deposition may occur on Al and spontaneous alloying (13) may ensue leading to the formation of LiAl. The thermogram shown in Fig. 20 indicates a strong exothermic reaction at the melting point of Li corresponding to the formation of Li-Al alloys. The two endotherms at higher temperatures correspond to the melting of two types of Li-rich alloys of Al. On cooling mode, three exotherms correspond to the freezing of the above two alloys and the excess Li. X-ray diffraction of the products indicated the presence of LigAl₄ and LiAl which remained in a solid state during the DTA run since the melting point (718°C) is much higher than the upper temperature limit of the DTA run. DTA runs with excess Al also had similar characteristics as shown in Fig. 20, except that there were no exotherm corresponding to Li freezing during cooling.

LiAl + AN: LiAl alloy prepared with excess Al was used for this run. The thermogram is shown in Fig. 21. The strong exotherm at 154°C represents the Li and AN reaction since DTA runs with Al + AN showed no significant reactivity. A comparison of the thermograms in Fig. 21 with the Li + AN thermogram in Fig. 8 shows that the reactivity as judged by the temperature of the exotherm is significantly reduced by the alloying of Li with Al. With pure Li (Fig. 8) AN reacted vigorously even at room temperature, whereas with the LiAl alloy, the reaction started at 154°C.

LiAl + S: LiAl alloy prepared with excess Al was used for this run. The alloy had 27% Li by weight and no free lithium remained in the alloy. The DTA thermogram for LiAl + S is shown in Figure 22 and it should be compared to Fig. 16, the Li + S thermogram. LiAl + S had a slow two peak reaction exotherm, over a

broad program temperature range as opposed to Li + S which reacted very strongly and rapidly. Also of interest was the fact that the reaction of LiAl + S did not initiate until Tp = 204°C, as opposed to 160°C for the Li + S reaction. This information augmented by the similar behavior of the LiAl + AN reaction discussed above, demonstrates that alloyed lithium is safer to use than the pure metal.

 $\underline{Al+S}$: Also in Figure 22 in a DTA run related to the above, it was shown that no reaction occured between aluminum and sulfur up to 470 °C. This demonstrates that the exotherms observed in the LiAl + S thermogram were from the reaction of alloyed lithium plus sulfur.

 $\underline{\text{LiAl} + \text{SO}}_2$: The thermogram showed no exothermic transitions up to 470°C, only endothermic transitions corresponding to the melting of lithium-rich alloys.

LiAl + AN + SO₂: AN and SO₂ were used in the volume ratio of 75:25. The thermogram is shown in Fig. 23. The major exothermic peak corresponding to the Li + AN reaction occurred at $420\,^{\circ}$ C, instead of occurring at $180\,^{\circ}$ C, as in the case of pure Li (Fig. 11). Furthermore, addition of SO₂ increased the temperature of the exotherm from $154\,^{\circ}$ C as in the case of LiAl + AN (Fig. 21) to $420\,^{\circ}$ C. Thus, the reactivity of the most reactive components of the Li/SO₂ batters viz Li and AN can be reduced by both the addition of SO₂ (film forming agent) and the alloying of Li and there appears to be a significant synergism when both are used together.

In addition to the above, DTA of other mixtures of various chemicals that may be formed in Li/SO₂ cells, were carried out and the results are summarized in Table 2. The DTA of Li with some organic solvents other than AN and with mixtures of AN and other solvents were carried out in an effort to find alternate less reactive solvents or solvent mixtures. DME (dimethox; "hane) appears to be a good substitute for AN. However, the performance characteristics of cells with this solvent and other prospective solvent mixtures, need to be established in order to determine the tradeoffs between cell performance and safety.

Conclusions:

DTA has been found to be an effective tool in the identification of the cell constituents responsible for the thermal runaway of the Li/SO₂ cells. The method was also useful in the development of approaches to deactivate the above active cell constituents. The specific conclusions from the DTA studies are listed below.

- 1. The cell discharge product $\text{Li}_2\text{S}_2\text{O}_4$ and analogous $\text{Na}_2\text{S}_2\text{O}_4$ undergo exothermic decomposition producing S as one of the products.
- 2. The presence of Li in a discharged cathode containing $\text{Li}_2\text{S}_2\text{O}_4$ leads to a stronger exothermic reaction most likely due to the exothermic reaction of Li and S formed from the decomposition of $\text{Li}_2\text{S}_2\text{O}_4$.
- 3. Moisture in the cell parts particularly in the cathode may lead to the production of additional heat due to its exothermic reaction with $\text{Li}_2\text{S}_2\text{O}_4$ and Li which is formed in the cathode during cell reversal.
- 4. Li and AN are the most reactive components of the Li/SO $_2$ cells, from the standpoint of internal heat generation at ambient temperatures.
- 5. Li and ${\rm SO}_2$ are extremely inert even at temperatures as high as 320 °C . This unexpected stability has been attributed to the formation of a protective film on Li.
- 6. PC is less reactive to Li than AN and the reactions of PC and AN mixtures is dependent upon the concentration of PC in the mixture.
- 7. Li alloys with Al exothermically near the melting point of Li producing primarily LiAl.
- 8. The reactivity of alloyed lithium with AN or with sulfur is significantly less than that of pure lithium.
- 9. The alloying of Li (to form LiAl) and the addition of SO_2 both reduce the reactivity of Li towards AN, but when used together, there is a synergistic effect which reduces the reactivity of Li towards AN to such an extent that the reaction occurred at $420\,^{\circ}\text{C}$ instead of at $150\,^{\circ}\text{C}$.
- 10. The above DTA results indicate that the following approaches may be useful in improving the abuse resistance of Li/SO_2 cells.
 - (a) Use of excess SO_2 in the cell to ensure its presence at all stages of use, storage and abuse.
 - (b) Use of mixtures of AN + PC instead of pure AN.
 - (c) Use of alternate solvents instead of AN and mixtures of solvents.
 - (d) Control of moisture levels in the cell components.

3. DTA of Spirally Wound Li/SO₂ Miniature Cell

We augmented the DTA studies of the cell constituents by DTA sutides on actual ${\rm Li/SO}_2$ cells. We chose to use a miniature spirally wound ${\rm Li/SO}_2$ cell instead of the LO26 cells (D size). The design of the miniature cell was such that it reflected the behavior of the larger D size cell insofar as the heat generation characteristics are concerned. The purpose of these DTA studies are to determine the heat generation characteristics of the actual ${\rm Li/SO}_2$ cells and compare them with the behavior predicted from the DTA studies of the cell constituents as well as to determine the effect of some of the cell design variables on the heat generation characteristics of the ${\rm Li/SO}_2$ cells. The cell design variables studies were: separator material (porous polyethylene and glass) electrolyte salt (LiBr and ${\rm LiAsF}_6$) and organic solvent (AN and PC + AN). The experimental details and the results are presented here.

Experimental

(a) Miniature Li/SO₂ Cell: The cross sectional view of the miniature cells is shown in Figure 24. The cell was made in a nickel plated cold rolled steel can, 0.302 inch diameter and approximately 1.5 inch high. The cell top consists of a G/M seal having a tantalum tube feed through which serves both as the positive terminal and as electrolyte fill port. The G/M seal was welded to the cell can. The cell bottom has a thermocouple well for the measurement of internal temperature. The cell was made with spirally wound electrodes: 1.2 ince x 1.3 inch x 0.012 inch cathode; 1.2 inch x 1.4 inch x 0.005 inch Li anode. The carbon cathode had expanded aluminum current collector but the Li anode did not have any current collector. The cells were filled with electrolyte having 70% SO₂ by weight. The fill tube was welded shut after the cell filling. The cells were made with the following variables:

Separator: porous polypropylene, (celgard) (standard)

glass filter paper.

Electrolyte Salt: LiBr (standard)

LiAsF₆

Organic Solvent: AN (standard)

PC + AN (1:1)

(b) <u>DTA Fixture</u>: A cross sectional view of the DTA fixture is shown in Fig. 25. It consists of an aluminum heating block having two cavities for the reference and the sample miniature cells. The differential thermocouples are inserted into the thermocouple wells (of the cells) by means of heat transfer compounds. The heating elements were wrapped around the aluminum black which was insulated all around by means of fiber glass. The heating block itself served as the negative terminal of the sample cell and the positive terminal was carefully insulated from the aluminum heating block. The DTA runs consisted of heating the aluminum block at a fixed rate from room temperature to a maximum of 250 °C and monitoring both the block temperature as well as the differential temperature on a strip chart recorder. The open circuit voltages of the cells were also monitored during the DTA run. In some experiments the differential temperature of the cell was monitored during discharge, reversal and charging of a cell.

Results and Discussion

The miniature cell was designed to reflect the thermal characteristics of the larger LO26S (D size) cells with the exception that the potential explosive energies involved would be substantially lower and hence less destructive of the available DTA fixtures. The electrochemical heat evolved per unit volume, as measured by the current density (i), over voltage (\P) and the cell volume, turned out to be 9.1 (i \P)_L watts/cm³ for the LO26S cells and 11.5 (i \P)_S watts/cm³ for the miniature cell. Thus, if the cells are discharged at comparable current densities where they would experience comparable overvoltages, the heat evolution per unit volume would be approximately the same for the two cells and so would their thermal excursions under adiabatic conditions.

The miniature cells delivered 227 mA.Hr at 1mA and 180, 210, 180 and 180 mA.Hr at 10 mA when discharged at 25°C. At -30°C, the cells delivered 90, 83 and 97 mA.Hr at 90 mA to a cutoff voltage of 2.0 volts. 90 mA current for the miniature cell corresponds to approximately 2A for the LO26S cells, in terms of equivalent current density.

DTA runs with two empty cell cans and with two cell cans filled with ${\rm Al}_2{\rm O}_3$ showed no transitions as expected. DTA runs with two fresh cells also showed no transitions. Cell cans filled with ${\rm Al}_2{\rm O}_3$ were chosen as a reference for all further DTA runs.

Altogether four different types of cells were tested. These will be referred to as (a) standard cells, (b) cells with PC (propylene carbonate), (c) cells with glass filter paper separator, and (d) cells with ${\rm LiAsF}_6$ electrolyte salt.

Almost all the DTA experiments were done in triplicate and the results were found to be quite reproducible.

(a) Standard Cells: The standard cells contained 0.005 inch thick Li anode, 70% SO₂ + 7% AN (acetonitrile) + 23% LiBr electrolyte and porous polypropylene (celgard) separator. The stoichiometric ratio of Li:SO₂ was approximately 1:1.3 based on the cell reaction

The cells were discharged at currents of 1, 10 and 90 mA at 25 °C and then these were subjected to DTA runs by heating from 25 °C to 170 °C. The differential thermocouple showed one small exothermic transition starting at temperatures of 150 °C. A typical thermogram is shown in Fig. 26. There was no significant effect of the discharge current on the size of this exotherm, although the exothermic transition was somewhat smaller for a partially discharged cell. The exothermic transition is attributed to the exothermic decomposition of the discharge product $\text{Li}_2\text{S}_2\text{O}_4$. However the upper limit of the temperature of the DTA run was too low for most of the other exothermic reaction. The sharp lowering of the open circuit voltage of the cell at temperatures of 140 °C was

probably due to the formation of shorts in the cell after melting of the polypropylene separator.

Miniature cells were force-discharged to reversal at 25° and -30°C in triplicate. One typical plot of the cell voltage, differential temperature and the aluminum block temperature during the cell discharge is shown in Fig. 27. The differential temperature increased sharply at the point of the cell polarization. The block temperature was increased only slightly. The cell was at reversal for only 0.75 hr corresponding to a capacity of 67.5 mA.Hr. There was no cell venting or explosion. The cell was then subjected to a DTA run. The thermogram, as shown in Fig. 28, has two strong exothermic peaks very similar to those observed in thermograms of mixtures of powdered Li and $\mathrm{Na_2S_2O_4}$ (analogous to $\mathrm{Li_2S_2O_4}$) . The first exotherm was attributed to the decomposition of $\text{Li}_2\text{S}_2\text{O}_4$ to produce S and the second one was most likely due to the Li + S reaction. Li + AN reaction may also occur simultaneously in view of the lower concentration of SO2. The similarity of the thermograms of actual cells with that of the synthetic mixtures of chemicals, done earlier, supports our conclusions regarding the identification of chemicals responsible for thermal runaway of Li/SO, cells. In the cell, Li,S,O, is formed during discharge and Li is formed during the reversal in the cathode. The presence of Li enhanced the exothermic caloric output of $\operatorname{Li}_2\operatorname{S}_2\operatorname{O}_4$ as observed earlier in DTA experiments with cathodes as well as in synthetic mixtures. A second DTA run (Fig. 29) with the same cell showed virtually no exothermic transition indicating that the active constituents (Li and $\text{Li}_2\text{S}_2\text{O}_4$) had reacted almost completely during the first DTA run, similar to our observations on Li/SOCl2 cells (14) .

The intensity of the exothermic transitions of the cells which were reversed appeared to be independent of the temperature at which the reversal occurred but dependent on the extent of reversal. Prolonged reversal produces more Li in the cathode than a short reversal and this leads to the increased caloric output as observed in the thermograms of mixtures of Li $+ Na_2S_2O_4$.

Miniature cells were also charged at 90 mA for 7 hours without any cell explosion. The DTA thermogram of the charged cell is shown in Fig. 30. Note that there is a small endotherm at $180\,^{\circ}\text{C}$ most likely indicating the melting of Li. The strong exotherm above $200\,^{\circ}\text{C}$ indicate the Li + AN reaction in the presence of excess SO_2 which protects Li from reaction with AN at a lower temperature. Since, the cell was not discharged, there was no strong exotherms corresponding to the decomposition of $\text{Li}_2S_2O_4$, although some $\text{Li}_2S_2O_4$ may have formed by chemical reaction with the dendritic Li formed on the anode during charging. Again, the thermograms of the cells appeared to be interpretable based on the DTA results of the individual chemicals. A repeat DTA run of the above cell showed considerably reduced exothermic transitions indicating the consumption of the active materials during the first run.

Cells with PC: These cells have the same size electrodes as the standard cells, only the electrolyte consists of 70% SO_2 + 23% mixture of AN and PC (3:1) + 7% LiBr. The thermogram of a discharged cell, as shown in Fig. 31 was found to be identical to that of the standard cell. Note that the upper limit of the temperature was only 170°C. The voltage and the differential temperature profile during discharge and reversal at 25 °C at 90 mA for 3 hours as shown in Fig. 32 also are very similar to those of the standard cell. However the DTA thermogram of the above reversed cell, as shown in Fig. 33, is interesting. Note that the upper limit of the temperature was 250°C. It shows three exothermic transitions prior to a very sharp exotherm occurring during the cooling cycle of the DTA. The repeat DTA run (Fig. 34) shows no significant exotherms. The thermogram of another cell force discharged at -30 °C for 3 hours at 90 mA, is shown in Fig. 35. Note that it shows only the three exothermic peaks. But on the repeat run, the fourth strong exothermic peak appears as shown in Fig. 36. The above experiment was repeated and the DTA thermograms were found to be identical to the above. We believe that the three peaks are due to the following three reactions, viz Li + AN, decomposition of Li2S2O4 and Li + PC. The fourth sharp peak in Fig. 33 is most likely due to the Li + S reaction. We found earlier that Li + S reaction produced the sharpest exothermic transitions indicating a very fast reaction.

All the DTA experiments were carried out at least one day after the discharge and reversal of the cells; thus the exothermic transitions reflect reactions of relatively stable species and not transient species.

(c) Cells with Glass Filter Paper Separator: These cells are similar to the standard cells in every respect except the separator is made of glass filter paper. The thermogram of a fresh cell heated to 170°C is shown in Fig. 37. Note that the OCV remained unchanged during the run indicating the absence of shorting that occurred in cells with celgard separator which melts at approximately 140°C causing shorting. Also, there was no significant transitions as expected. The thermogram of a completely discharged cell, as shown in Fig. 38, showed a small exotherm very similar to that of the standard cells, most likely because the upper limit of the temperature was 170°C. Note also that the OCV of the cell did not drop to zero; indicating lack of cell shorting. The repeat run did not show any transition as before.

The DTA thermogram of a cell which was force-discharged at -30°C at 90 mA showed only a small exotherm (as shown in Fig. 39) when the upper limit of the DTA run was kept at 170°C. However, when the upper limit of the DTA temperature was increased to 250°C of a similarly force-discharged cell, stronger exothermic transitions were observed again (Fig. 40) very similar to those of the standard cells.

The efficacy of the glass separator in preventing cell shorting at elevated temperatures is demonstrated from the above experiments. However, the exothermic reactions at $150\,^{\circ}\text{C}$ is not thus preventable, as expected.

(d) Cells with LiAsF $_6$ Electrolyte Salt: These cells are identical to the standard cells except the electrolyte salt is LiAsF $_6$ instead of LiBr. The electrolyte consisted of 70% SO $_2$ + 21% AN + 9% LiAsF $_6$. The thermogram of a fresh cell is shown in Fig. 41. The open circuit voltage of the cell curiously increased above 132°C from 2.95 volt to 3.66 volt. We found this phenomenon to be quite reproducible. There is a small exotherm in the thermogram corresponding to this increase in OCV. Our earlier DTA studies were incomplete insofar as this electrolyte salt is concerned and as such the reason for this increased OCV is not quite clear. The thermogram showed an endotherm corresponding to the melting of Li. Curiously, the cell did not short in spite of the fact that the cell temperature exceeded the melting point of the celgard separator. It is possible

that the electrode assembly was not tight enough to create a short when the separator melted. The thermogram then showed a sharp exothermic transition corresponding to the shorting of the cell as indicated by the sudden drop of OCV. This cell did not explode at this point although another cell did in a subsequent run. A repeat run of the same cell showed no significant transitions as shown in Fig. 42, indicating complete decomposition of any electrochemically and thermally active materials including $\operatorname{Li}_2S_2O_4$ formed during shorting. The temperature of the cell must have been high enough to complete all the thermally active processes discussed earlier.

The thermograms of discharged cells showed relatively smaller exotherms (Fig. 43) compared to those of a force-discharged cell (Fig. 44) as observed earlier with the standard cells. The thermogram of a charged cell (Fig. 45) was similar to that of a fresh cell with the exception that the OCV was higher initially (3.44 volts) and it was reduced to 2.85 volts prior to shorting which resulted in a very large exotherm corresponding to both electrochemical and chemical heats. Note that the cell shorting occurred after the lithium melting as indicated by the small endotherm prior to the sharp drop of OCV. Repeat run showed no transitions as before.

The above results demonstrate the applicability of the cell DTA technique, in resolving the chemical processes occurring in cells during thermal excursions, and this method, in conjunction with the DTA of cell constituents, provides a useful tool for studying the thermal runaway processes of Li/SO_2 and other cells.

Conclusions

The differential thermal analysis (DTA) of miniature ${\rm Li/SO_2}$ cells was found to be a useful tool in elucidating the chemical processes that occur in a cell during thermal excursions, as in thermal runaways. The DTA data of cell constituents were particularly useful for the identification of the various processes occurring in the cell by comparing the nature of the transitions of the cell with those of synthetic mixtures of cell constituents. The effect of the cell construction variables such as glass filter paper separator on the DTA thermograms of the

miniature cells was found to be predictable in most cases based on the DTA data of the cell constituents. The major reactions which contribute to the thermal runaway processes are the Li-organic solvent reaction and the decomposition of $\text{Li}_2\text{S}_2\text{O}_4$ as well as the Li + S reaction, where S was produced from $\text{Li}_2\text{S}_2\text{O}_4$. The cell reversal results in stronger exothermic transitions due to the formation of Li in the cathode containing $\text{Li}_2\text{S}_2\text{O}_4$.

4. Kinetics of Lithium-Organic Solvent Exothermic Reactions

From the DTA studies we have shown that the reactions most likely to initiate a thermal runaway are the Li-organic solvent reactions, particularly the exothermic Li-acetonitrile reaction which occurs at room temperature. For this reason, we chose to concentrate on the study of the kinetics of this reaction in an effort to find ways and means of quenching it. We also carried out kinetic study of several other organic solvents in an effort to find suitable candidates for replacing acetonitrile in the electrolyte of the Li/SO₂ cells or adding to it, if possible. The extent of the reaction is proportional to the heat evolved and the rate of the reactions is proportional to the rate of the heat evolution at a constant temperature and at a constant surface area of the Li. Therefore, an isothermal DTA technique was used to study these reactions. The experimental details and the results are reported here.

Experimental:

The Mettler TA2000 Differential Thermal Analysis System with the high pressure hermetic crucibles described earlier, was used for the isothermal DTA runs. A 0.098 inch diameter piece of 0.005 inch thick Li foil weighing 0.00029 gm was placed in the DTA sample crucible in an argon filled dry box. 20 microliters of the appropriate organic solvent was injected into the crucible and the crucible sealed. The Li disc size, weight and the location inside the sample container as well as the volume of the organic solvent were kept as constant as possible from run to run. The mixtures were then heated very quickly to various temperatures in the DTA furnace and maintained at those temperatures while the differential temperatures were recorded as a function of time yielding isothermal DTA thermograms at the various temperatures.

All the organic solvents used were of the highest purity available from Eastman Kodak and were used as received except for PC which was vacuum distilled over Li foil prior to use.BL, DME and MF were monodistilled.

The Li foils were used as received from the Foote Mineral Co. and contained 1% Na as impurity. The foils were shiny in appearance and all the

experiments were carried out using freshly punched Li from one roll except for some preliminary experiments with AN for which the Li discs were punched several days prior to the experiments. Although the Li foil was shiny in appearance it is reasonable to assume that it has a thin protective film and the freshly punched areas of the discs are probably most active towards the organic solvents. Therefore, the duration between the punching of a Li disc and the isothermal run was kept constant from run to run in order to reduce any variation of the activity of the Li surface from run to run.

Results and Discussion:

Some typical isothermal DTA thermograms at various temperatures for the Li + AN system are shown in Fig. 46. It can be shown that the slopes of the rising portion of the DTA thermogram at the point of inflection of the temperature-time curve can be expressed as

$$\frac{d \Delta T}{dt} = k \left(\frac{\Delta H}{L + S} \right)$$

where $\triangle H$ = heat of the reaction

k = zeroth order rate constant

L = heat capacity of reaction mixture

S = heat capacity of container

when the DTA furnace is maintained at a constant temperature and the chemical reaction obeys zeroth order kinetics.

Since \triangle H, L and S are constants, the slope is proportional to the rate constant of the Li + solvent reaction which is controlled by the reaction temperature and the surface area of the Li disc which were kept constant for all the runs.

An Arrhenius plot of the above slopes as a function of the reaction temperature for the Li + AN system with Li discs cut several days prior to the experiment is shown in Fig. 47. The plot is linear and the energy of activation, as determined from the least square slope (excluding the point at the lowest temperature) was 13 K.cal mole⁻¹ with a frequency factor of 8. A similar plot

of the same system with freshly cut Li discs as shown in Fig. 44 was also linear and had a higher reaction rate and a slightly lower activation energy; 10 K.cal mole⁻¹. This probably reflects the effect of the Li film (formed during storage in the dry box) on the kinetics of the Li + AN reaction.

The effect of LiBr on the kinetics of the Li + AN reaction was studied and the Arrhenius plot is also shown in Fig. 47. The activation energy of the reaction was reduced further to 6 K.cal mole⁻¹ possibly indicating the catalytic effect of Li + (15) on the Li + AN reaction.

Although PC was found to be rather inert towards Li at room temperature, it reacted with Li at higher temperatures. The energy of activation as determined from the linear Arrhenius plot, shown in Fig. 48, was $22 \text{ K.cal mole}^{-1}$.

The effect of addition of PC on the Li and AN reactivity was studied. The results are shown in Fig. 48. The addition of PC, up to 20%, resulted in a lowering of the reaction rates without altering the energy of activation significantly. This probably indicates that the Li + AN reaction is occurring through a film which only lowers the reaction rates without altering the activation energy. PC is known (12) to form an insoluble film of Li_2CO_3 on Li thus protecting it from further attack. With 50% PC, the reaction rates were reduced drastically, and the Arrhenius plots showed two linear regions corresponding to activation energies of 22 and 113 K.cal mole $^{-1}$ for the lower and the upper region respectively. In this mixture, the reaction temperatures are very high and as such complex reactions may occur to give rise to this type of behavior.

The addition of small amounts of SO_2 (3%) to the AN resulted in a sharp reduction of the reaction rates as shown in Fig. 48, without altering the energy of activation. This demonstrates the excellent film forming ability of small amounts of SO_2 and its efficacy in reducing the Li + AN reactivity, the key element in the safety of the Li/ SO_2 cells.

The kinetics of the Li + AN/BL system were studied and the results are shown in Figure 49. The Arrhenius plot for the Li + BL reaction had two straight line segments as shown in Figure 49. As in the case with PC, the very high reaction temperatures may be expected to cause some complex reactions to occur in the reaction of Li + BL. The lower temperature, steeper segment is the more significant portion of the Li + BL reaction and the data show that BL is more reactive than PC with lithium at the temperatures of interest. The steeper portion of the Li + BL Arrhenius plot had a higher activation energy but also a higher frequency factor than the Li + PC reaction (items 4 and 18, Table 3).

Although BL was more reactive with lithium than PC, it was found to be as effective an additive as PC in reducing the Li + AN reactivity. The Arrhenius plots for Li + AN/BL (95/5) and Li + AN/PC (95/5) virtually coincide as seen in Table 3 (items 5 and 16). 5% BL or 5% PC in acetonitrile decrease the Li + AN reaction rate by nearly one order of magnitude.

When the concentration of BL in acetonitrile was increased from 5% to 20%, both the activation energy and the frequency factor were increased by 73%. At the lower temperatures of interest (50-100°C), 20% BL marginally reduced the Li + AN reaction rate compared to 5% BL.

Li was found to be stable in MF (methyl formate) at ambient temperature and reacted only at very high temperatures. Surprisingly, the reaction rates were found to be considerably lower than those of the Li + PC. Also the energy of activation, as determined from the Arrhenius plot shown in Fig. 50 was almost twice that of the Li + PC, viz 43K.cal mole⁻¹.

The effect of MF on the Li + AN reaction was studied. The reaction rates increased significantly with 5% MF present giving rise to a non-linear plot as shown in Fig. 50. At higher concentration of MF, the reaction was too rapid, particularly at the higher temperature, so that it was not possible to measure the rates by the isothermal DTA method. A substantial part of the reaction was completed during the heating period so that the slopes were not representative of the reaction rates. The Arrhenius plots with 20% MF were found to be meaningless as shown in Fig. 50. In a normal isothermal DTA run,

as shown in Fig. 51 (a), the first short peak represents the difference in temperature between the sample and the reference during the short heating period. Note that the differential temperature reached the base line before it shot up as a result of the exothermic reaction. Also the area under this major peak representing the heat released, is very similar for all the runs at various temperature for a particular system, indicating the correctness of our assumptions regarding reasonable adiabaticity. The abnormal isothermal runs with the Li + AN + MF system, is shown in Fig. 51 (b). Note that the differential temperature does not reach the base line after the first short peak (corresponding to the heating of the sample) prior to the reaction exotherm, indicating that the reaction was already initiated during the heating up period. Also the areas under these exothermic peaks are different from run to run. These results demonstrate the limitation of this technique which is applicable to only those heterogeneous reactions which have a sufficiently long induction period during which the samples may be heated without any substantial reactions. In systems such as Li + AN + MF, the induction periods are too short, most likely due to the increased solubility of the reaction products in the mixed solvents. Thus, although MF by itself is less reactive to Li, addition of it to AN increased the Li solvent reactivity to a greater extent than the reactivity with the individual solvents. The above results indicate that although pure MF may be used by itself in Li/SO₂ cells, the mixture of MF and AN may be deleterious from a safety standpoint. The reported (5) unsafe behavior of Li/SC2 cells with MF in the electrolyte may be due to the presence of other impurities which may act as cosolvent with MF to dissolve the protective lithium film.

The Li + DME (dimethoxyethane) reaction was found to be extremely slow at the moderate to high temperatures used in our studies. However, the reactivities of AN + DME mixtures to Li were examined successfully. The Arrhenius plots, shown in Fig. 52 were found to be linear. The reaction rates were increased significantly by the addition of DME to AN and the activation energies were reduced. The results again point to a solubilizing effect of the AN + DME mixed solvents towards the lithium film formed as a result of the Lisolvent reaction.

Similar runs with AN + DG (diglyme) and AN + THF (tetrahydrofuran) systems (Fig. 53) also showed enhanced reactivity.

The energy of activation and the frequency factors of all the above reactions are presented in Table 3.

Conclusions:

The isothermal DTA technique developed for studying the kinetics of the heterogeneous reactions involving Li and organic solvents at various temperatures provided an effective tool to assess the usefulness of solvent additives to the Li/SO_2 electrolyte in improving the safety of the Li/SO_2 cells. The results show that whereas SO_2 and PC are effective in reducing the Li + AN reactivity, organic solvents such as MF, DME, THF and DG enhance the Li + AN reactivity and are unsuitable electrolyte additives for safety, although these may be used in place of AN in the electrolyte.

5. Exotherm Initiation Temperature: Effect of Solvent Additives on the Li-Solvent Reactions

We have shown earlier that the exothermic reaction of Li and acetonitrile, (the reaction most responsible for initiating a thermal runaway) may be mitigated by the addition of other less reactive solvents. We have attempted to determine the optimum concentration of the additive solvent required for suppressing the Li-AN reaction. For this, we have phosen the exotherm initiation temperature (defined as the temperature at which the Li-solvent reaction exotherm starts) as a measure of the Li-solvent reactivity. The higher exotherm initiation temperature represents lower reactivity and vice a versa. We have determined the Li-solvent exotherm initiation temperature as a function of the organic solvent concentrations at a fixed heating rate using DTA. The purpose of these experiments is to select the specific organic solvent compositions which are promising for improving the safety of the Li/SO₂ cells.

Experimental

The Mettler TA2000 DTA system was used with the asual Nemonic crucibles. 20 μ l of the solvents of interest were run with the standard 0.00029 g Li discs at the 5.0°C/min heating rate. The resulting thermograms were interpreted as follows: The programmed temperature, T_p , was determined where the steepest slope of the Li-solvent reaction exotherm intersected the projected baseline. The exotherm initiation temperature was determined by subtracting the thermal lag of the sample crucible, ΔT_{LAG} , from the intersect temperature. Figure 54 shows the DTA thermogram at 5°C/min for two samples and the typical determination of the exotherm initiation temperature.

For the effort centering on the use of AN with an additive we generally used 5% (volume) additive and 95% AN. Promising solvent systems were studied in more detail by determining the exotherm initiation temperature at various additive concentrations.

A problem in data interpretation arose with the Li + AN/BL system as seen in the thermograms of Figure 55. For the run with AN/BL (99/1) there is only one exotherm initiation temperature as determined from the point of intersection of the base line and the slope for thermogram but for the run with AN/BL (92/8) there are two slopes leading to the points of intersections at 95.7°C or 114.7°C. We elected to plot the first slope because it is more realistic for the problem under consideration. This resulted in more scatter in the results for Li + AN/BL than was observed for the other three systems.

Results and Discussion:

We compiled a survey of the reactivity of lithium with various solvents and solvent mixtures, in order to determine the least reactive solvent mixtures. The more desirable solvent mixtures are unreactive with lithium at about 100°C or higher as determined by the described technique.

We investigated many chemicals encompassing a wide variety of organic functional groups including alcohol, aldehyde, ketone, acetate, anhydride, amide, amine, acid, carbonate, glycol and sulfoxide compounds and others. Table 4 lists the systems that were studied, in the order of ascending exotherm initiation temperatures with ternary solvents listed separately.

Item 1 in Table 4 shows that although Li + AN react at room temperature, the reaction is slow enough to give DTA exotherms up to 50°C in some cases. It is desirable to increase this exotherm initiation temperature range with appropriate solvent mixtures or additives.

Table 4 shows that the systems numbered 1-17, inclusively, has initiation temperatures below 50°C. They provided no reduction in the reactivity of lithium with acetonitrile. Item 18, acrylonitrile, an impurity of AN, had a negligible effect on the initiation temperature of the Li + AN reaction. Similarly, items 19 through 27 were only marginally beneficial. Items 28 through 37 gave a marked improvement over item 1, Li + AN. Of great interest in this group were PC, BL and acetic anhydride (AA). PC and BL have been studied before but AA has not. In the initial survey, AA appeared to be slightly more effective than PC or BL in decreasing the Li + AN reaction rate.

Methyl formate worked well as a reaction inhibiting solvent in 50/50 mixes with AN or PC or as an exclusive solvent. AN/MF (95/5) was not acceptable effective in limiting the Li + AN reaction, however, and this finding supported our kinetics studies on this mixture. We are cautioned in using MF as a solvent due to reports of methyl formate decomposing in cells to form methane gas which is flammable and would increase the internal pressure of the Li-SO₂ cells.

DME and other ethers were discussed in the previous section. A study of the exotherm initiation temperature verified our findings that lithium is very unreactive with ethers but ethers as additives to AN enhance the Li + AN reaction. In the ternary solution, AN/PC/DME (90/5/5), the Li + AN exotherm initiation temperature was increased to 104°C. This demonstrates that the tenacious protective film formed in the presence of PC is insoluble in DME. Ethers therefore may be useful in certain ternary solvents.

We have seen that PC decreased the reactivity of lithium in AN/PC/DME mixtures so we studied a few more ternary solvents in items 38 through 44. In items 38 and 39 we found that neither PC nor BL could protect Li adequately in AN and methanol (5%). Unlike DME or some other ethers we studied, methanol reacts with lithium. Apparently, solvent components which may be useful in improving the electrolyte conductivity should be selected from compounds which do not react readily with lithium. We also explored ternary mixtures using two of the three "protective" solvents (PC, BL, and AA) with AN. No beneficial synergistic effects were found and the systems behaved as if they contained only one "protective" solvent.

For the more promising solvent systems, we studied the initiation temperature as a function of the concentration of the additive solvents in solutions where AN was the principal solvent. The data for these investigations are presented in Figures 56 to 58.

In Figure 56 the data for the ternary solvent system AN/PC/DME are shown. The data indicates that the amount of PC present determines the exotherm initiation temperature. With PC held constant at 5% (vol.), the

exotherm initiation temperature for the Li + AN reaction was 98.4 ±5.3°C for DME concentrations of 1 to 20% (vol). With the DME held constant at 5%(vol) the exotherm initiation temperature for the Li + AN reaction rose rapidly with increasing PC concentration. With 8% to 28% (vol) PC the initiation temperature leveled off at better than 110°C.

We also studied the binary systems AN/PC and AN/AA and the data appear in Figure 57. The additive constituents, PC and AA were varied between 1% and 28% (vol) as before. Both sets of data mirrored the performance of the AN/PC/DME (5%) system. The scatter in the data was reasonable for all three of the above systems.

Finally, we studied the Li + AN/BL system. The exotherm initiation temperature for a given amount of BL was apparently less than with the other additives discussed, but there was great scatter with the BL additive as mentioned above. The exotherm initiation temperature of the Li + AN reaction as a function of BL concentration is shown in Figure 58. Despite the problems involving scatter, BL still proved to be an effective inhibitor of the Li + AN reaction.

To demonstrate the extent to which SC_2 in AN protects lithium we combined some assorted data to produce the curve of Figure 59. A rapid rise in the exotherm initiation temperature with SO_2 concentration in AN is demonstrated. Note that in a discharging cell the chance of initiating the Li + AN reaction increases as the SO_2 concentration decreases. When the SO_2 depletes to below about 5%, the Li could react with the AN solvent if the cell temperature was elevated to near 100° C through resistance heating during discharge. It is for this reason we wish to find a non-depleting additive to protect the lithium from reaction with the acetonitrile.

Conclusions:

The exotherm initiation temperature is a simple and revealing parameter for screening organic solvent systems for increasing safety. Our survey as shown in Table 4 revealed many solvent systems with the potential to improve the safety of Li-SO₂ cells, particularly by lessening the thermal runaway problem. We found that many improved solvent systems increased the exotherm initiation temperature of the Li + AN reaction from around room temperature to

around 100°C.

In studying the effect of additive concentration we found the maximal inhibition of the Li + AN reaction occurring at additive concentrations of about 8% to 28% for all the additives: PC, AA, BL and PC/DME (5%).

It has been demonstrated that some useful additives can effectively inhibit the reaction of lithium and acetonitrile. The solvents of most interest are PC, BL, AA, MF and DME.

We selected a series of organic solvent compositions based on the above studies for further screening based on the electrical conductivity of the finished electrolytes containing 70% SO₂ and LiBr.

6. Electrical Conductivity of the Prospective Electrolytes

The study of the exotherm initiation temperature revealed several electrolyte solvents and solvent mixtures which lessened the threat of thermal runaway in Li-SO₂ cells. To further evaluate the efficacy of these and other solvents of interest, SO₂ electrolytes were prepared and a study was made of the conductivities of the electrolytes at various temperatures. The purpose is to select a few specific electrolytes with conductivities similar to or superior to that of the standards. The experimental methods and the results are presented here.

Experimental:

Two conductivity cells were built as shown in Figure 60. The aluminum surfaces which were exposed to electrolyte were found to need a baked on protective teflon coating to prevent corrosion. Electrolytes 1A, 1B, 2 and 3 were run in a cell without the teflon and the conductivity results were unaffected. The parallel platinized platinum conductivity cell electrodes were protected by a pyrex tube as shown in the illustration. The platinum feedthrough wires were run through EPR septa for the screw-down external electrical connections. The septa retainer held the septa in place and insulated the feedthrough wires from the solutions of the constant temperature bath. The assembled cell employed an EPR O-ring inside of a 2-3/8" bolt circle.

The following procedures were used in the conductivity determinations. Pressurized SO₂ electrolytes were made up in 115 ml polypropylene cylinders fitted with polypropylene ball valves on each end and an additional 3-way stainless steel valve on one end. Vacuum dried LiBr and appropriate distilled solvents (except acetic anhydride) were introduced into the polypropylene electrolyte cylinder and SO₂ was condensed into the chilled cylinder through the three-way valve. An assembled cell was filled with argon and then connected to the electrolyte filling station via the fill valve. At the filling station the conductivity cells were evacuated to facilitate the introduction of electrolyte which was introduced through the fill valve. The filled cells were equilibrated at various temperatures between -40°C and 98°C. At thermal equilibrium, the solution resistances

were measured with a GenRad GS1657 Digibridge which applied a 1KHz test frequency (0.3V rms maximum) across the cell electrodes and the series equivalent circuit was used. Figures 61 through 71 show the conductivities of the various SO₂ electrolytes. In Figures 61 through 71 the Specific Conductance in millimhos/cm is plotted as a function of the electrolyte temperature in °C.

Results and Discussion:

The specific conductances of the electrolytes were determined from the equation

$$L_s = \frac{K}{R}$$

where

 $L_s = Specific conductance, \Omega^{-1}cm^{-1}$

K = The cell constant, cm⁻¹

R = Solution resistance, 1

To employ the above equation the cell constant, K, was determined for our two conductivity cells using several 0.1 Demai KCI solutions for which the specific conductance is known to great accuracy. Four measurements were made to determine each cell constant and the results were:

Cell #1:
$$K_1 = 0.2831 \pm 0.0021 \text{ cm}^{-1}$$

Cell #2: $K_2 = 0.09107 \pm 0.00090 \text{ cm}^{-1}$

In order to get a more meaningful comparison between electrolytes, we used consistent volume ratios of the electrolyte constituents. Therefore, during electrolyte preparation we used 6.0g LiBr (dried), 30.0 ml solvent, and about 72g ($\pm 5\%$) SO₂. The weight ratios of the finished electrolytes vary due to the different densities of the various solvents. In Table 5 is a list of the SO₂ electrolytes which were studied.

The plots of the specific conductance versus temperature for the electrolytes are shown in Figures 61 through 71. By visually comparing these graphs we were able to rank the electrolytes in order of decreasing conductivity as listed in Table 6 where the electrolytes are differentiated according to the solvents used. Acceptable conductivities were found for all but the last seven electrolytes on the list. Electrolyte 14 and those above it on Table 6 had conductivities that were as good as, or better than the standard electrolyte (AN solvent). We rated the conductivity of electrolyte 9 as marginal whereas its specific conductance plot fell within the band of values found for electrolyte 3A. Electrolyte 5 and those below it in Table 6 seemed to be clearly inferior to the standard electrolytes in conductivity. Some of the inferior electrolytes had good conductivities initially, but observations over a few days revealed a severe loss of conductivity. Electrolytes 4 and 7, as seen in Figures 63 and 66 respectively, suffered most severely in this respect.

We did not study the apparently stable electrolytes over prolonged time periods but there was a slight tendency for almost all of the electrolytes to lose conductivity while maintained above about 72°C. It seemed characteristic that a loss of conductivity was accompanied by the salting out of an unknown white precipitate. Such a precipitate was examined by KEVEX (SEM) and x-ray diffraction for electrolytes 3A and 4. The analyses revealed that similar compounds were salted out from electrolytes 4A and 8. The unknowns contained sulfur and bromine and were apparently single compounds.

In a cursory survey, one cannot be sure of the batch to batch differences which may be found for a given electrolyte composition but the comparison of standard electrolytes 3 and 3A (Figures 61 and 62) demonstrate the kind of variability which might be expected. Electrolyte 3A (Figure 62) initially had a slightly lower conductivity than electrolyte 3 above 15°C, and electrolyte 3A suffered a slight loss in conductivity with time. The last conductivities measured for electrolyte 3A were 25-30% lower than the conductivities of electrolyte 3 at the same temperatures.

Conclusions:

By determining the conductivity of the SO₂ electrolytes we were able to make a general assessment of their utility in actual cells by comparing their conductivities to the standard (type 3, 3A) electrolytes. Based on conductivity

alone, we find that the electrolytes at the top of Table 6 that are noted to have acceptable or marginal conductivities are candidates for further study.

7. Selection of Electrolytes for Improved Safety

The selection of electrolytes for further study is based on the information obtained in the preceding sections. In Section V we obtained information on solvent compositions which were relatively inactive in the presence of lithium. In Section VI we determined the conductivity of several SO₂ electrolytes of interest. The following electrolytes merit further study as candidates for improving the safety of Li-SO₂ cells.

1. LiBr in AN/PC (90/10):

We have shown that about 10% propylene carbonate is sufficient to protect lithium from the attack of acetonitrile. Although propylene carbonate leads to the voltage delay problem it is expected to be less severe with only 10% propylene carbonate in the solvent mixture. The conductivity of this electrolyte was the best of the candidates tested in Section VI.

2. LiBr in AN/AA (1)/10:

Acetic anhydride (AA) was discovered to protect lithium from acetonitrile. The thermogram for the Li + AN/AA (95/5) reaction is shown in Figure 54. Acetic anhydride has not been tested in actual Li-SO₂ cells, but our preliminary tests showed that the electrolyte with acetic anhydride was stable. The conductivity was measured for two of these electrolytes. One was found to be as good as An/PC (90/10) above and the second was about 15% poorer but still better than electrolytes with acetonitrile as the exclusive solvent.

3. <u>LiBr in AN/BL/DME (85/10/5):</u>

This ternary solvent mixture offered marked improvement in electrolyte conductivity compared to a similar electrolyte which lacked the dimethoxyethane. Other synergistic benefits may accrue from the use of ternary solvents in the ${\rm SO}_2$ electrolytes such as lessened voltage delay or improved protection of the lithium from the reaction with solvent.

4. LiBr in AN/MF (50/50):

In this electrolyte the acetonitrile was only 50% of the solvent mixture and the Li + AN reaction was significantly inhibited as measured by the exotherm initiation temperature (140°C). Because of its potential benefits we believe this electrolyte is worth studying in SO₂ cells despite the possible problems associated with the use of methyl formate.

5. LiBr in PC/DME (50/50):

This electrolyte which does not contain acetonitrile is expected to protect lithium from reacting with the solvent to temperatures above the melting point of lithium. The Li + PC exotherm initiation temperature was 244°C. The conductivity of this electrolyte was about the same as electrolytes with acetonitrile as the exclusive solvent. The severity of the voltage delay problem due to propylene carbonate is unknown for this electrolyte.

6. LiBr in BL/DME (50/50):

As above, this electrolyte does not contain acetonitrile and the lithium protection is therefore good. The Li + BL exotherm initiation temperature was 168°C. The conductivity of this electrolyte was about the same as standard electrolytes which use acetonitrile exclusively as the organic solvent. This electrolyte may have less problems with voltage delay than the similar electrolyte above with propylene carbonate.

The above list of electrolytes for improved safety in Li-SO_2 cells was culled from candidates which were examined in our DTA and conductivity studies. All of the selected electrolytes are expected to significantly decrease the possibility of lithium reacting with solvent in the cell while offering equivalent or superior conductivity as compared to standard Li-SO_2 cells with acetonitrile as the organic solvent.

In tests involving actual cells, electrolyte compositions other than the above may suggest themselves. For example improved performance or safety may result from the use of other component ratios or from the introduction of new components such as a different solute. The suggested electrolytes offer a

reasonable starting point for the study of actual Li-SC $_2$ cells designed for improved safety.

8. Conclusions and Recommendations

In our DTA work we studied the thermal stability of the various components of Li-SO₂ cells. We showed that Li reacts very slowly with SO₂ even in the molten state up to the maximum temperature (370°C) examined in this study. The excellent stability of lithium is due to the kinetic effect of the protective film on the lithium. The DTA results corroborate the observed excellent shelf life and the relative safety of the Li/SO₂ batteries under various conditions of use and abuse.

The cell discharge product, $\text{Li}_2\text{S}_2\text{C}_4$ was found to decompose exothermally producing S and as such could contribute in sustaining a thermal runaway (initiated by other means) but could not initiate one since the decomposition temperature is above 100°C .

The organic solvent AN was found to be the most reactive constituent of the cell. AN was found to react with unprotected lithium at around room temperature. The heat released from the Li + AN reaction is suspected to initiate other detrimental exothermic reactions in the Li-SO₂ cells.

The DTA results on the miniature Li/SC₂ cells corroborated our conclusions from the DTA of individual cell constituents and it was found to be a useful tool for studying the thermal runaway process.

The kinetic studies of the Li-organic solvent reactions were useful in determining the effectiveness of the organic solvent additive (to AN) in reducing the Li and AN reactivity for increased safety. The results show that the solvents MF, DME, DG and THF, although stable by themselves, were unsuitable as additives since they enhance the Li and AN reactivity; most likely due to an enhanced solubilizing effect of the mixed solvent on the Li film. PC was found to be a beneficial solvent in that respect.

We studied the lithium-solvent reaction for many combinations of organic solvents using the exotherm initiation temperature as a measure of the reactivity of lithium with the assorted solvents. We discovered a new solvent additive, acetic anhydride, to be effective in protecting lithium from reaction with acetronile. Also effective in the role of additives (small amounts) were propylene carbonate and Y -butyrolactone, two familiar non-aqueous electrolyte solvents. Of interest as major solvent constituents (without AN) were propylene carbonate, butyrolactone, methyl formate and the ethers discussed above.

The conductivity measurements of SO₂ electrolytes with prospective organic solvents showed that several of these electrolytes had conductivities equal to or better than the standard SO₂ electrolyte which used acetonitrile as the exclusive organic solvent. Based on both the DTA results and the conductivity studies we recommended six specific electrolyte systems for further evaluations in practical cells in order to determine the performance, storability and safety of the Li/SO₂ batteries using the above electrolytes. Two of these electrolytes contain no AN, the reactive component of the electrolyte. All of these recommended electrolytes possess equivalent or superior conductivity to that of the standard electrolyte containing AN.

9. References

- P. Bro, R. Holmes, N. Marincic and H. Taylor, Paper No. 45,
 Proc. Intl. Power Sources Symposium, Brighton, England, 1974.
- P. Bro, H. Y. Kang, C. Schlaikjer and H. Taylor, Tenth Intersociety Energy Conversion Engineering Conference, Newark, Delaware, p. 432 (1975).
- H. Taylor and B. McDonald, p. 66, Proc. 27th Power Sources
 Symposium, Atlantic City, 1976.
- 4. E. S. Brooks, p. 42 Proc. 26th Power Sources Symposium, Atlantic City, 1974.
- H. F. Hunger, and J. A. Christopulos, R&D Technical Report ECOM-4292, February 1975.
- A. N. Dey, Proc. 28th Power Sources Symposium, Atlantic City, 1978.
- W. Behne, G. Jander, and H. Hecht, Z. Anorg. Allegem. Chem. 269, 249 (1952).
- 8. P. Shah, p. 59, Proc. 27th Power Sources Symposium, Atlantic City, 1976.
- 9. G. DiMasi, p. 75, ibid.
- J. J. Helstrom and G. A. Atwood, Ind. Eng. Chem. Process Res. Dev.,
 16, 148 (1977).
- 11. D. D. Wagman, National Bureau of Standard, (Private Communication).
- 12. A. N. Dey, Thin Solid Films 43, 131 (1977).
- 13. A. N. Dey, J. Electrochem. Soc. <u>118</u>, 1547 (1971).

- 14. A. N. Dey, Paper No. 23, Proc. ECS Symp. on Design and Optimization, Pittsburg Meeting, October 1978.
- 15. A. Soffer and E. Yeager, Abstract No. 548, Proceedings ECS Meeting Seattle, May 1978.

TABLE 1

List of Possible Chemicals Present in ${\rm Li/SO_2}$ Batteries at the Various Stages and Types of Use and Abuse

(a)	Start	ing Materials		
	1.	Li	8.	Acrylonitrile
	2.	so ₂	9.	Acetamide
	3.	Carbon black	10.	Propylene
	4.	Teflon	11.	Li ₂ CO ₃
	5.	Aluminum	12.	Li ₃ N
	6.	Nickel plated cold rolled steel: Ni, Fe	13.	Li ₂ O
	7.	Polypropylene (c)	Chen	nicals Generated
	8.	LiBr	1.	Li ₂ SO ₄
	9.	Acetonitrile	2.	Br ₂
	10.	Propylene carbonate	3.	Li ₂ SO ₃
	11.	LiAsF ₆	4.	S
	12.	Methyl formate	5.	S2Br2
	13.	Other prospective organic solvents	6.	SOBr ₂
		such as THF, Y-BL, DME, Dioxolane, etc.	7.	Undefined polymers of AN, PC
	14.	Tantalum	8.	Li ₂ S ₂ O ₄
(b)	Poss	ible Impurities	9.	CH ₄
	1.	н ₂ о	10.	CS ₂
	2.	Mg	11.	H ₂ S
	3.	Na	12.	CO ₂
	4.	LiOH	13.	LiCN
	5.	Propylene glycol		
	6.	СН ₃ СООН		
	7.	Ni, Fe, Ta salts, heavy trace		

metals

TABLE 2

Summary of DTA Results of the Various Chemicals

And Their Combinations From Table 1; Heating Rate 5 °C/minute

	Chemicals Program Temperature of Transitions °C <u>Exothermic Endothermic</u>		
r.	Li		188
2.	Carbon		
3.	Celgard (Porous Polypropylene	e)	156
4.	Acetonitrile (AN)		
5.	Propylene Carbonate (PC)		- -
6.	Teflon powder	en rem unit unit unit en	245
7.	Sulfur		112, <u>120</u>
8.	Na ₂ S ₂ O ₄ (sodium dithionite)	91, 125, 211, 284	
9.	LiBr		sassuf C
10.	Li + Celgard	comulato an	152, 191
11.	Li + LiBr	124	<u>188</u>
12.	Li + Teflon powder	279	191
13.	Li + SO ₂	nos ru nt erra auctoripura	192
14.	Li + AN	<u>89, 149</u>	502 2.5
15.	Li + PC	<u>264</u> , 306	189
16.	Li + AN/PC (50:50)	<u>180</u> , 226	
17.	Li + AN/PC (95:5)	98	nni sidiangi (a-
18.	Li + SOZAN/LiBr (40:40:20)	<u>182</u> , 211	-
19.	Cathode mix from discharged cell	179	
20.	Above after exposure to air	64, <u>159</u> , <u>210</u>	
21.	Cathode mix from a reversed (force-discharged) cell	58, 177, <u>237</u>	
22.	Li + Carbon + Na ₂ S ₂ O ₄	198, <u>292</u>	184
23.	Li + S	160	110, 121
24.	Li + Li ₂ SO ₃ (as received)	126, <u>151</u> , 190	187
25.	Li + Li ₂ SO ₃ (dried)		189
26.	Li + Al	188	281, 346
27.	LiAl alloy + AN	<u>157</u> , 327	
28.	LiAl alloy + S	204, 298	
29.	Al + AN	 46	

TABLE 2 (continued)

	Chemicals	Program Temperature of T Exothermic	ransitions °C Endothermic
30.	Al + S		in west
31.	LiAl alloy + SO,		
32.	LiAl alloy + AN/SO ₂ (75:25)	424	345
33.	PC + Br	68, 150, 200, 247	
34.	Na ₂ S ₂ O ₄ + Br ₂	143,204	
35.	Br ₂ + AN/SO ₂ /LiBr (40:40:20)	119,173	
36.	CH ₄ + Br ₂	324	
37.	Li + CH		191
38.	Li + Diglyme	187,280,374	44 14 12 <u>-</u>
39.	Li + AN/PC (95:5)	103	stani) iš
40.	Li + AN/PC (80:20)	86,114,148,190	4.46 9.21 F
41.	Li + DME	432	188
42	Li + AN/DME (95:5)	<u>30</u>	CAR P. C. C.
43.	Li + AN/MF (95:5)	78	
44.	Li + AN/MF (80:20)	102	WE + 13
45.	Li + AN/MF (50:50)	148	-
46.	Li + AN/THF (95:5)	<u>34</u>	Mikada da 🚣
47.	Li + THF		188
48.	Li + MF	<u>184</u> , 318	73.413. 111 <u>.</u>
49.	Li + MF/PC (50:50)	184, 325	ya el tu
50.	Li + AN + Napthalene	<u>75</u>	
51.	Li + LiAs F ₆	282	190, <u>269</u>
52.	Li + LiAs F ₆ + AN	189	
53.	Li + S ₂ Br ₂	362,386,400	124 mili 122 <u>1.</u> 134 mili 13 mili

TABLE 3

The Activation Energy and the Frequency Factor of Various Li-Organic Solvent Heterogeneous Reactions Determined by Isothermal DTA Method.

	465	Activation Energy	
	Reactions	K.Cal Mole ⁻¹	Frequency Factor
1.	Li + AN	13.1 ± 0.5	8.3
2.	Li (freshly cut) + AN	10.3 ± 0.3	7.1
3.	Li + 0.32 M LiBr, AN	5.9 ± 0.6	4.3
4.	Li + PC	22.3 ± 3.2	9.8
5.	Li + AN/PC (95/5)	15.0 ± 0.6	8.8
6.	Li + AN/PC (80/20)	11.1 ± 0.6	6.6
7.	Li + AN/PC (50/50)	$\begin{cases} 21.7 \pm 2.5 \\ 112.9 \pm 22.6 \end{cases}$	10.8 56.8
8.	Li + AN/SO ₂ (97/3)	12.5 ± 2.1	7.0
9.	Li + MF	42.7 ± 5.2	16.7
10.	Li + AN/DME (95/5)	5.9 ± 0.5	3.9
11.	Li + AN/DME (80/20)	9.1 ± 0.9	6.4
12.	Li + AN/DG (95/5)	9.5 ± 0.3	6.6
13.	Li + AN/DG (80/20)	10.2 ± 0.6	7.2
14.	Li + AN/THF (95/5)	9.6 ± 0.8	6.6
15.	Li + AN/THF (80/20)	8.6 ± 1.0	6.2
16.	Li + AN/BL (95/5)	16.2 ± 1.1	9.4
17.	Li + AN/BL (80/20)	28.1 ± 2.8	16.3
18.	Li + BL	$\begin{cases} 13.5 \pm 1.3 \\ 65.6 \pm 7.8 \end{cases}$	6.9 32.1

TABLE 4

Solvent and Additive Search for System to Protect Lithium in SO Cells. DTA @ 5 °C/min. 0.00029g Li + $20\mu l$ of Indicated Solution.

ITEM NO.	SOLUTION	INITIATION TEMP.
1	AN	RT-50°C
2	AN/DME (95/5)	RT
3	AN/carbon tetrachloride (95/5)	RT
4	AN/diglyme (95/5)	25°C
5	AN/THF (95/5)	26
6	A N/bromobenzene (95/5)	33
7	AN/pyridine (95/5)	37
8	AN/allyl alcohol (95/5)	38
9	AN/diethylamine (95/5)	42
10	AN/diethyl carbonate (95/5)	42
11	AN/butyl acetate (95/5)	43
12	AN/acetamide (.0043 g/ml)	44
13	AN/Triton surfactant, .5%	45
14	AN/dioxolane (95/5)	46
15	AN/oleic acid (95/5)	47
16	AN/benzaldehyde (95/5)	47
17	AN/methanol (95/5)	49
18	AN/acrylonitrile (95/5)	52
19	AN/ethyl acetate (95/5)	55
20	AN/di-tert butyl dicarbonate	55
21	AN/N, N, -dimethyl formamide (95/5)	58
22	AN/acetone (95/5)	60
23	AN/methyl ethyl ketone (95/5)	62
24	AN/dimethyl sulfoxide (95/5)	63
25	AN/ethylene glycol (95/5)	64
26	AN/naphthalene (.015g/ml)	67

TABLE 4 (continued)

ITEM NO.	SOLUTION	INITIATION TEMP
27	AN/MF (95/5)	71
28	AN/PC (95/5)	96
29	AN/BL (95/5)	98
30	AN/acetic anhydride (95/5)	107
31	AN/BL (80/20)	130
32	AN/MF (50/50)	140
33	BL TALL THE PROPERTY OF THE PR	168
34	MF/PC (50/50)	171
35	MF .	173
36	PC	244
37	DME	425
38	AN/PC/methanol (86/9/5)	48
39	AN/BL/methanol (86/9/5)	63
40	AN/DME/acetic anhydride (90/5/5)	92
41	AN/PC/acetic anhydride (90/5/5)	101
42	AN/PC/DME (90/5/5)	104
43	AN/BL/acetic anhydride (90/5/5)	111
44	AN/PC/BL (90/5/5)	111

NOTE: PC, BL and dioxolane were distilled

TABLE 5
SO₂ ELECTROLYTE COMPOSITIONS FOR CONDUCTIVITY STUDY

Electrolyte #	Solut	e	Solvents (Solvent Ratio)	SO ₂
1A	LiBr	6.1%	AN 18.0%, AA 2.8% (90/10)	73.2%
1B	LiBr	5.8	AN 20.9, AA 3.2 (90/10)	70.1
2	LiBr	5.9	AN 20.8, PC 3.6 (90/10)	69.7
3	LiBr	6.3	AN 24.5	69.2
3A	LiBr	6.2	AN 24.3	69.5
4	LiBr	5.9	AN 21.0, BL 3.4 (90/10)	69.7
5	LiBr	5.2	PC 31.3	63.5
6	LiBr	5.7	THF 25.1	69.2
7	LiBr	5.7	AN 19.1, PC 3.5, DME 1.2 (85/10/5)	70.5
8	LiBr	5.7	DME 24.8	69.5
9	LiBr	5.3	BL 30.0	64.7
10	LiBr	5.3	MF 13.0, PC 16.1 (50/50)	65.6
11	LiBr	5.7	AN 11.1, MF 13.8 (50/50)	69.4
12	LiBr	5.7	AN 20.3, PC 1.7, BL 1.6 (90/5/5)	70.6
13	LiBr	5.4	PC 16.3, DME 11.7 (50/50)	66.7
14	LiBr	5.7	BL 16.1, DME 12.3 (50/50)	66.0
15	LiBr	5.8	AN 19.2, PC 3.5, MeOH 1.1 (85/10/5)	70.4
16	LiBr	5.7	AN 19.2, BL 3.2, DME 1.2 (85/10/5)	70.6

Electrolyte No.	Solvents	Notes
2	AN/PC (90/10)	0 W41
1 A	AN/AA (90/10)	.8 V81.1
15	AN/PC/MeOH (85/10/5)	4 400
16	AN/BL/DME (85/10/5)	Conductivity
11	AN/MF (50/50)	Acceptable
12	AN/PC/BL (90/5/5)	3 301
1B	AN/AA (90/10)	A SHE
13	PC/DME (50/50)	3 65
3	AN 2 Standard	
3 A	AN Selectrolyte	
14	BL/DME (50/50)	
9	BL	Marginal
5	PC	4
10	MF/PC (50/50)	Conductivity
7	AN/PC/DME (85/10/5)	Тоо
8	DME	Low
6	THF	0.0003
4	AN/BL (90/10)	2 0962

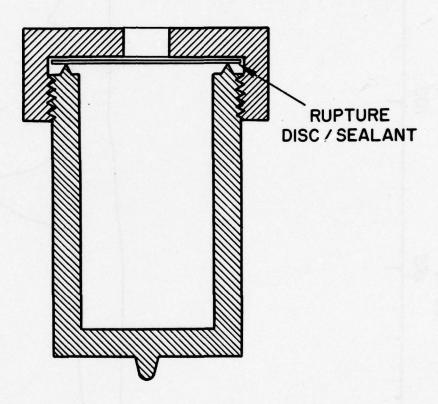


Fig. 1. Cross-Sectional View of the High-Pressure Hermetic Crucible.

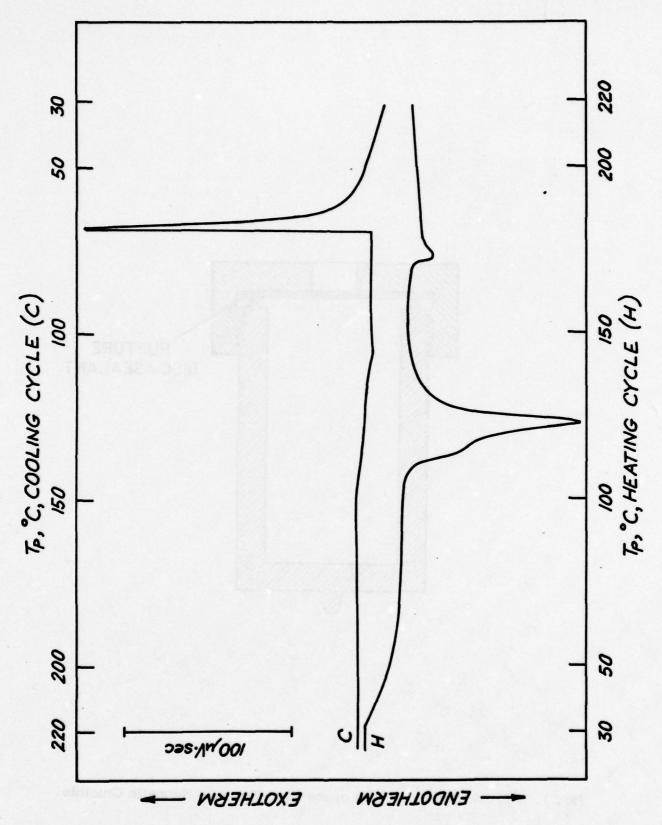


Fig. 2. Thermogram of S (0.0240 gm); 5°C/Minute.

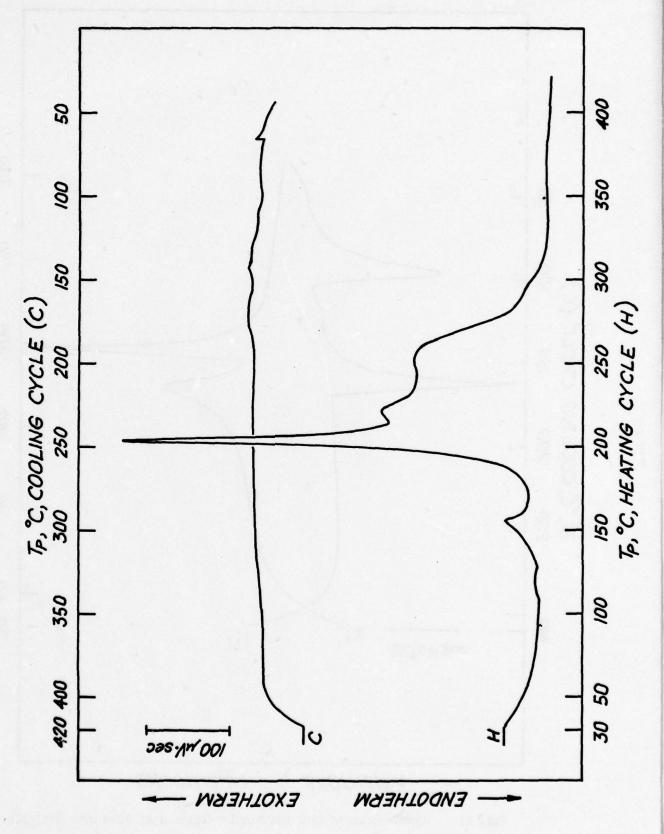


Fig. 3. Thermogram of $Na_2S_2O_4$ (0.0333 gm); 5°C/Minute.

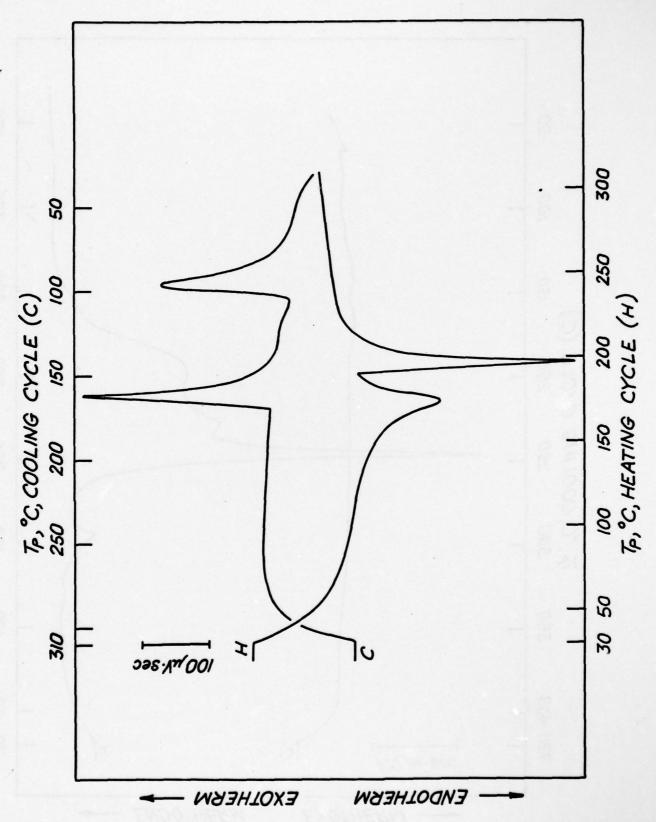


Fig. 4. Thermogram of Li(0.0123 gm) + Celgard (0.0634 gm); 5°C/Minute.

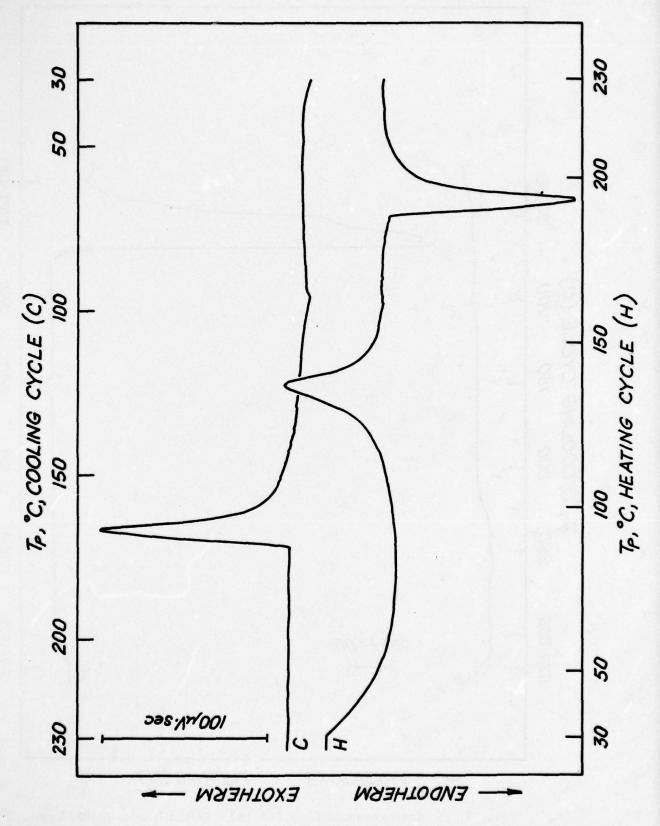


Fig. 5. Thermogram of Li (0.0031 gm) + LiBr (0.0799 gm); 5°C/Minute.

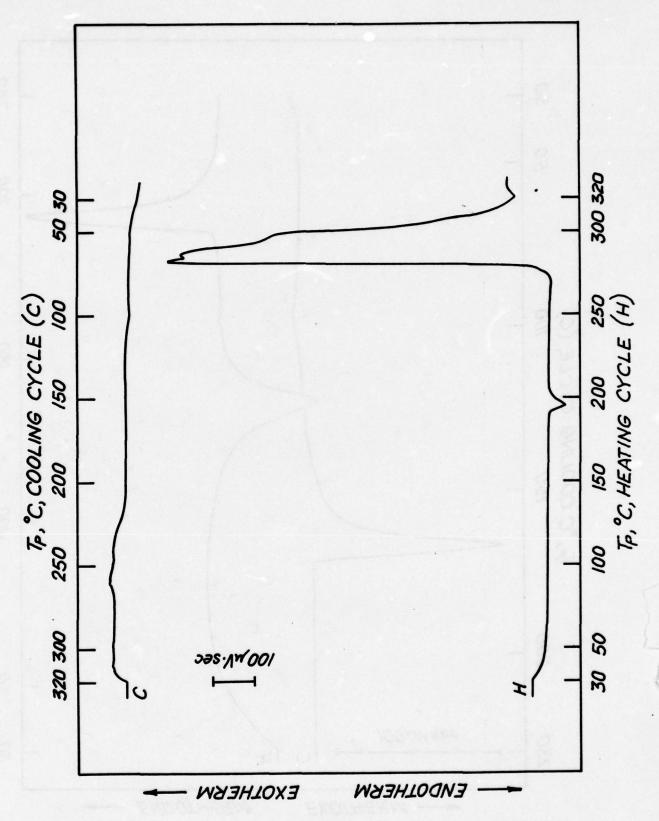


Fig. 6. Thermogram of Li (0.008 gm) + Teflon Powder (0.0234 gm); 5°C/Minute. 58

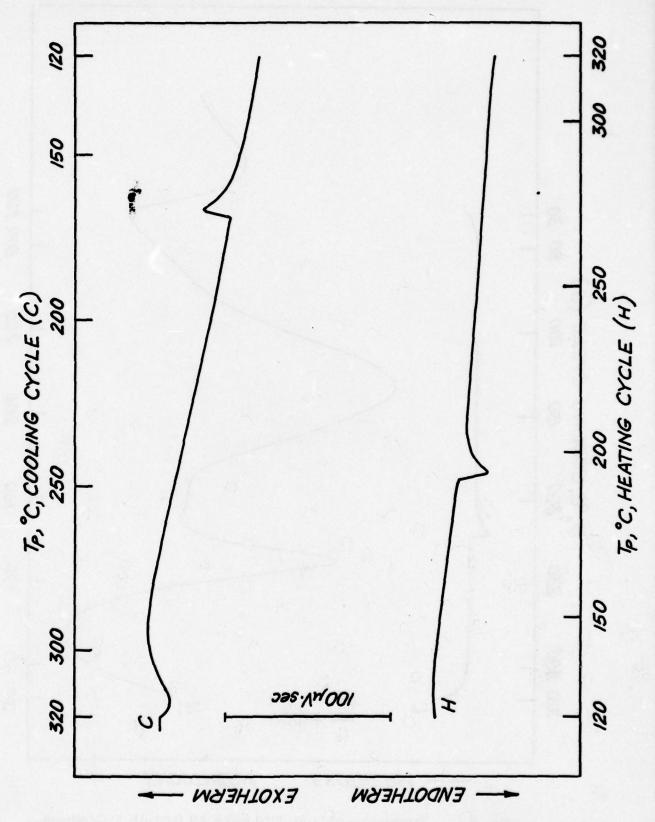


Fig. 7. Thermogram of Li (0.00029 gm) + SO₂; 5°C/Minute.

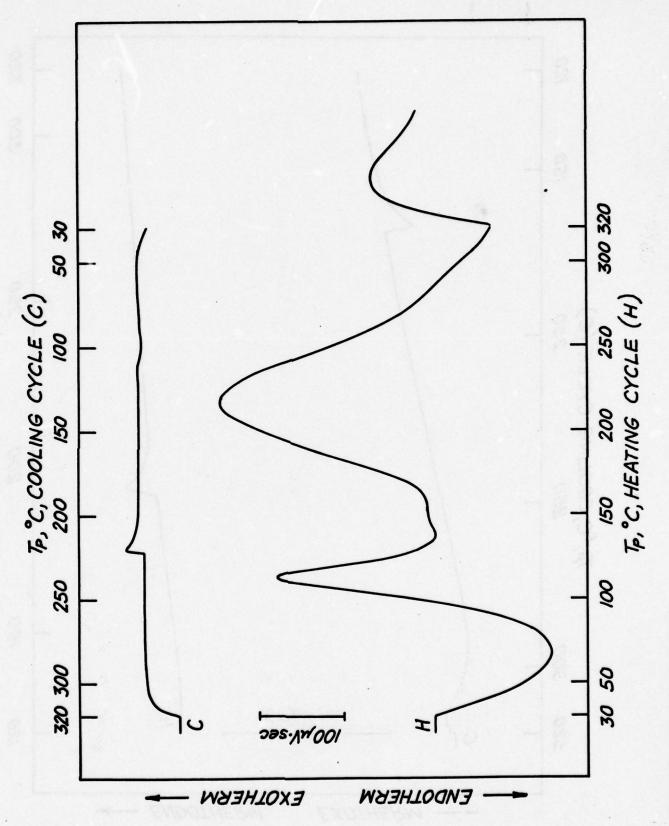


Fig. 8. Thermogram of Li (0.0010 gm) + AN (100 μl); 5°C/Minute.

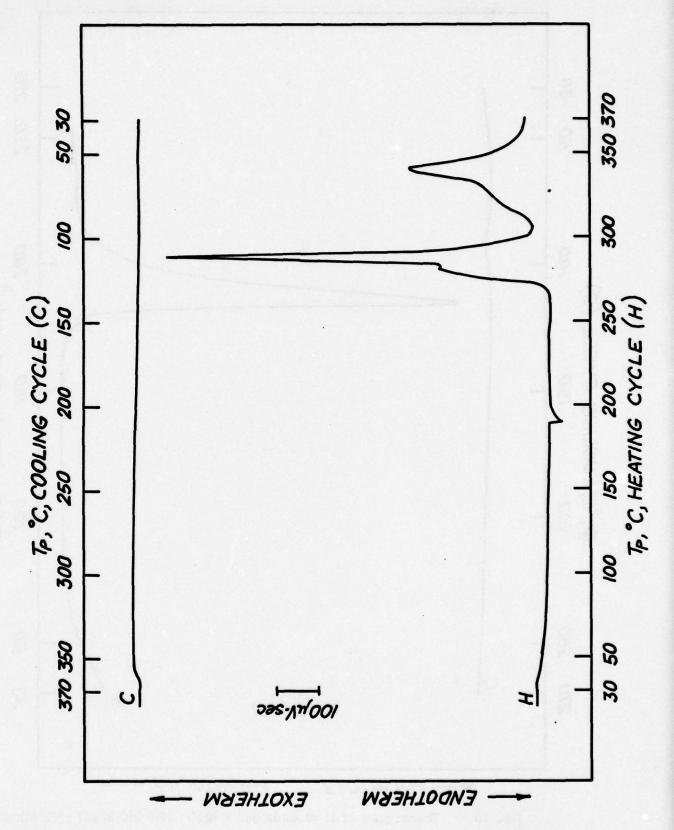


Fig. 9. Thermogram of Li $(0.0008 \text{ gm}) + PC (20 \mu\text{l}); 5 °C/Minute.$

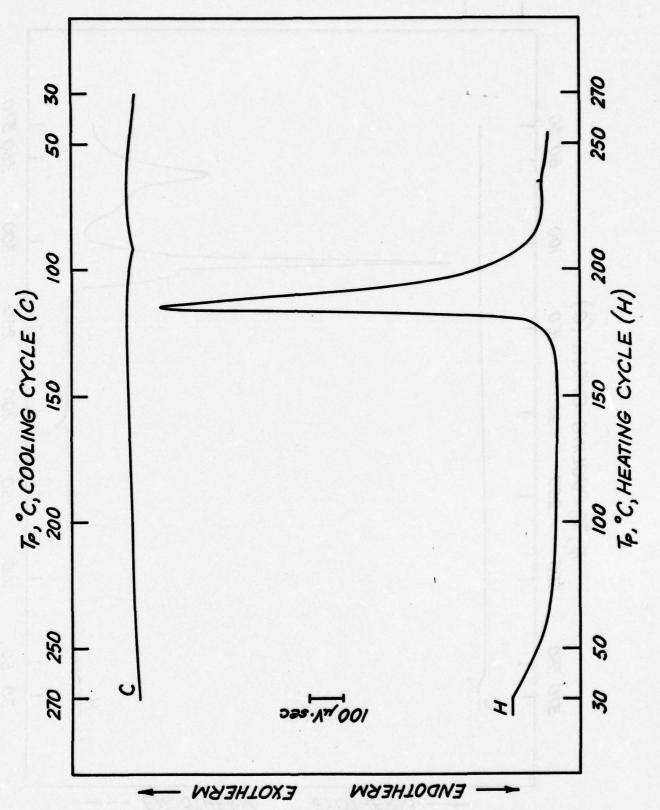


Fig. 10. Thermogram of Li (0.0003 gm) + AN/PC (50:50) 80 μ l; 5°C/Minute.

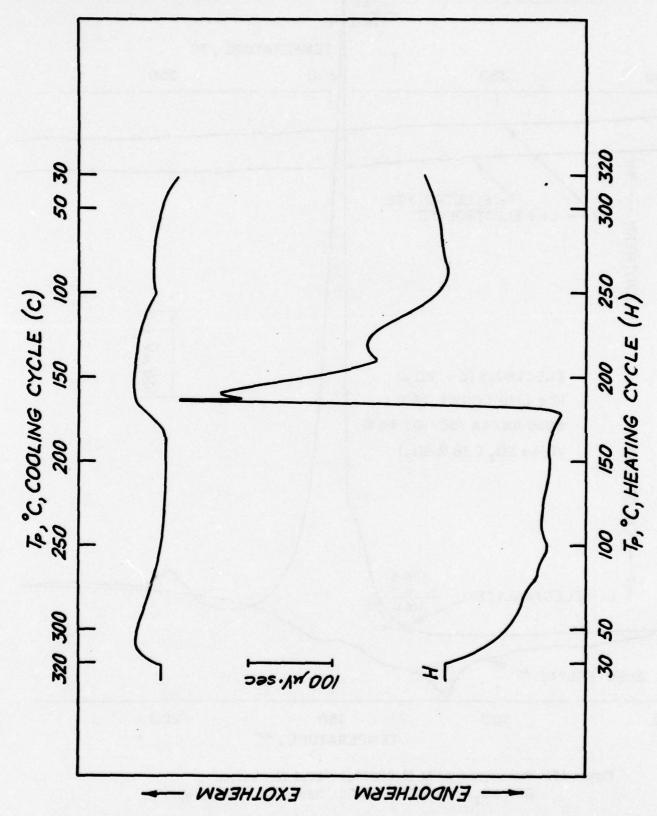


Fig. 11. Thermogram of Li (0.00085 gm) + Electrolyte (40% SO₂, 40% AN, 20% LiBr) \sim 25 μ l; 5 °C/Minute. 63

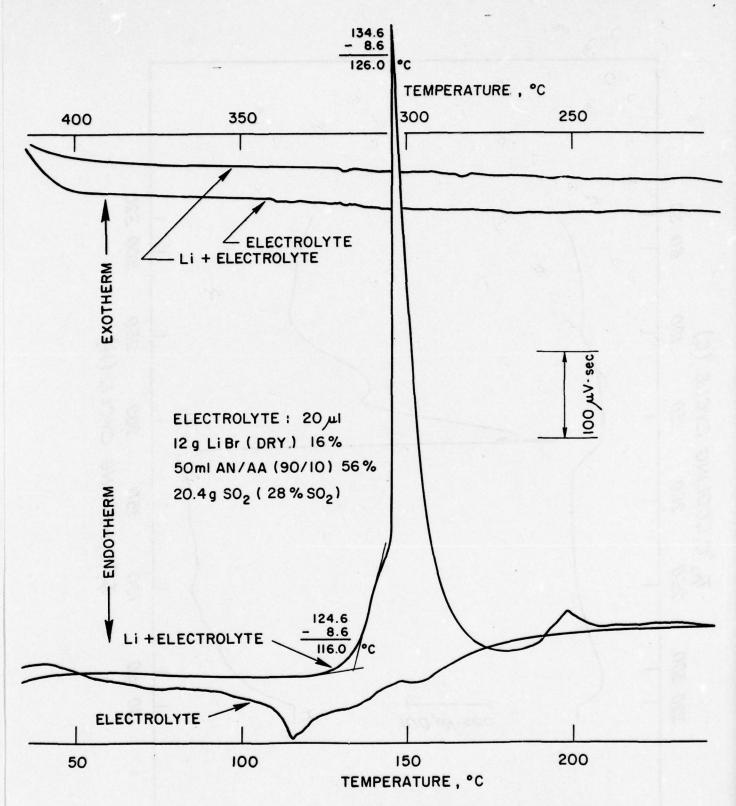


Figure 12. Thermogram of Li (0.00029g) + 20µl Electrolyte (28% SO₂, 56% AN/AA (90/10), 16% LiBr). 5°C/Minute.

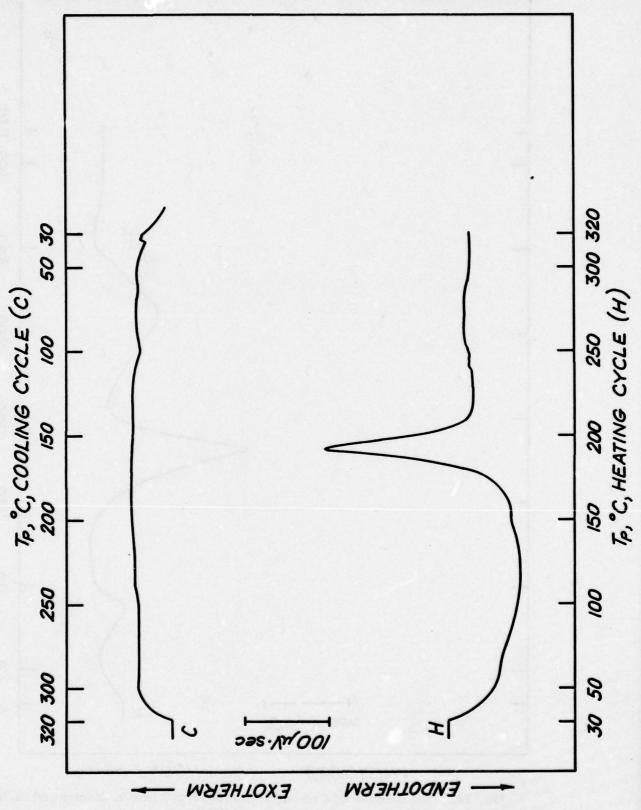


Fig. 13. Thermogram of Cathode Mix (0.0661 gm) from a Discharged Li/SO₂ Cell; 5°C/Minute.

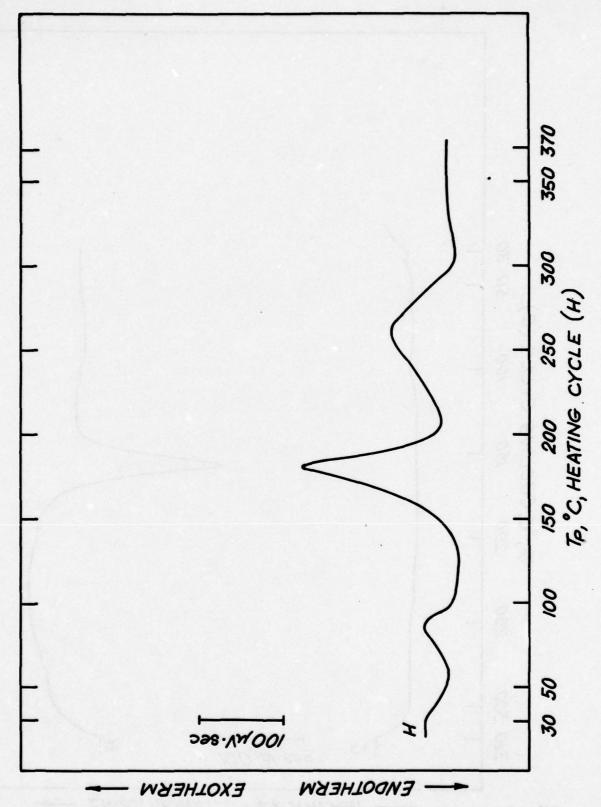


Fig. 14. Thermogram of Cathode Mix (0.0819 gm) from a Discharged Li/SO₂ Cell after Exposure to Air; 5°C/Minute.

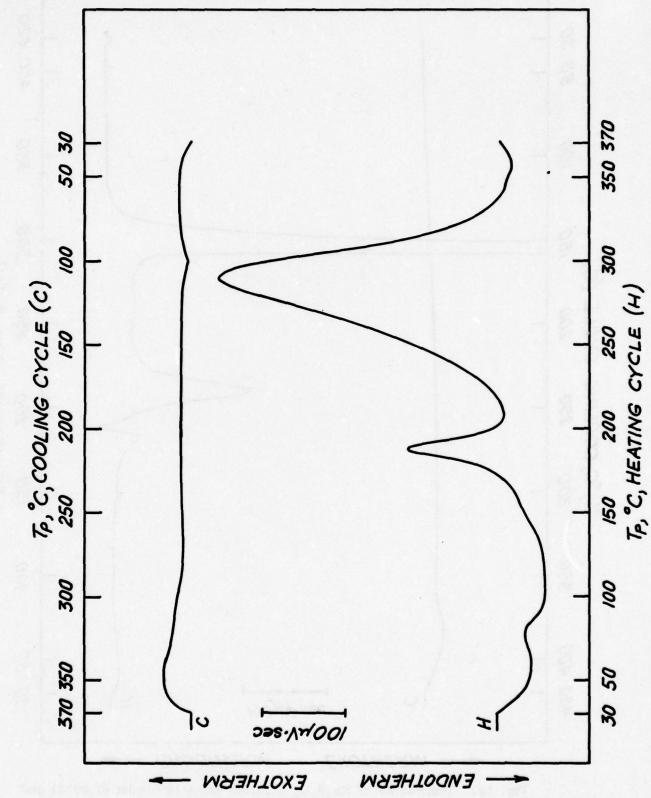


Fig. 15. Thermogram of Cathode Mix (0.0624 gm) from a Li/SO₂ Cell which was Discharged and then Driven into Reversal for 10% of Its Discharged Capacity; 5°C/Minute. 67

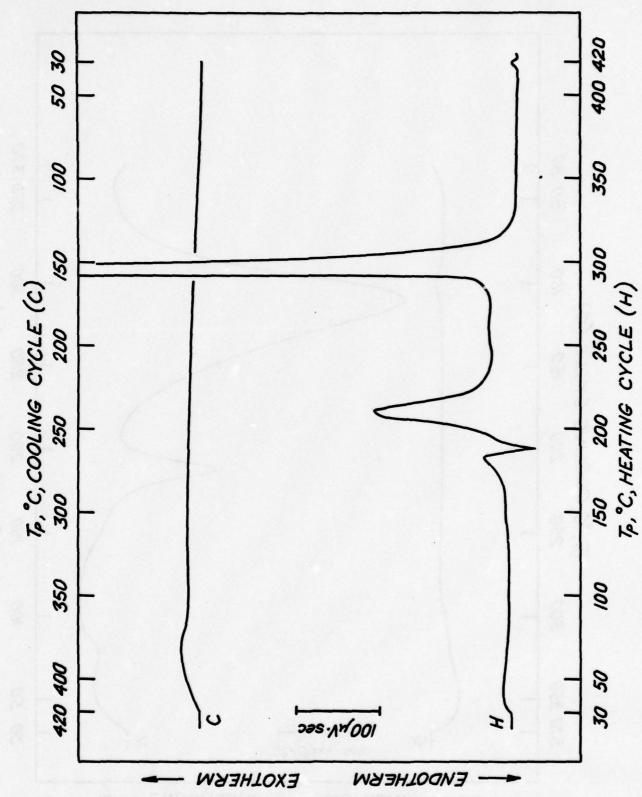


Fig. 16. Thermogram of $Na_2S_2O_4$ (0.01007'gm) + Li Powder (0.00131 gm) + Carbon (0.00284 gm); 5°C/Minute.

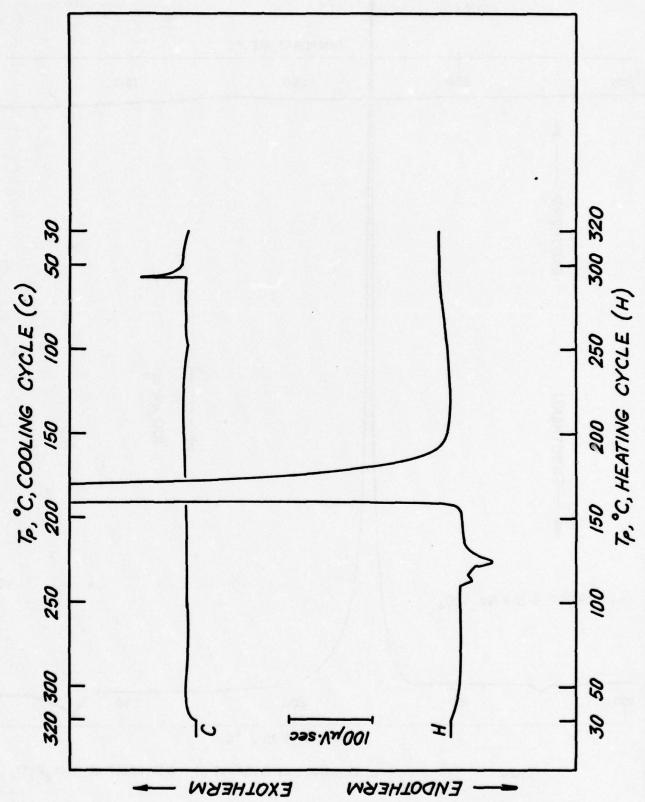


Fig. 17. Thermogram of Li (0.0015 gm)+ S (0.0079 gm); 5°C/Minute.

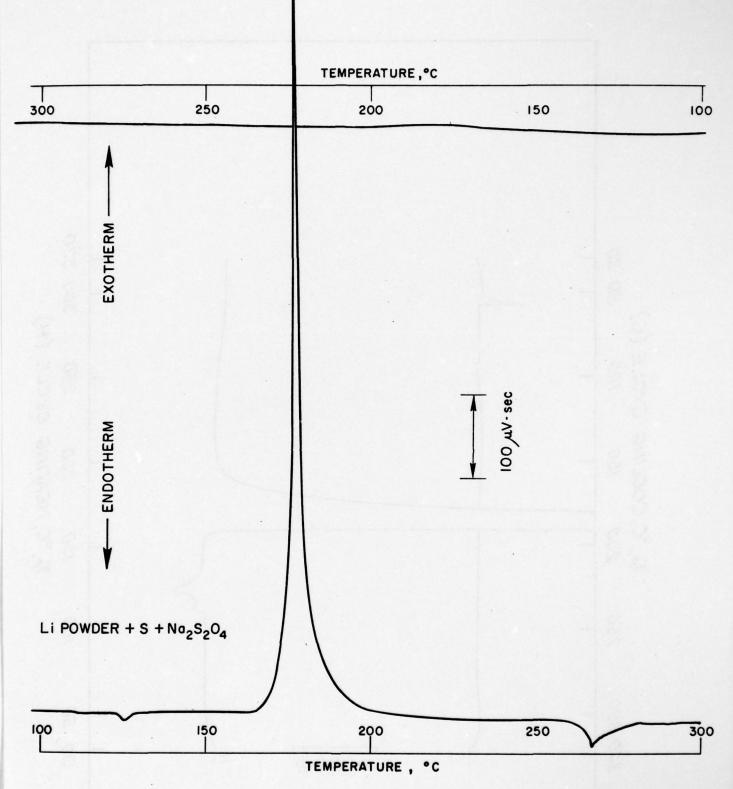


Figure 18. Thermogram of Powdered Li (0.00039 g) + S (0.00147 g) + Na $_2$ S $_2$ O $_4$ (0.00644 g)

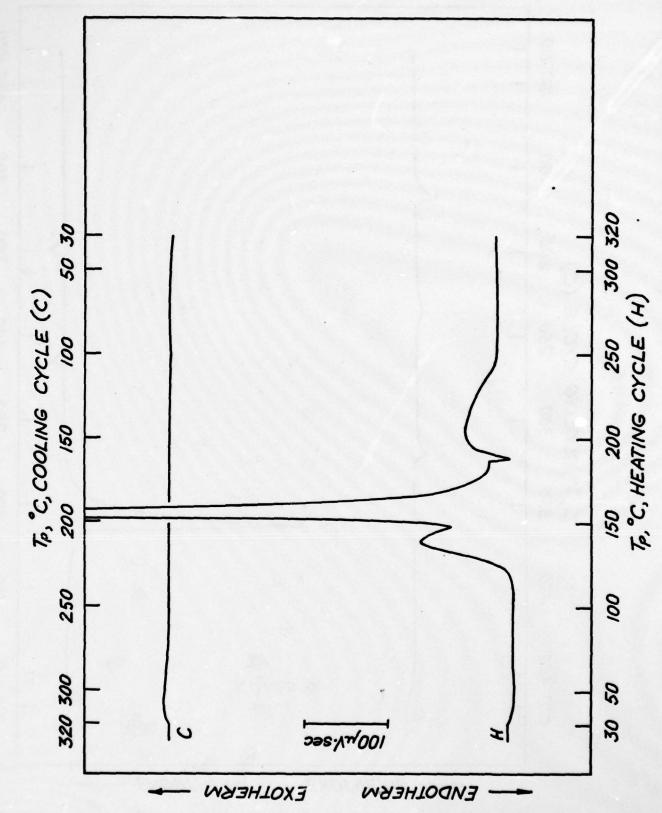


Fig. 19. Thermogram of Li $(0.00094 \text{ gm}) + \text{Li}_2\text{SO}_3$ (0.0075 gm) As-Received; $5 \, ^{\circ}\text{C/Minute}$.

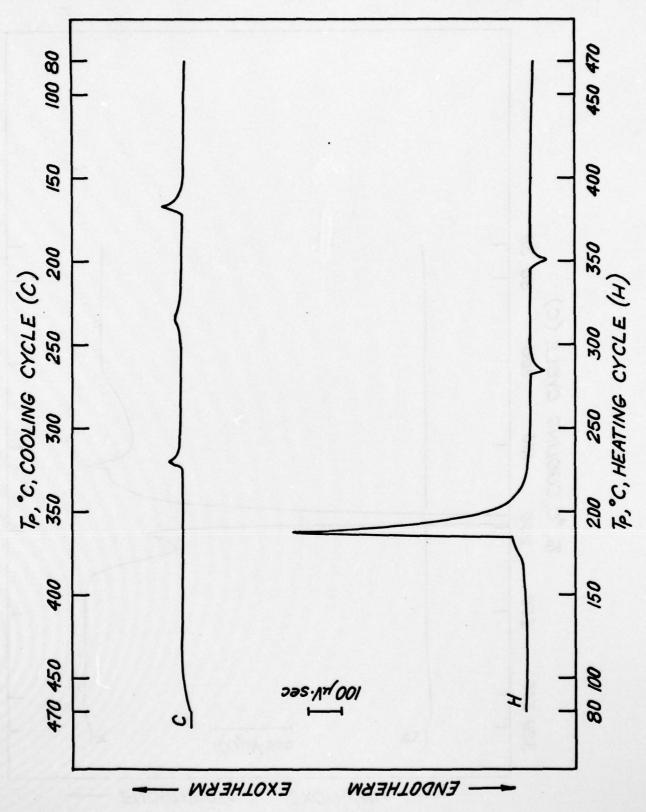


Fig. 20. Thermogram of Li (0.00572 gm) + Al (0.00720 gm); 5°C/Minute. 72

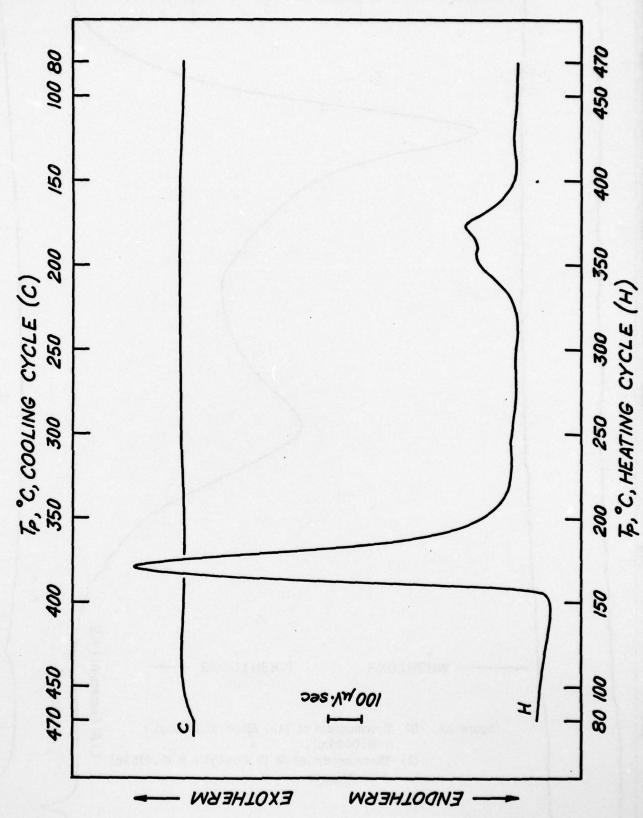
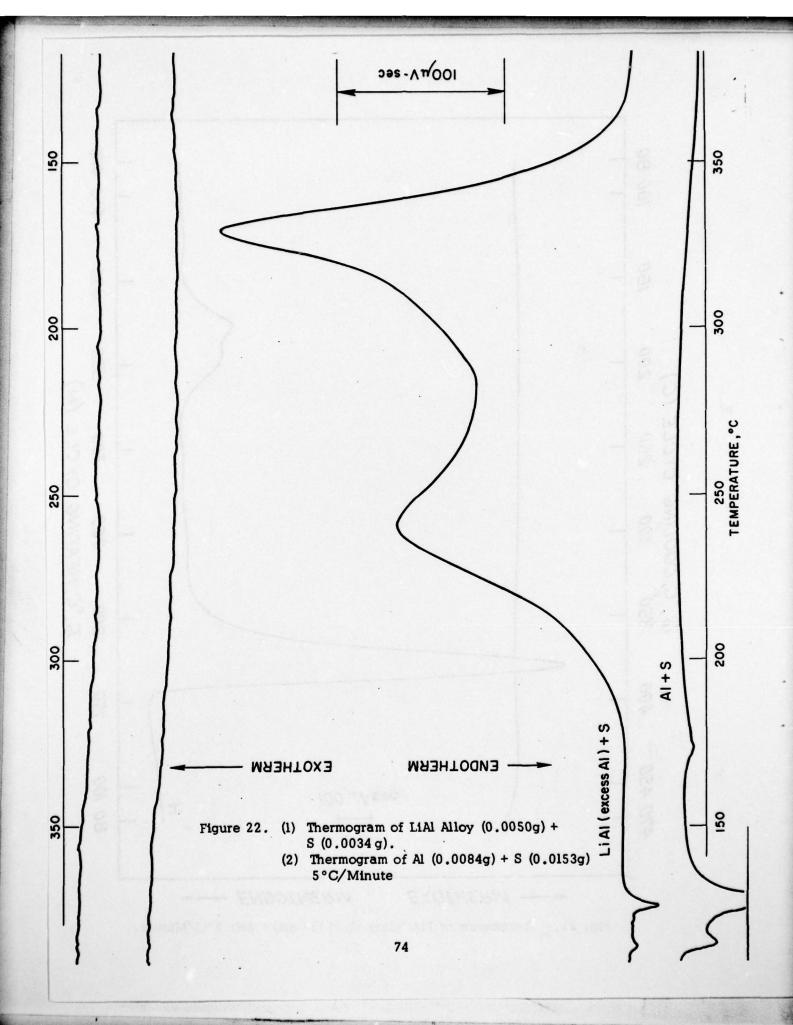


Fig. 21. Thermogram of LiAl Alloy (0.01333 gm) + AN; 5°C/Minute.



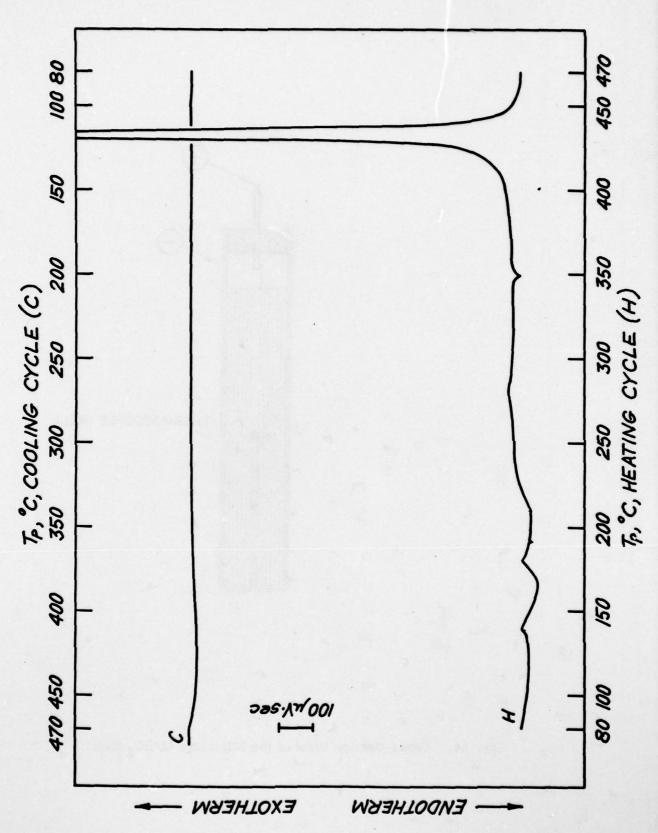


Fig. 23. Thermogram of LiAl Alloy + AN/SO_2 (75:25) 20µl; 5°C/Minute.

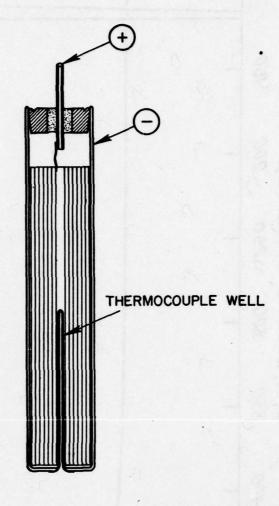


Fig. 24. Cross-Section View of the Miniature Li/SO₂ Cell.

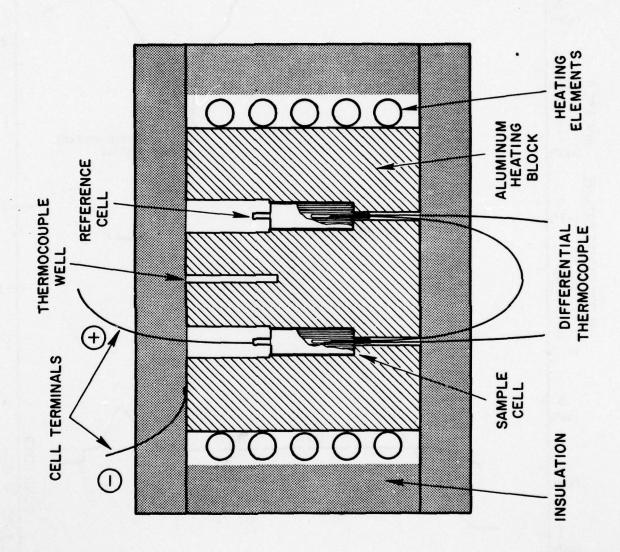


Fig. 25. Fixtures for DTA of Miniature Cell.

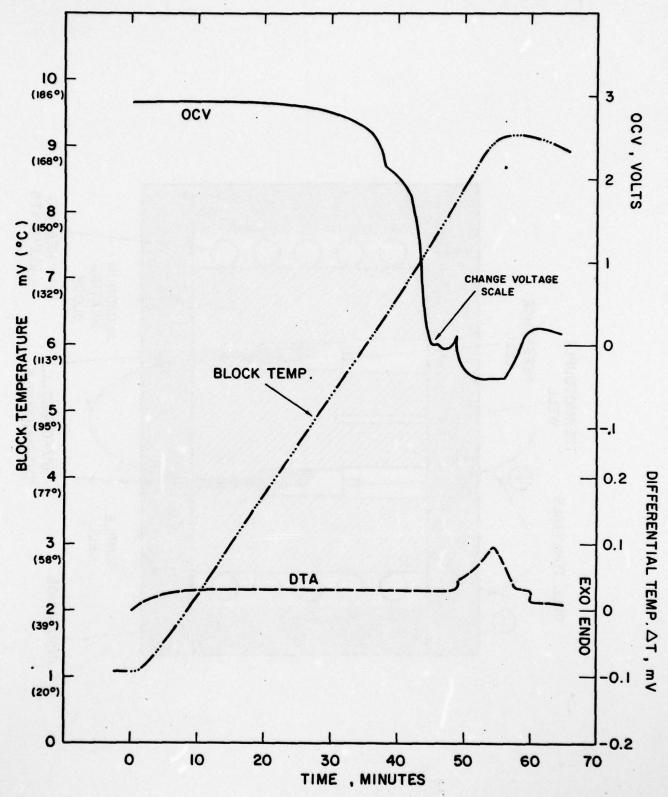
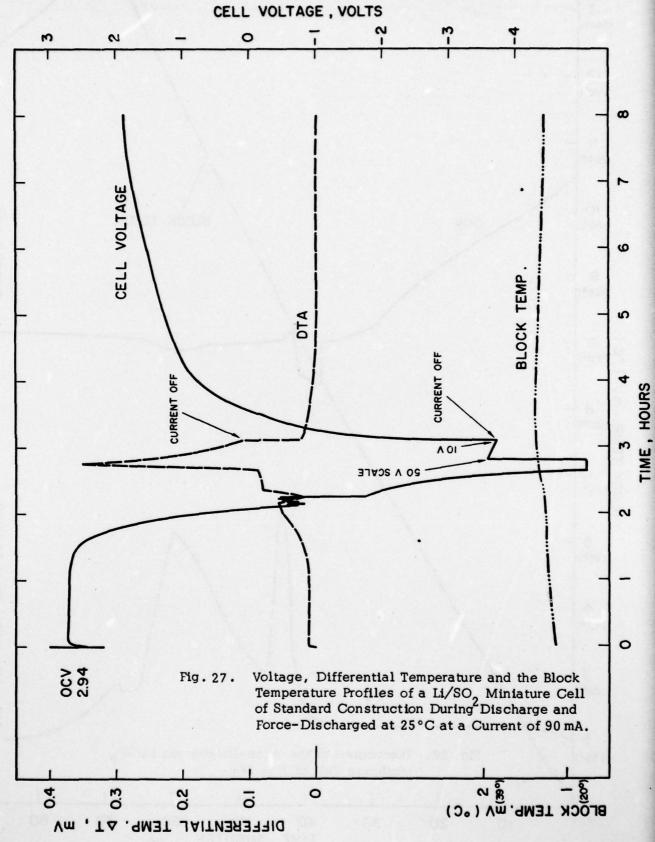
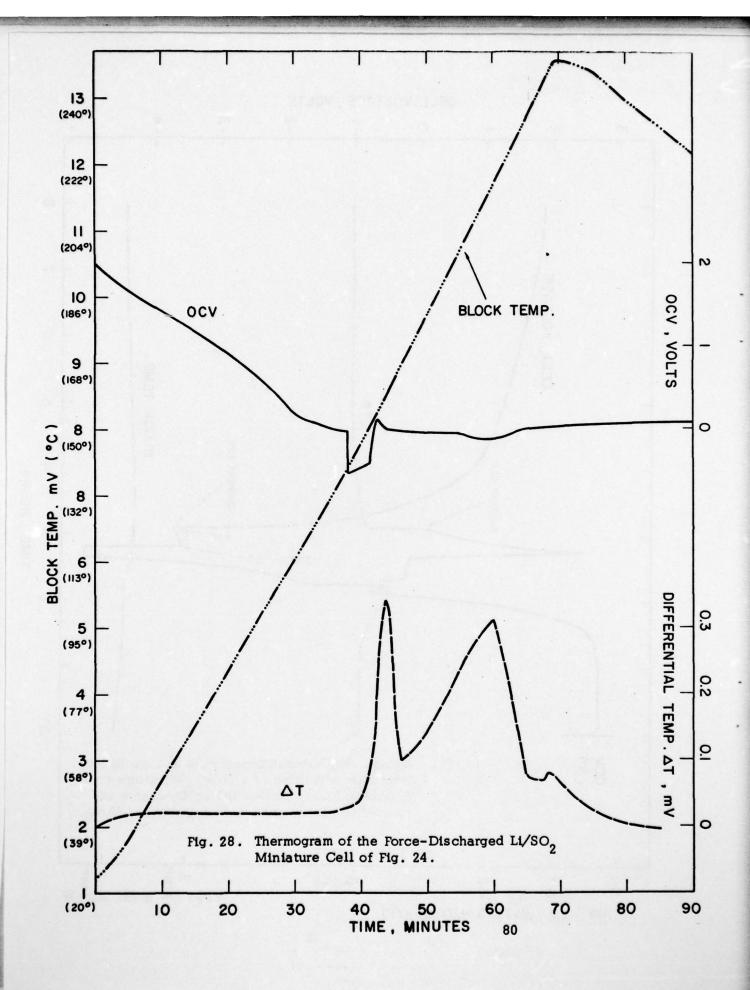
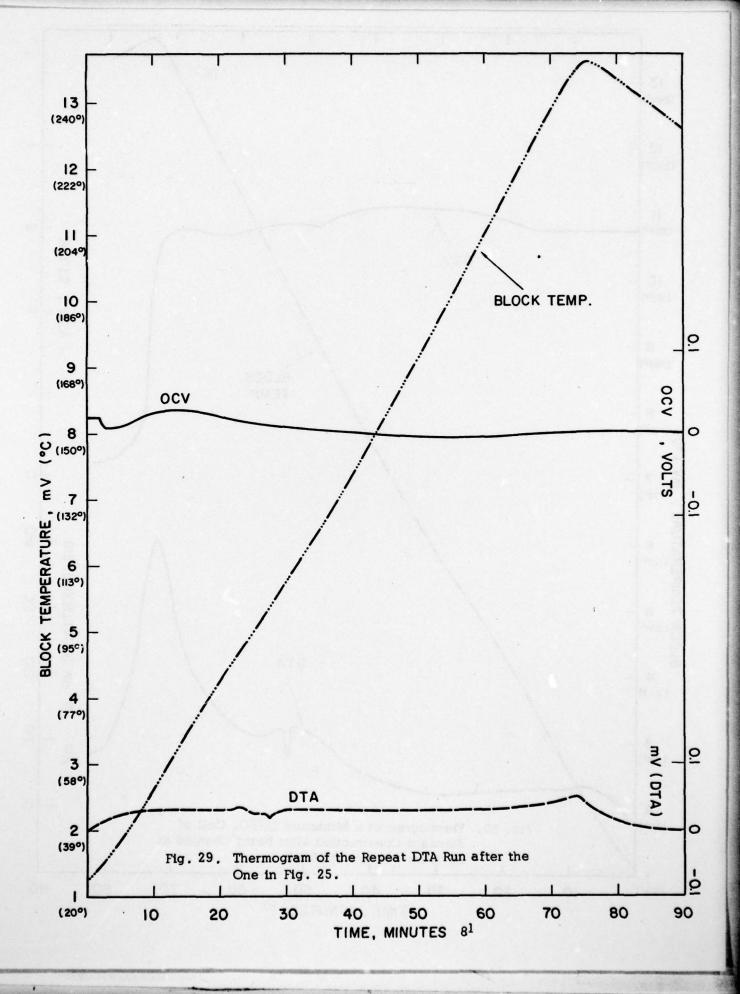


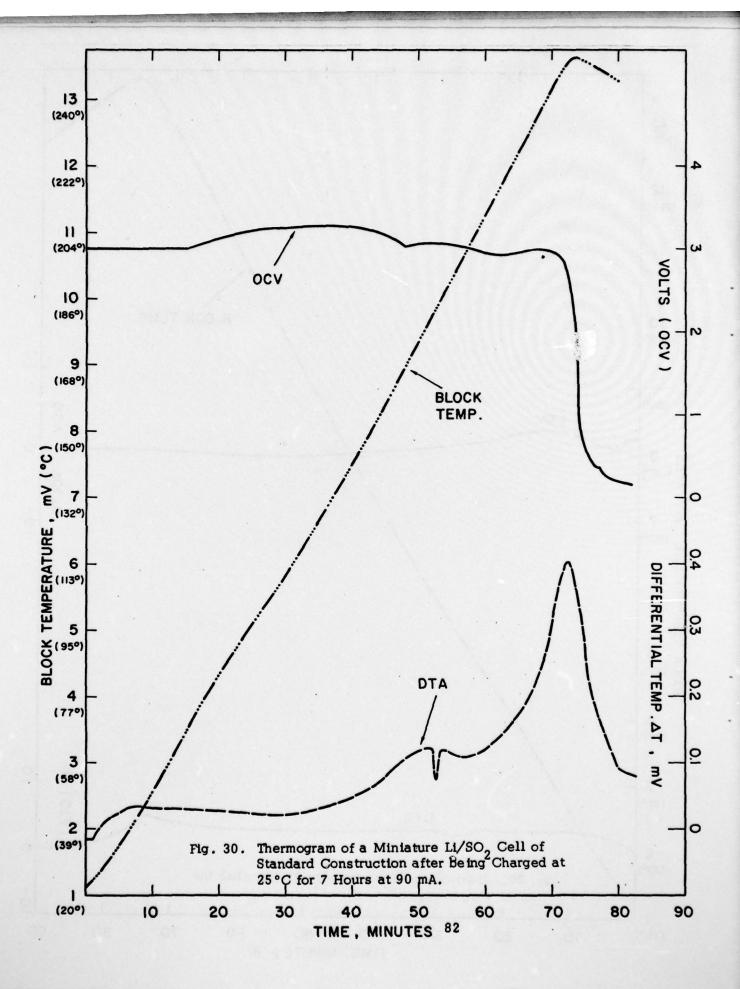
Fig. 26. Thermogram of a Discharged Miniature Li/SO, Cell of Standard Construction, Discharge Current 1 mA; Discharge Capacity 193 mAHr.

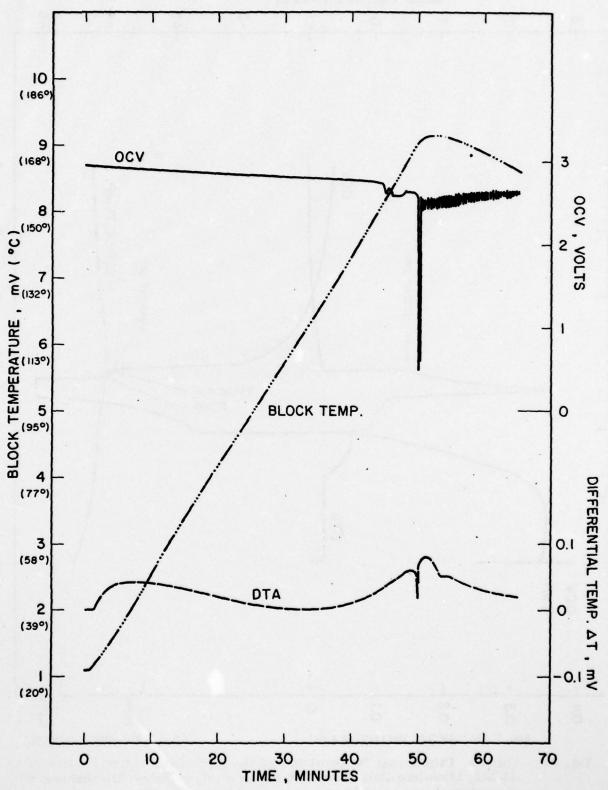












Pig. 31. Thermogram of a Discharged Miniature Li/SO₂ Cell with PC in the Electrolyte; Discharge Current, 10 mA; Discharge Temperature, 25°C. 83

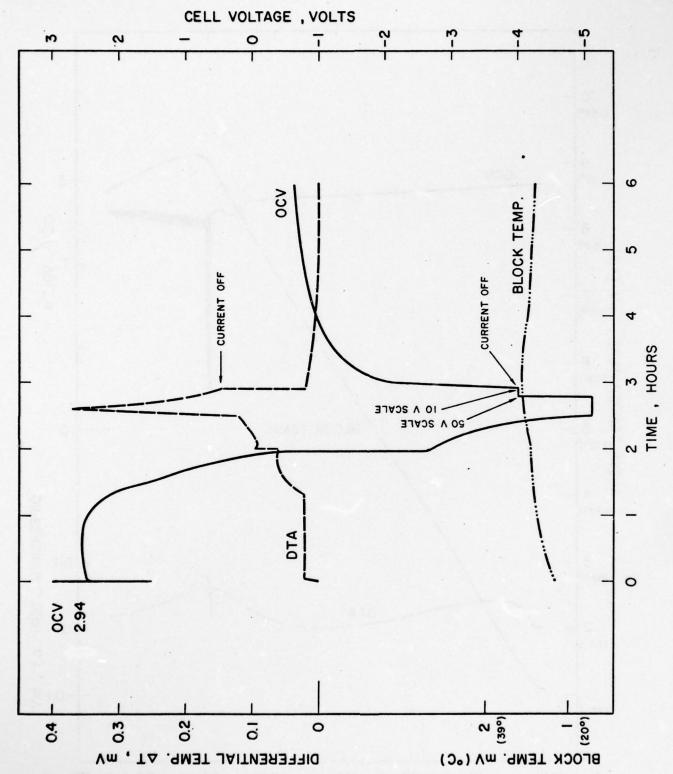
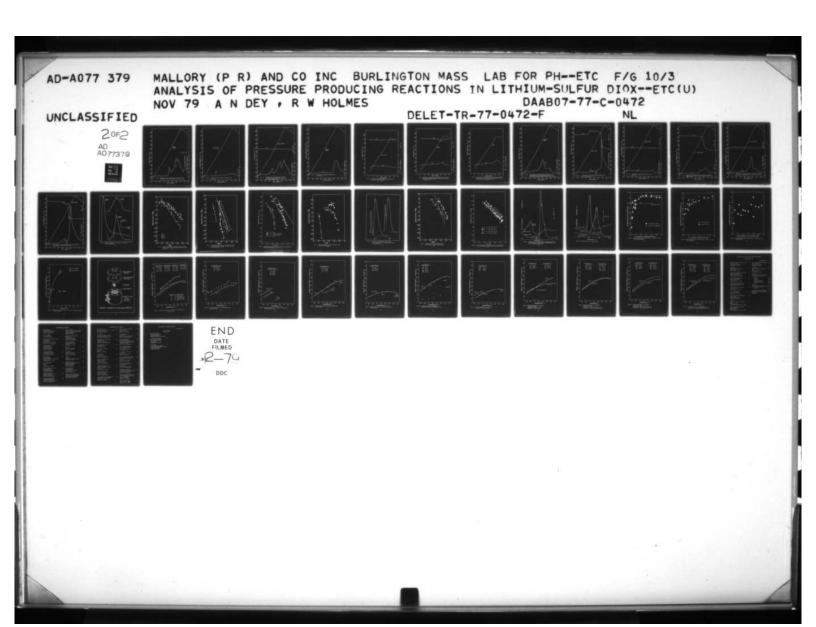
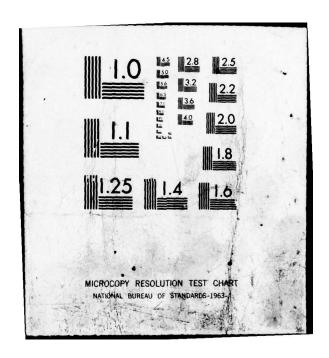
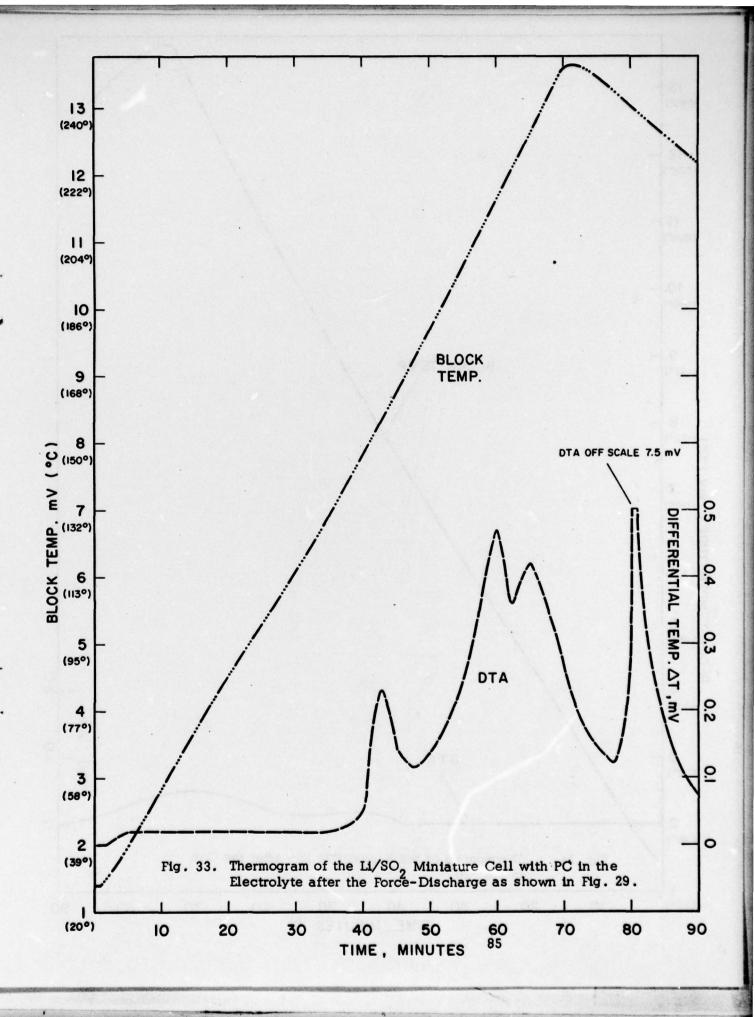
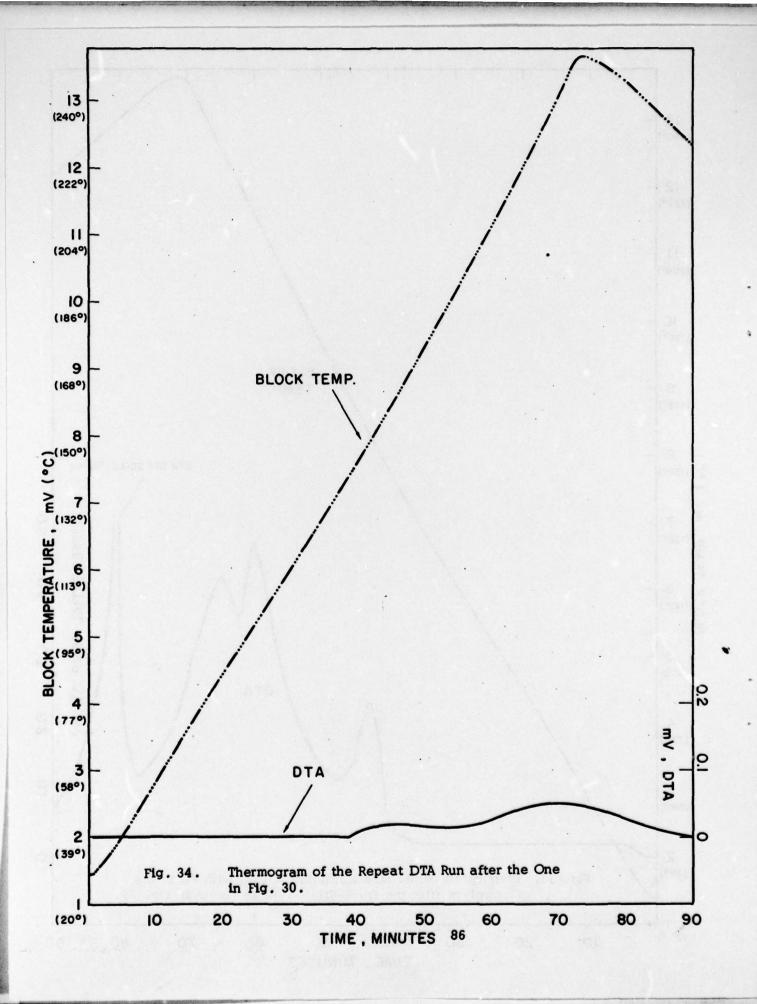


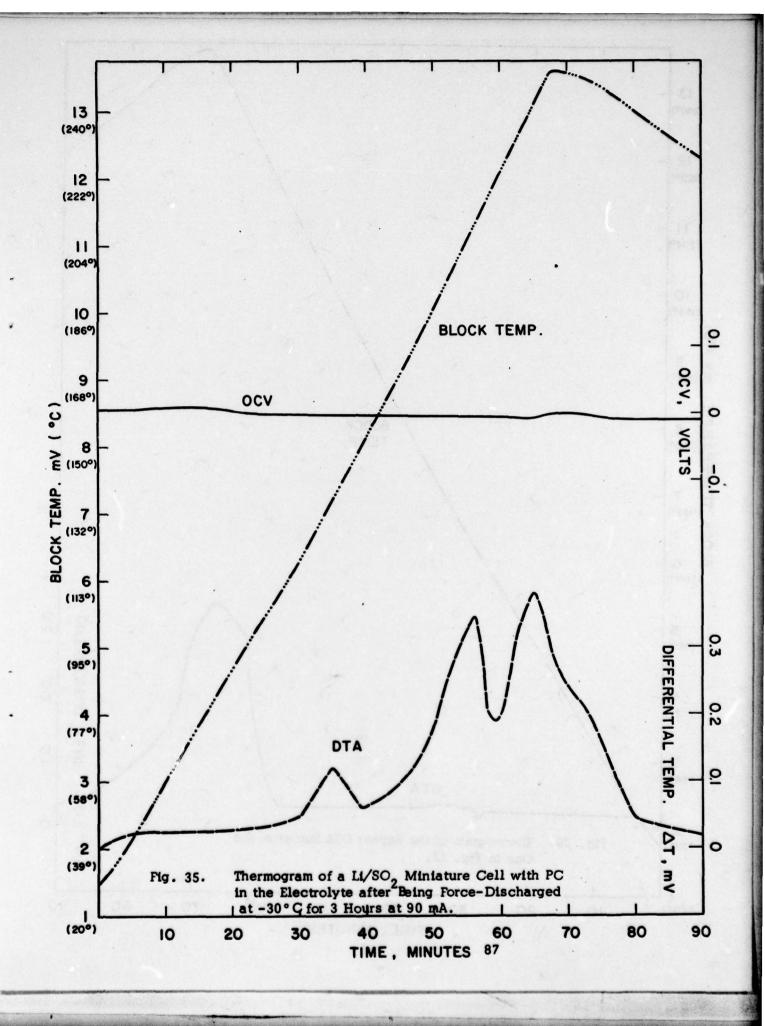
Fig. 32. Voltage, Differential Temperature and the Block Temperature Profiles of a Li/SO₂ Miniature Cell with PC in the Electrolyte During Discharge and Force-Discharge at 25°C at a Current of 90 mA.

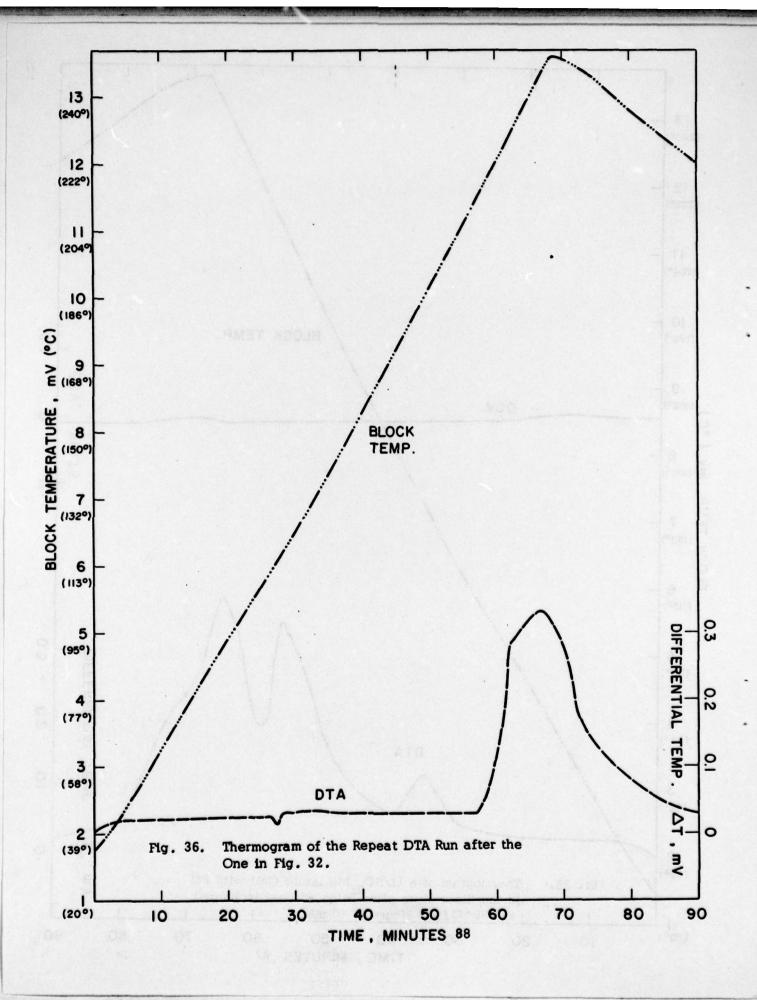












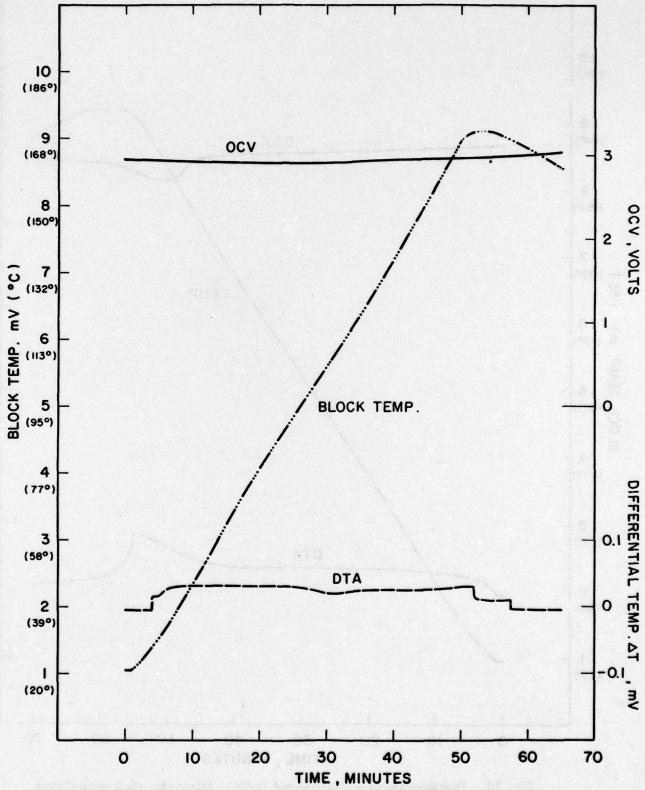


Fig. 37. Thermogram of an Undischarged Li/SO $_2$ Miniature Cell with Glass Filter Paper Separator.

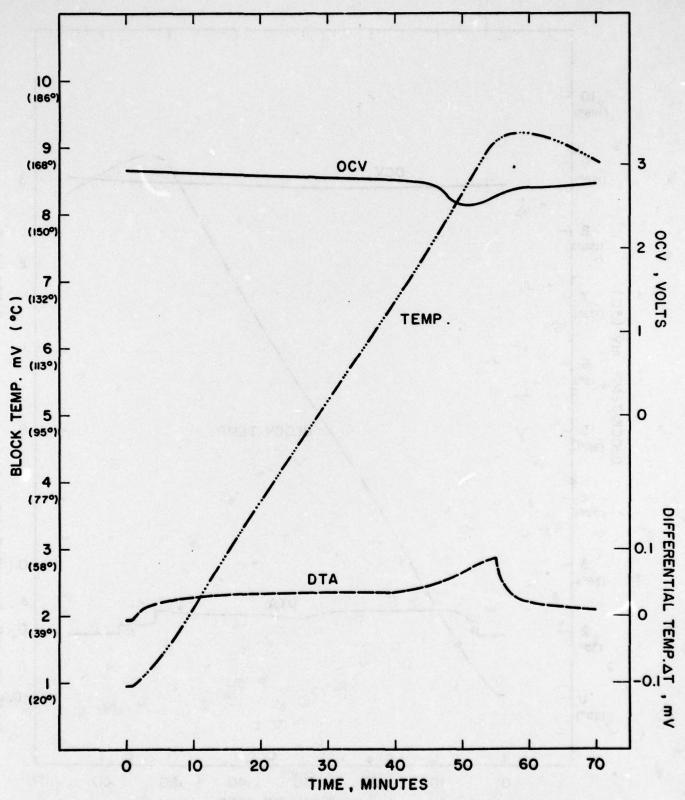


Fig. 38. Thermogram of a Discharged Li/SO, Miniature Cell with Glass Filter Paper Separator; Discharge Current, 10 mA; Discharge Temperature, 25°C. 90

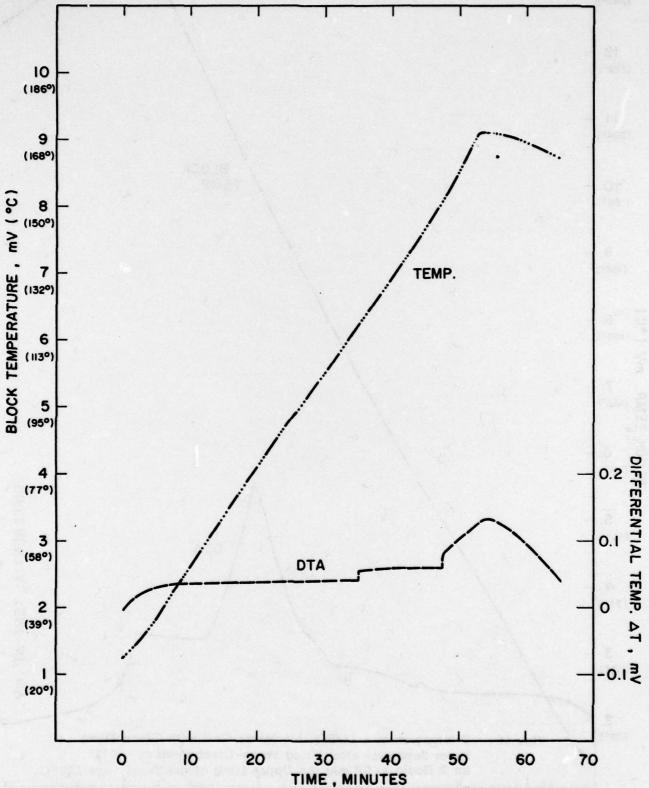
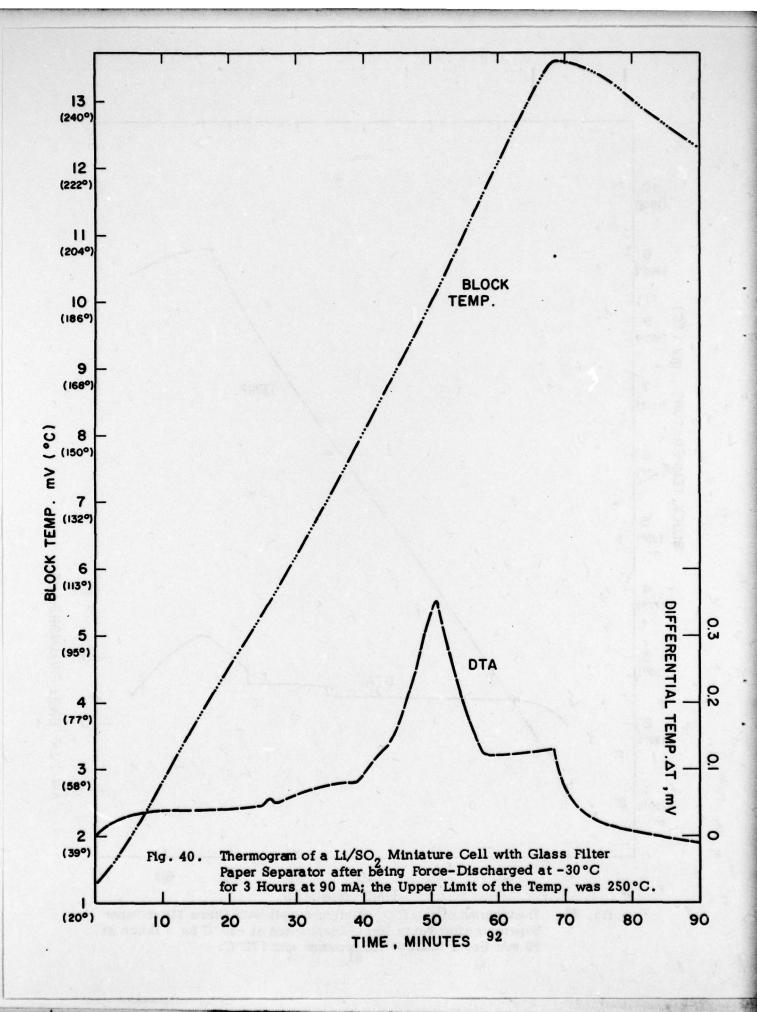
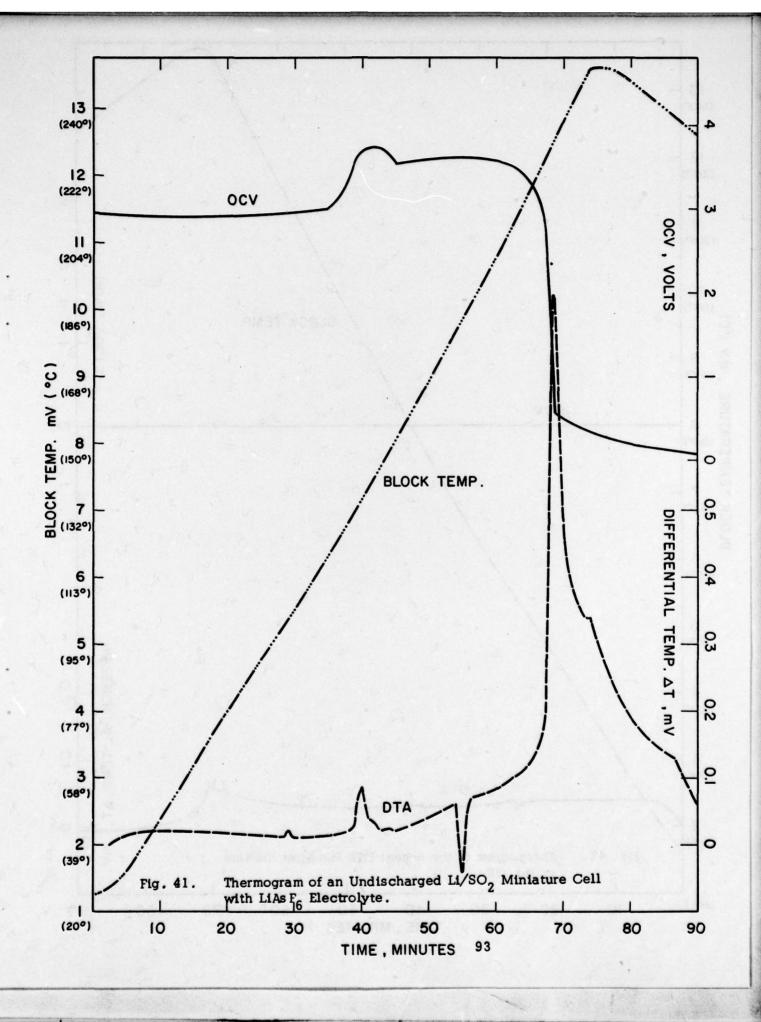
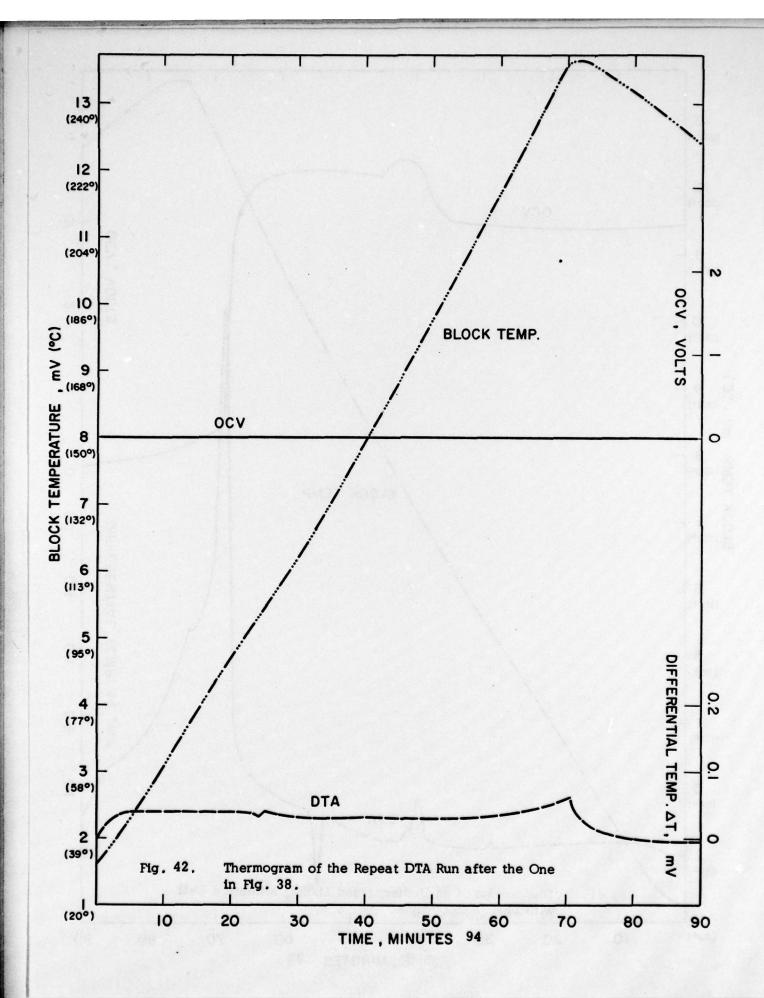
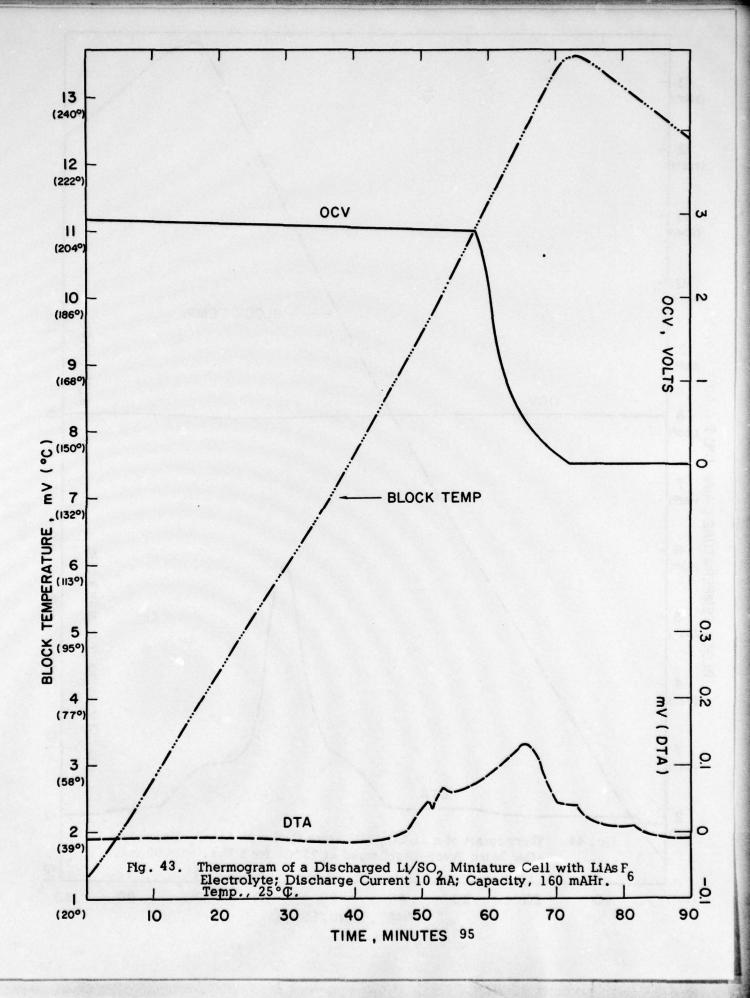


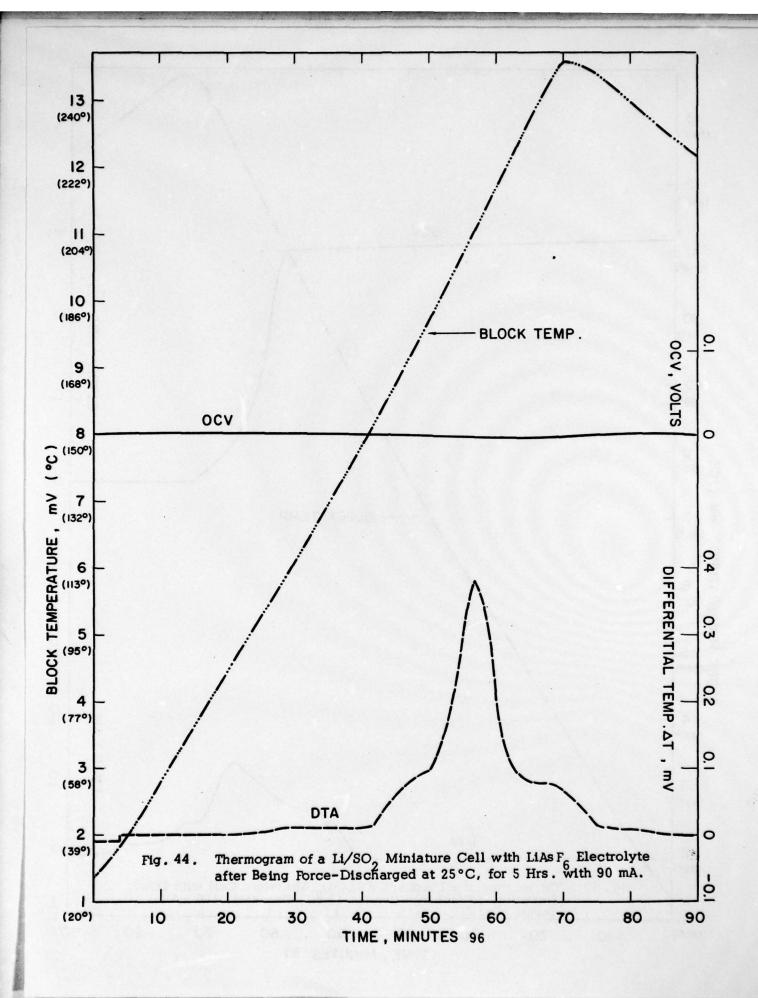
Fig. 39. Thermogram of a Li/SO, Miniature Cell with Glass Filter Paper Separator after being Force-Discharged at -30°C for 3 Hours at 90 mA; Upper Limit of Temperature was 170°C.

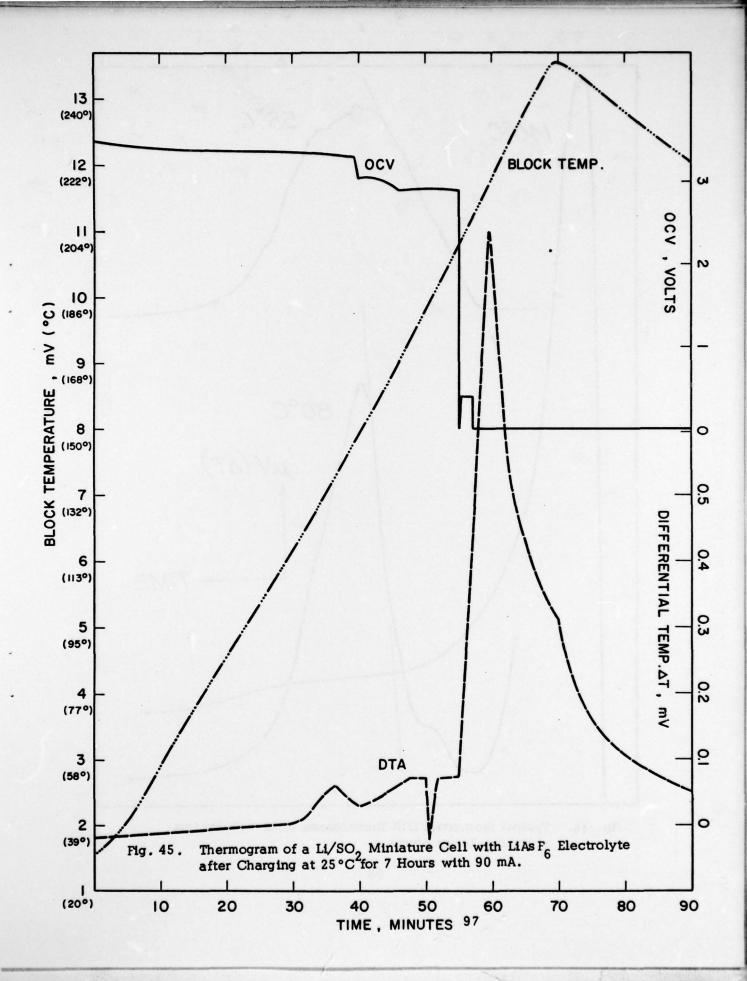












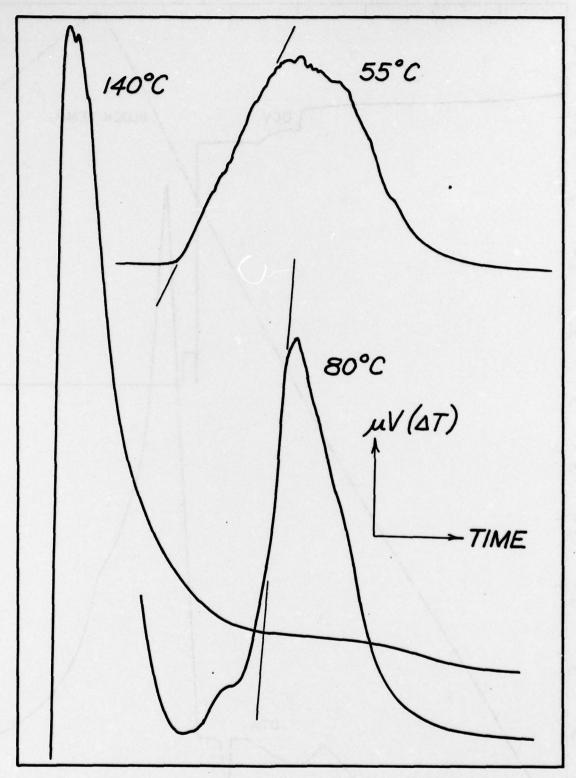


Fig. 46. Typical Isothermal DTA Thermograms of Li + AN Sys tem at Various Temperatures.

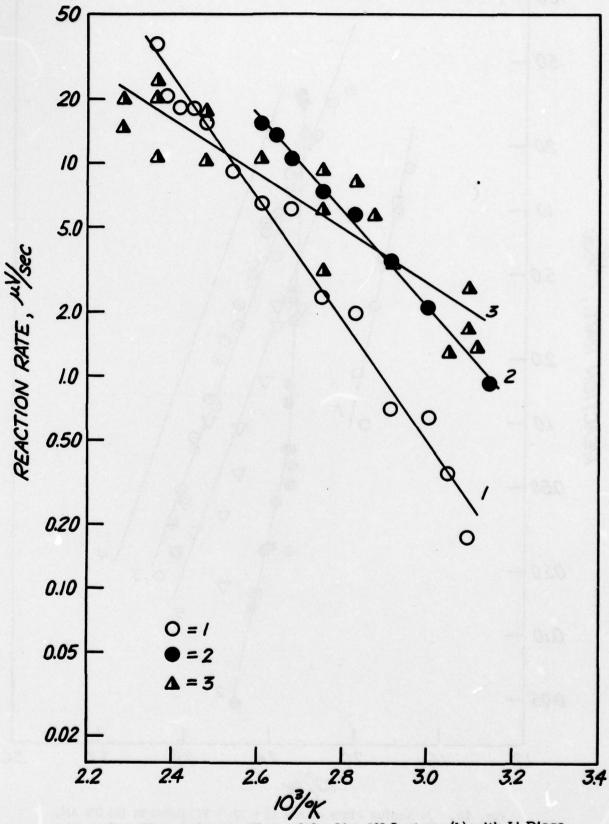


Fig. 47. Arrhenius Plots of the Li + AN System; (1) with Li Discs Aged in Dry Box, (2) Freshly Cut Li Discs, (3) with 0.32 M LiBr in AN. 99

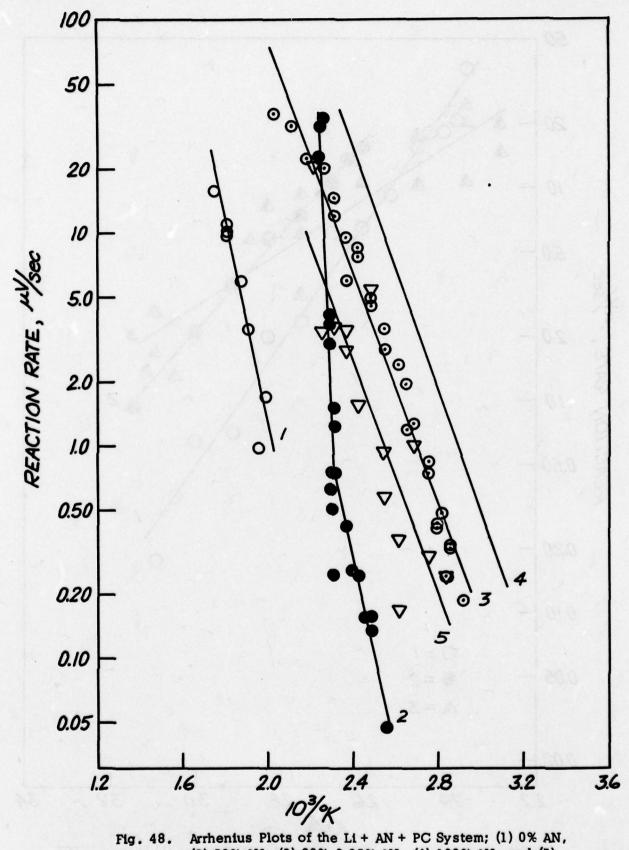


Fig. 48. Arrhenius Plots of the Li + AN + PC System; (1) 0% AN, (2) 50% AN, (3) 80% & 95% AN, (4) 100% AN, and (5) 0% PC and 3% SO₂.

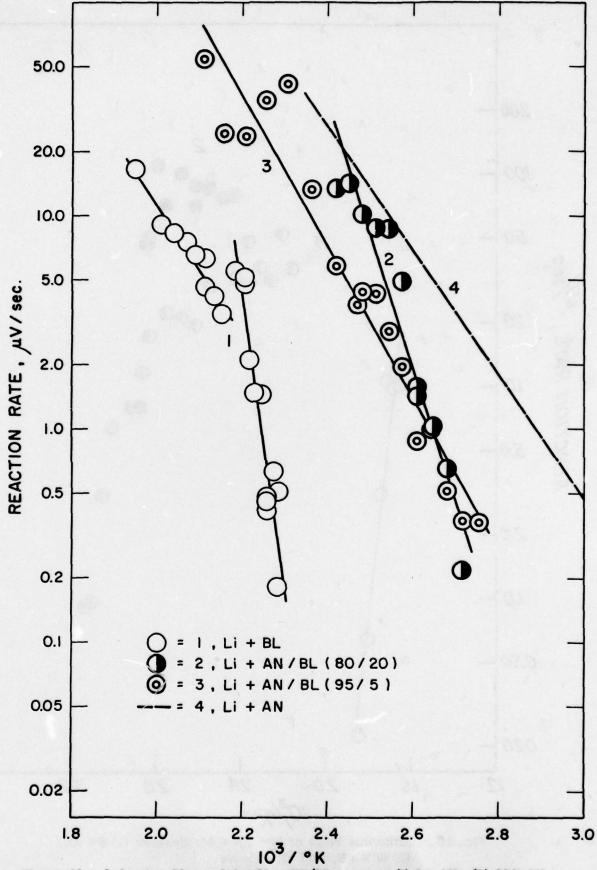


Figure 49. Arrhenius Plots of the Li + AN/BL system; (1) 0% AN, (2) 80% AN, (3) 95% AN and (4) 100% AN. 101

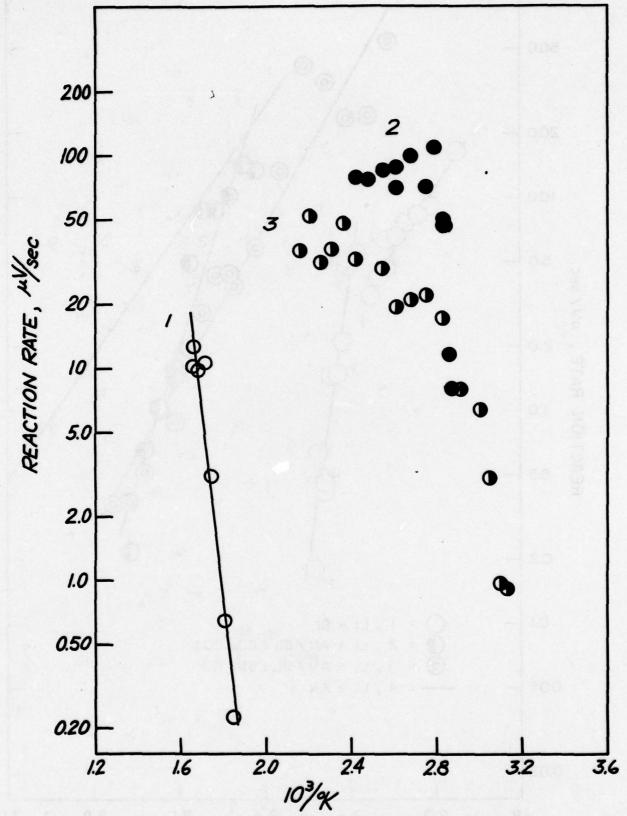


Fig. 50. Arrhenius Plots of Li + AN + MF System; (1) 0% AN, (2) 80% AN, and (3) 95% AN. 102

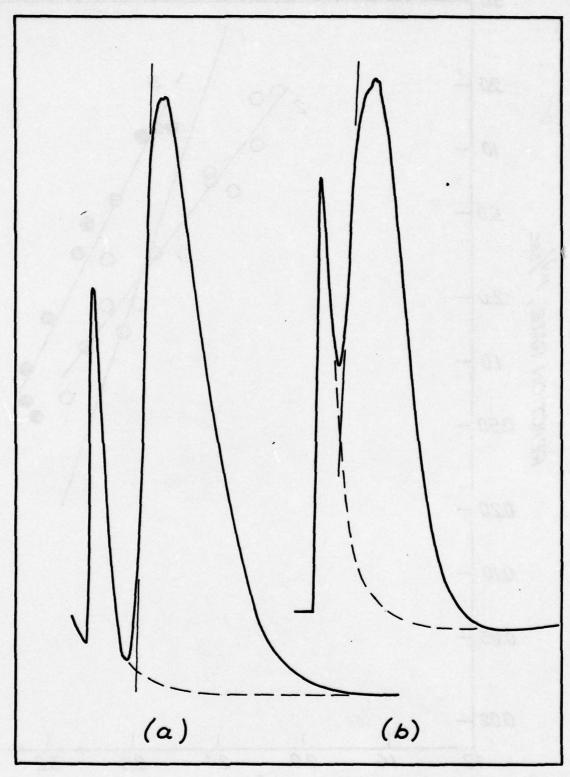


Fig. 51. Isothermal DTA Thermograms (a) Normal Runs, (b) for Reactions with Short Induction Periods as with Li + AN/MF (80/20).

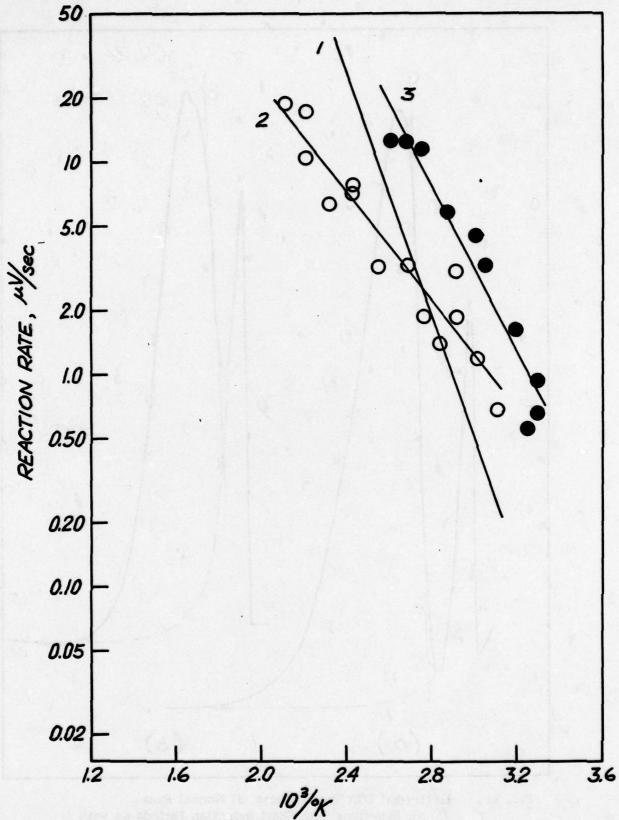
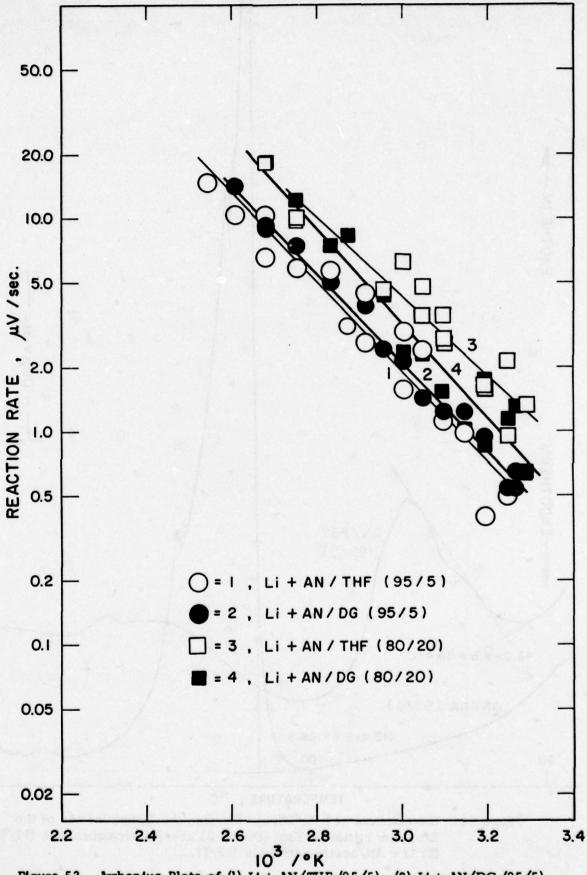


Fig. 52. Arrhenius Plots of Li + AN + DME System;
(1) 0% DME, (2) 5% DME, and (3) 20% DME.
104



10³ /°K
Figure 53. Arrhenius Plots of (1) Li + AN/THF (95/5), (2) Li + AN/DG (95/5), (3) Li + AN/THF (80/20), and (4) Li + AN/DG (80/20) Systems.

105

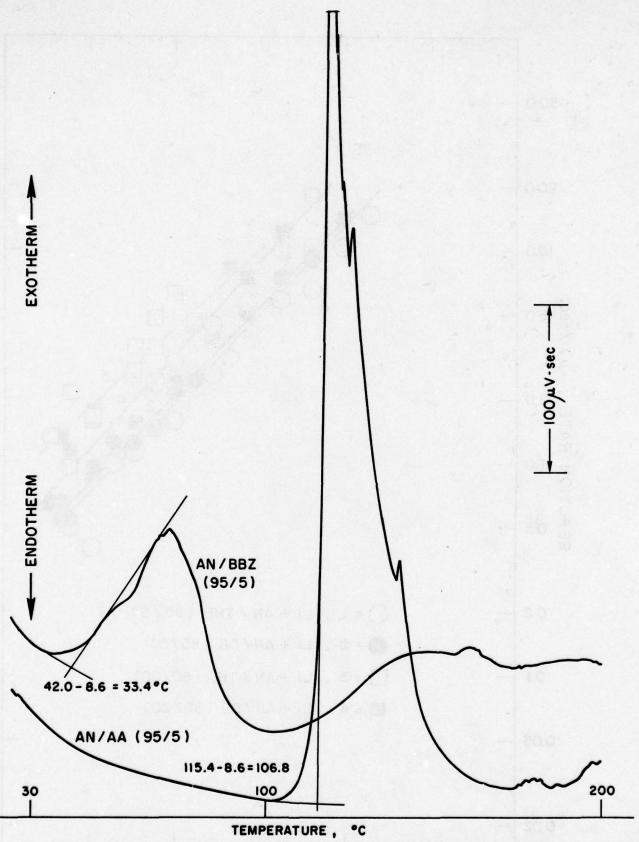


Figure 54. Thermograms at 5°C/Minute Showing the Determination of the Exotherm Initiation Temperature (1) Li + AN/bromobenzene (95/5), (2) Li + AN/acetic anhydride (95/5).

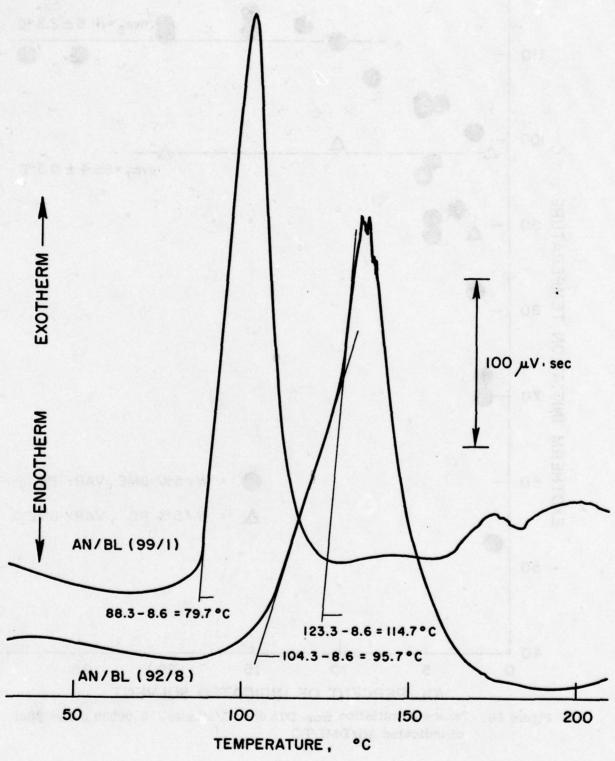


Figure 55. Thermograms for the Li + AN/BL Reaction

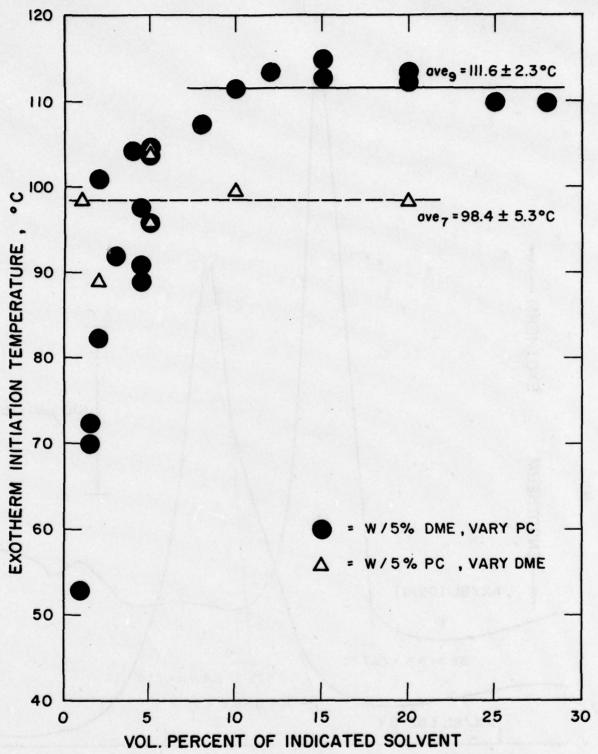


Figure 56. Exotherm initiation from DTA @ 5°C/Minute. 0.00029 g Li + $20\mu l$ of indicated AN/DME/PC

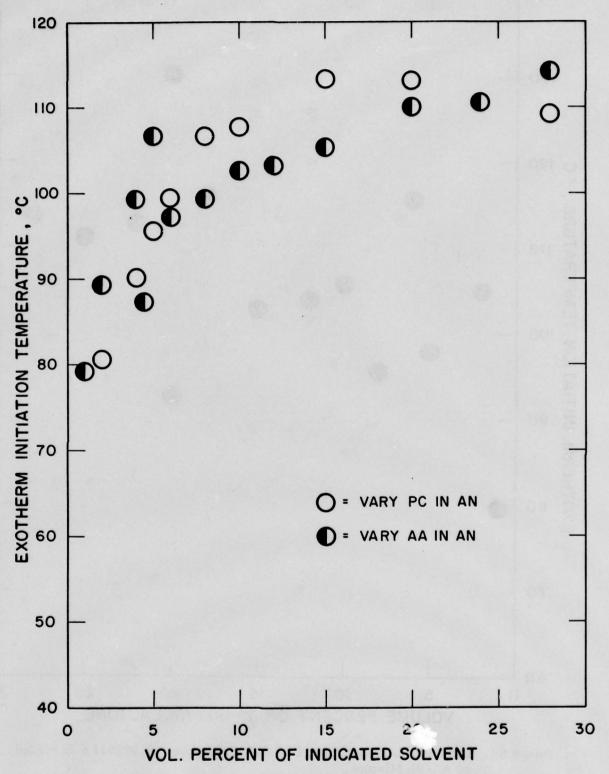


Figure 57. Exotherm Initiation from DTA @ $5\,^{\circ}$ C/Minute. 0.000291 g Li + 20μ l of Solvent Mixture.

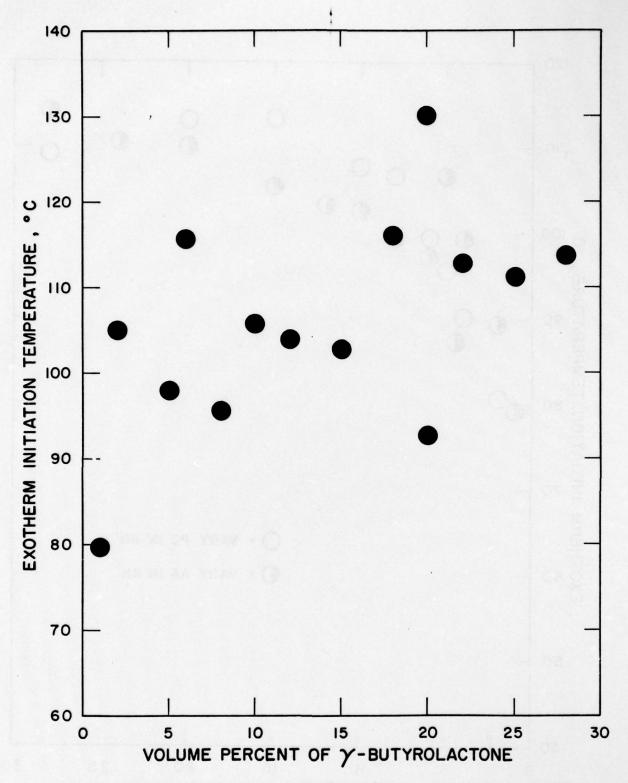


Figure 58. Exotherm Initiation from DTA @ $5\,^{\circ}$ C/Minute. 0.000291 g Li + $20\mu l$ of AN/BL Mixture.

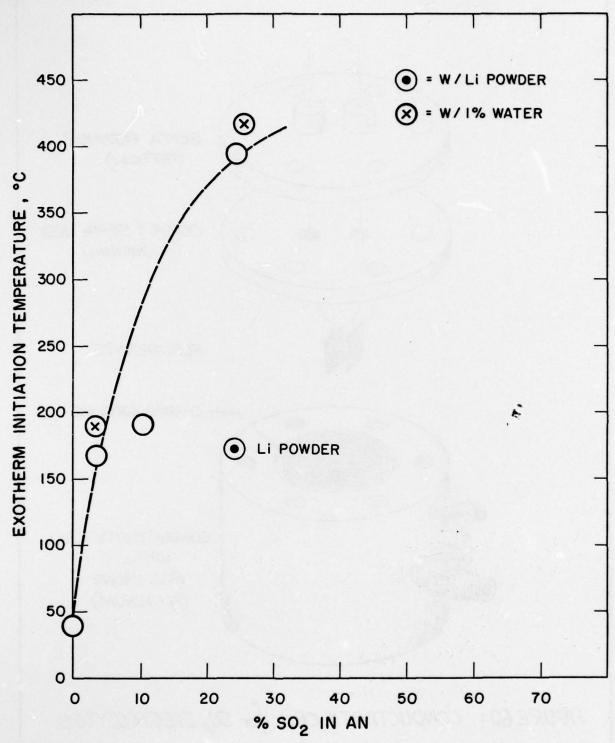


Figure 59. Exotherm Initiation Temperature of the Li + AN. Reaction as a Function of SO_2 concentration

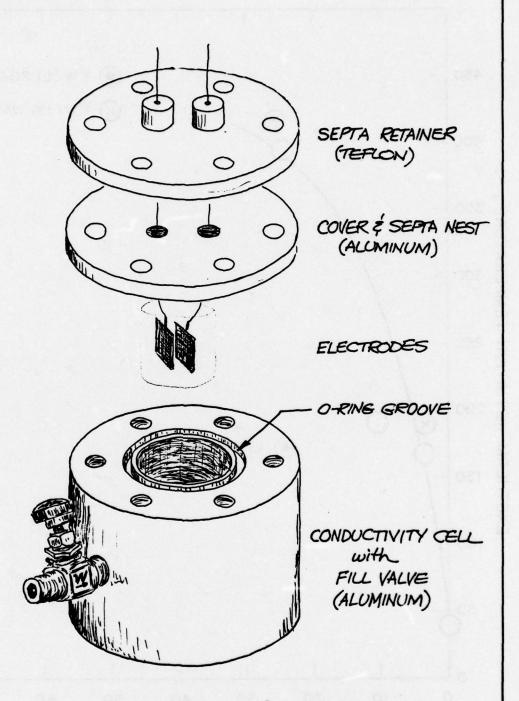


FIGURE 60: CONDUCTIVITY CELL for SO2 ELECTROLYTES

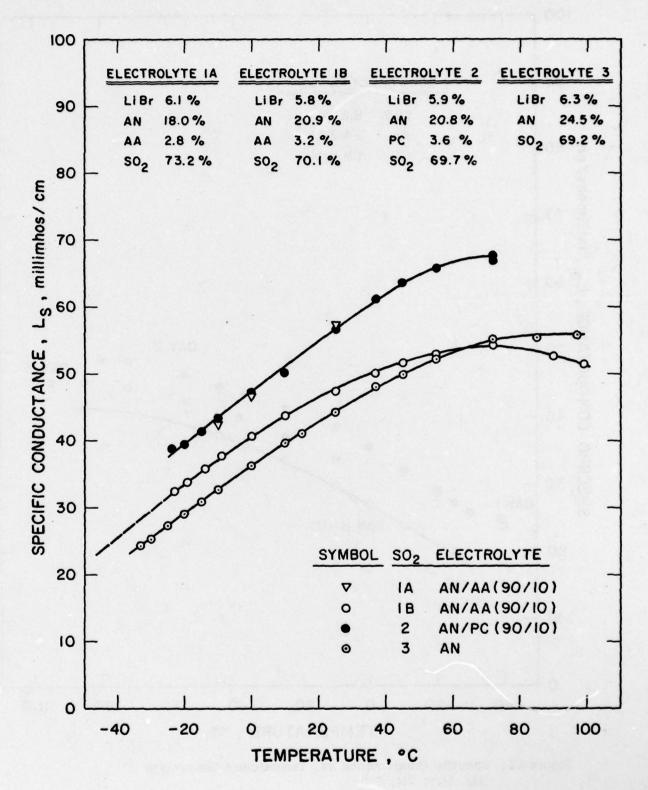


Figure 61. Specific Conductance vs. Temperature for SC₂ Electrolytes, in Aluminum Cell.

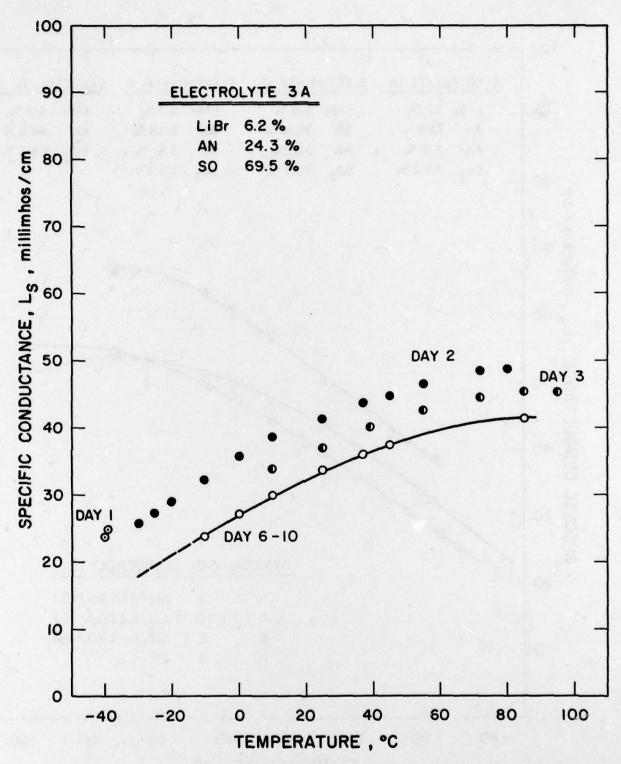


Figure 62. Specific Conductance vs. Temperature Electrolyte 3A: LiBr, AN, SO₂

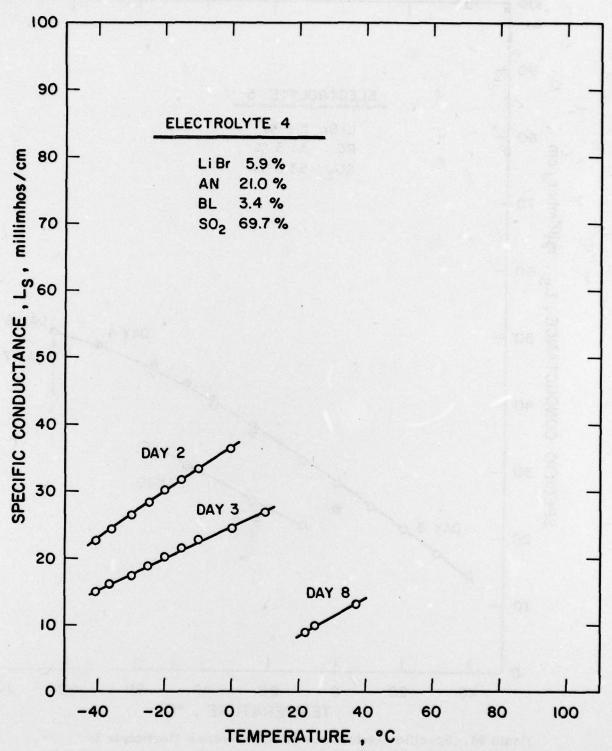


Figure 63. Specific Conductance vs. Temperature for Electrolyte 4: LiBr, AN/BL (90/10), SO₂.

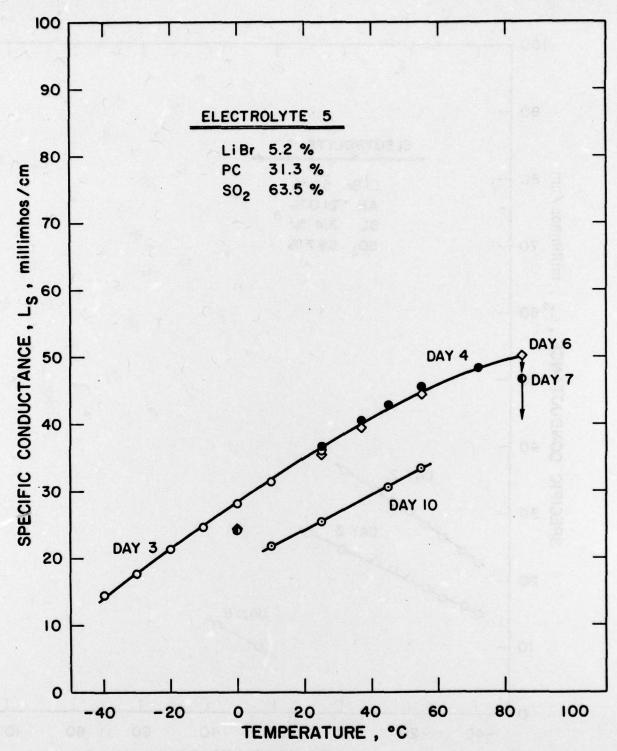


Figure 64. Specific Conductance vs. Temperature Electrolyte 5: LiBr, PC, SO₂.

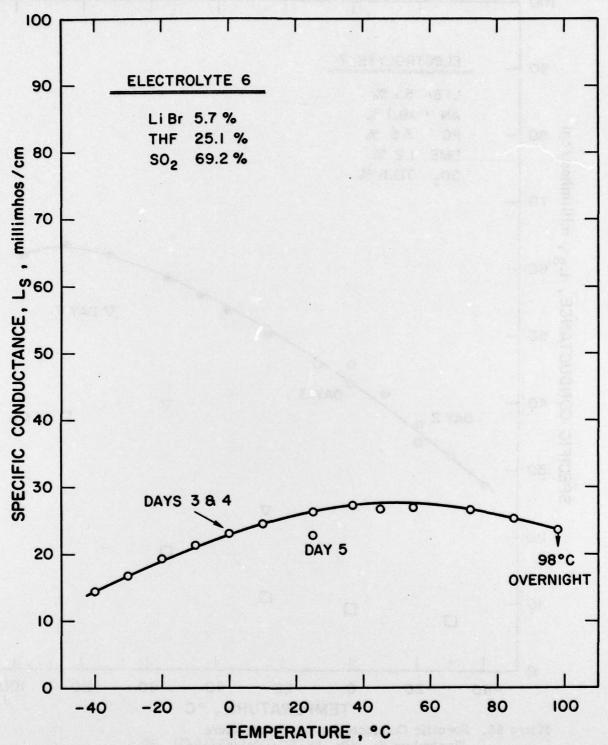


Figure 65. Specific Conductance vs. Temperature Electroltye 6: LiBr, THF, SO₂.

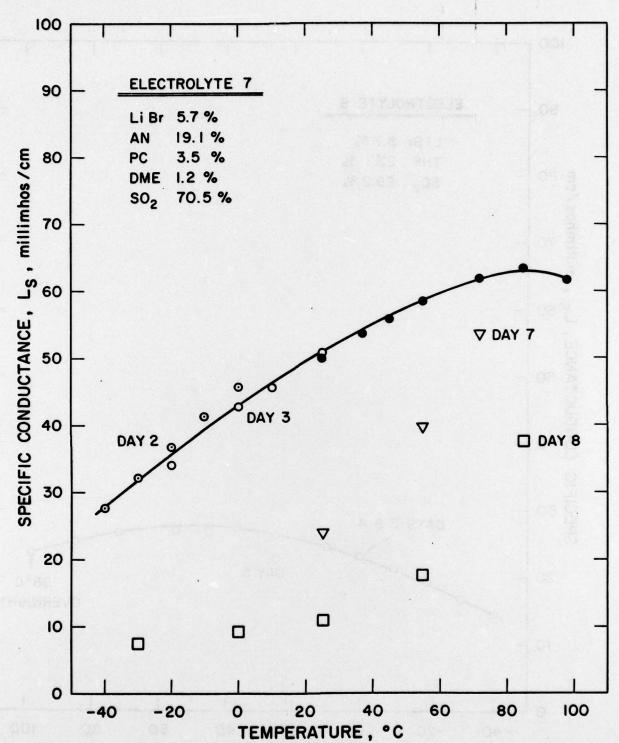


Figure 66. Specific Conductance vs. Temperature Electrolyte 7: LiBr, AN/PC/I)ME(85/10/5), SO₂

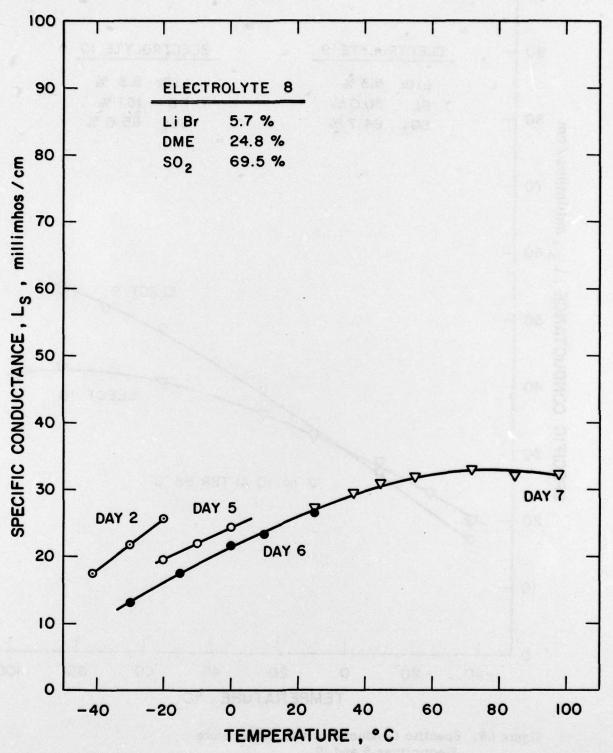


Figure 67. Specific Conductance vs. Temperature Electroltye 8: LiBr, DME, SO₂

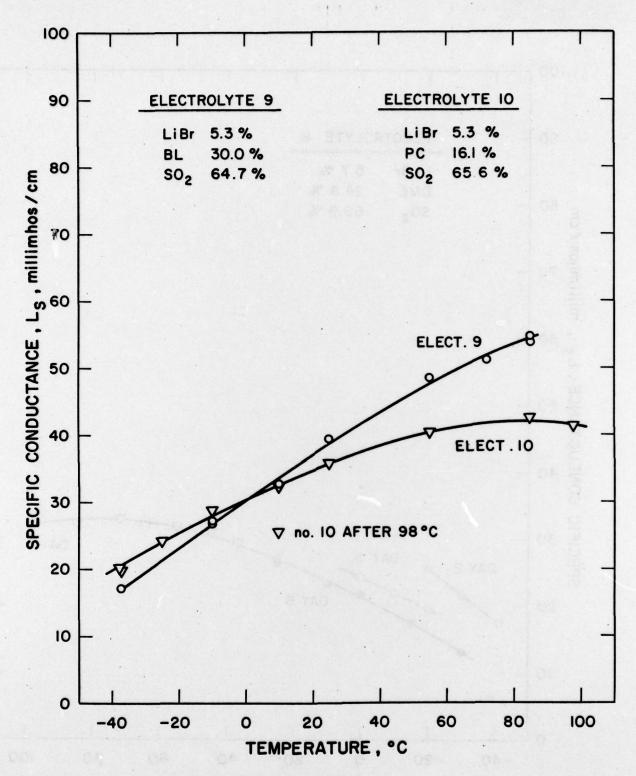


Figure 68. Specific Conductance vs. Temperature Electroltyes 9 and 10. Electrolyte 9: LiBr, BL, SO₂ and Electrolyte 10: LiBr, PC, SO₂

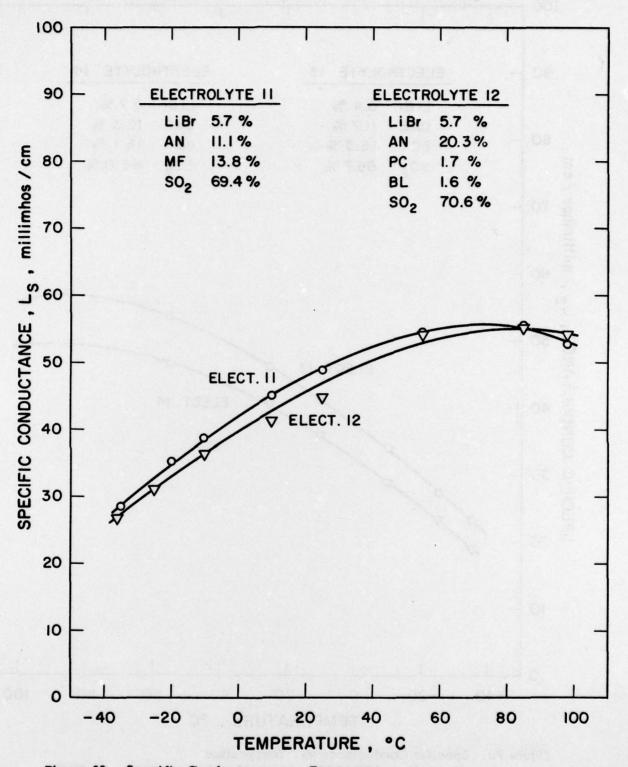


Figure 69. Specific Conductance vs. Temperature Electrolytes 11 and 12.

Electrolyte 11: LiBr AN/MF (50/50) SO₂ and Electrolyte 12: LiBr, AN/PC/BL (90/5/5), SO₂

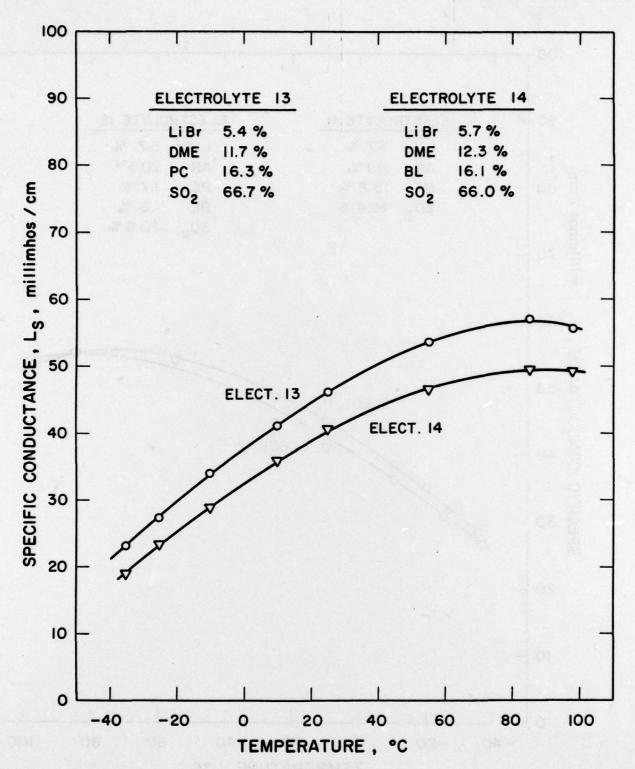


Figure 70. Specific Conductance vs. Temperature Electroltyes 13 and 14.
Electrolyte 13: LiBr, DME/PC (50/50), SC₂
Electrolyte 14: LiBr, DME/BL (50/50), SO₂

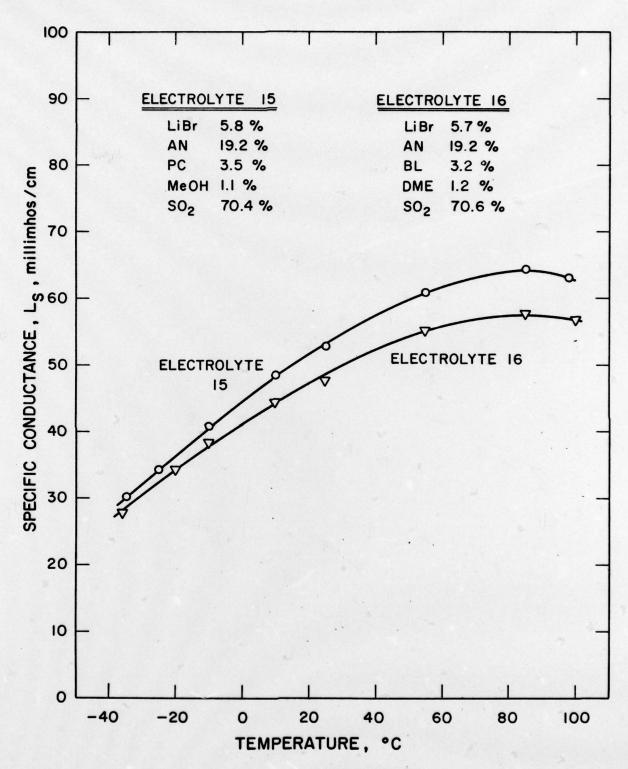


Figure 71. Specific Conductance vs. Temperature Electrolyte 15: LiBr, AN/PC/MeOH(85/10/5), SO₂ Electrolyte 16: LiBr, AN/BL/DME(85/10/5), SO₂

ELECTRONICS TECHNOLOGY AND DEVICES LABORATORY

DISTRIBUTION LIST

1 February 1979

Defense Technical Information Center ATTN: DDC-TCA Cameron Station (Bldg 5) Alexandria, VA 22314	(12)	CDR, US Army Signals Warfare Lab ATTN: DELSW-OS Vint Hill Farms Station Warrenton, VA 22186	(1)
Commander Naval Ocean Systems Center ATTN: Library San Diego, CA 92152	(1)	Commander US Army Mobility EQP Res & Dev CMD ATTN: DRDME-R Fort Belvoir, VA 22060	(1)
CDR, Naval Surface Weapons Center White Oak Laboratory ATTN: Library Code WX-21 Silver Spring, MD 20910	(1)	Commander US Army Electronics R&D Command Fort Monmouth, NJ 07703	
Commandant, Marine Corps HQ US Marine Corps ATTN: Code LMC	(2)	DELET-P DELET-DD DELET-DT	(1) (1) (2)
Washington, D.C. 20380		DELSD-L (TECH LIB) DELSD-L-S (STINFO) DELET-PR	(1) (2) (25)
Rome Air Development Center ATTN: Documents Library (TILD) Griffiss AFB, NY 13441	(1)	Commander US Army Communications R&D Comma	
Air Force Geophysics Lab/SULL ATTN: S-29	(1)	Fort Monmouth, NJ 07703 USMC-LNO	(1)
Hanscom AFB, MA 01731 HQDA (DAMA-ARZ-D) Dr. F. D. Verderame Washington, DC 20310	(1)	NASA Scientific & Tech Info Facility Baltimore/Washington Intl Airport PO Box 8757 MD 21250	(1)
CDR, Harry Diamond Laboratories ATTN: Library 2800 Powder Mill Road Adelphi, MD 20783	(1)		
Director US Army Materiel Systems Analysis ACTV ATTN: DRXSY-MP Aberdeen Proving Ground, MD 21005	(1)		
CDR, US Army Research Office ATTN: DRXRO-IP	(1)		
PO Box 12211 Research Triangle Park, NC 27709			

Distribution List - Continued

Electrochimica 2485 Charleston Road Mountain View, CA 94040 ATTN: Dr. Eisenberg	(1)	Mr. J. R. Moden Energy Conversion Branch Code 3642 Naval Underwater Systems Center Newport Laboratory Newport, RI 02840	(1)
Dr. Hugh Barger	(1)		
P. O. Box 2232 Davidson, NC 28036	ν-/	NASA Lewis Research Center Mail Stop 6-1 21000 Brookpark Road	(1)
Energy Storage & Conversion Lept. TRW Systems One Space Park	(1)	Cleveland, OH 44135 ATTN: Dr. Stuart Fordyce	
Redondo Beach, CA 90278		Mr. Joe McCartney	(1)
ATTN: Dr. H. P. Silverman		Naval Undersea Center Code 608	
Sanders Associates, Inc.	(1)	San Diego, CA 92132	
24 Simon Street			
Mail Stop NSI-2208		EIC, Inc.	(1)
Nashua, NE 03060		ATTN: S. B. Brummer	
ATTN: J. Marshall		Newton, MA 02158	
Power Conversion, Inc.	(1)	Altus Corp.	(1)
70 MacQuesten Pkwy		440 Page Mill Road	
Mount Vernon, NY 10550		Palo Alto, CA 94306	
ATTN: Stuart Chodosh		ATTN: Douglas Glader	
Dr. D. Pouli	(1)	J. Bene	(1)
Portfolio Manager		MS 488	
Hooker Chemicals & Plastics Corp.		NASA Langley Research Center	
M.P.C. Box 8		Hampton, VA 23665	
Niagara Falls, NY 14302			
	/11	Mr. Eddie T. Seo	(1)
Dr. Leonard Nanis G207	(1)	Research and Development Div. The Gates Rubber Co.	
S.R.I.		999 S. Broadway	
Menlo Park, CA 94025		Denver, CO 80217	
Dr. J. J. Auborn, Rm 1A-317	(1)	Mr. Sidney Gross	(1)
Bell Laboratories	(1)	Mail Stop 8C-62	(1)
600 Mountain Avenue		Boeing Aerospace Company	
		P. O. Box 399	
Murray Hill, NJ 07974		Seattle, WA 98124	
Stonehart Associates, Inc.	(1)	Seattle, WA 30124	
34 Five Fields Road	(-)	Honeywell Technology Center	(1)
Madison, CT 06443		ATTN: Dr. H. V. Venkatasetty	(-,
ATTN: Mr. Thomas Reddy		1701 Lyndale Avenue South	
ATTN. MI. Inomas Reday		Bloomington, MN 55420	
Jet Propulsion Laboratory	(1)		
4800 Oak Grove Drive			
Pasadena, California 91103			
ATTN: Mr. Harvey Frank			

Distribution List - Continued

Mr. Aiji Uchiyama	(1)	Argonne National Laboratories	(1)
Jet Propulsion Laboratory - M.S.198-220		9700 South Cass	
4800 Oak Grove Drive		Argonne, IL 60439	
Pasadena, CA 91103		ATTN: Dr. E. C. Gay	
Mr. Frank Dic	(1)	GTE Sylvania, Inc.	(1)
Mr. Frank Bis Naval Surface Weapons Center	(-)	77 A Street	
White Oak Laboratory, Code R-33		Needham Heights, MA 02194	
Silver Spring, MD 20910		ATTN: Mr. Richard Pabst	
onvoi opinia, me			
Transportation Systems Center	(1)	General Motors Corp.	(1)
Kendall Square		Research Laboratories	
Cambridge, MA 02142		General Motors Technical Center	
ATTN: Dr. Norman Rosenberg		12 Mile and Mounds Roads	
		Warren, MI 48090	
GTE Laboratories, Inc.	(1)	ATTN: Dr. J. L. Hartman	
40 Sylvan Road		Union Carbide Corporation	(1)
Waltham, MA 02154		Parma Research Center	(-,
Reads Minaral Company	(1)	P. O. Box 6116	
Foote Mineral Company Route 100	(-)	Cleveland, OH 44101	
Exton, PA 19341			
ATTN: Dr. H. Grady		P. R. Mallory & Co. Inc.	(1)
AIII. Die III. Casa,		S. Broadway	
Honeywell, Inc.	(1)	Tarrytown, N.Y. 10591	
104 Rock Road		ATTN: J. Dalfonso	
Horsham, PA 10944			// //
ATTN: C. Richard Walk		North American Rockwell Corp.	(1)
		Atomics International Division	
Sanders Associates, Inc.	(1)	Box 309 Canoga Park, CA 91304	
Sonobuoy Division		ATTN: Dr. L. Heredy	
95 Canal Street		AIIN: Dr. E. Heledy	
Nashua, N.H. 03060 ATTN: Dr. David Dwyer		General Electric Pesearch &	(1)
Alin: Dr. David Dwyer		Development Center	
Eagle-Picher Industries, Inc.	(1)	P. O. Box 8	
Electronics Division		Schenectady, N.Y. 12301	
ATTN: Mr. Robert L. Higgins		ATTN: Dr. Stefan Mitoff	
P.O. Box 47			
Joplin, Missouri 64801		University of California	(1)
		Department of Science & Research	
Yardney Electric Company	(1)	Santa Barbara, CA 93100	
82 Mechanic Street		ATTN: Dr. J. Kennedy	
Pawcatuck, CT 06379		The Electric Storage Battery Co.	(1)
ATTN: Technical Library		Carl F. Norburg Research Center	(-,
Exxon Research and Engineering Co.	(1)	19 W. College Avenue	
Corporate Research Laboratory		Yardley, PA 19067 ATTN: Dr. A. Salkind	
Linden, N.J. 07036		ATTN: Dr. A. Barking	
ATTN: Dr. R. Hamlen		Gulton Industries, Inc.	(1)
		Metuchen, N.J. 08840	
		ATTN: Mr. S. Charlip	

SUPPLEMENT TO DISTRIBUTION LIST

13 January 1978

Other Recipients

Mr. Donald Mortel (1)
AF Aero Propulsion Lab.
ATTN: AFAPL-POE-1
Wright Patterson AFB, Ohio 45433

Mr. Richard E. Oderwald (1)
Department of the Navy
Hqs., US Marine Corps
Code LMC 4
Washington, DC 20380

Commander (1)
Harry Diamond Laboratories
Attn: DELHD-RDD (Mr. A. Benderly)
2800 Powder Mill Road
Adelphi, MD 20783